



University of Tennessee, Knoxville
**Trace: Tennessee Research and Creative
Exchange**

Doctoral Dissertations

Graduate School

8-2018

Preservation of Proterozoic Microbial Mats

Ashley Rene Berg

University of Tennessee, aberg@vols.utk.edu

Recommended Citation

Berg, Ashley Rene, "Preservation of Proterozoic Microbial Mats." PhD diss., University of Tennessee, 2018.
https://trace.tennessee.edu/utk_graddiss/5080

This Dissertation is brought to you for free and open access by the Graduate School at Trace: Tennessee Research and Creative Exchange. It has been accepted for inclusion in Doctoral Dissertations by an authorized administrator of Trace: Tennessee Research and Creative Exchange. For more information, please contact trace@utk.edu.

To the Graduate Council:

I am submitting herewith a dissertation written by Ashley Rene Berg entitled "Preservation of Proterozoic Microbial Mats." I have examined the final electronic copy of this dissertation for form and content and recommend that it be accepted in partial fulfillment of the requirements for the degree of Doctor of Philosophy, with a major in Geology.

Linda C. Kah, Major Professor

We have read this dissertation and recommend its acceptance:

Christopher M. Fedo, Andrew D. Steen, Steven W. Wilhelm

Accepted for the Council:

Dixie L. Thompson

Vice Provost and Dean of the Graduate School

(Original signatures are on file with official student records.)

Preservation of Precambrian Microbial Mats

**A Dissertation Presented for the
Doctor of Philosophy
Degree
The University of Tennessee, Knoxville**

**Ashley Rene Manning Berg
August 2018**

Copyright © 2018 by Ashley Rene Manning Berg
All rights reserved.

DEDICATION

To my husband, Chris, for his unwavering support and encouragement, and to the many educators and colleagues who have encouraged my passion for learning and knowledge

ACKNOWLEDGEMENTS

Funding for the work in this dissertation was provided by the Society for Sedimentary Geology, the Paleontological Society, Southeastern GSA, The Society for Organic Petrology, the NASA Astrobiology Early Career Collaboration Award, and the JPL Collaborative Academic Partnership. Field work was funded by the Robert W. Rex Research Fund, the Lewis and Clark Astrobiology Grant, and the Kenneth R. Walker Professorship fund. The Polar Continental Shelf Project provided logistical support for our field season. I would also like to thank the JPL Astrobiogeochemistry Laboratory for collaborating with me.

I want to thank my advisor, Dr. Linda Kah for encouraging and supporting me while I pursued my graduate degrees. I'd like to acknowledge my committee, Drs. Andrew Steen, Christopher Fedo, and Steven Wilhelm for their support. I'd also like to thank Drs. Julie Bartley, Michael Tuite, and Kenneth Williford for their continued guidance, support, and encouragement while completing this dissertation. I would also like to acknowledge my friends in the Department of Earth and Planetary Sciences, especially Joy Buongiorno-Altom, Keenan Golder, Miles Henderson, Jason Muhlbauer, Cameron Hughes, and countless others. Finally, I'd like to thank my husband, Chris, for his support, patience, and strength over the last four years.

ABSTRACT

Meso- to Neoproterozoic peritidal carbonate strata commonly contain early diagenetic chert deposits that can record evidence of mineral and organic precursors. Exceptional morphologic preservation can be used to place time constraints on silicification, often indicating silicification is penecontemporaneous with mat growth. Silica-rich sedimentary deposits have also been suggested as potential targets for the search for extraterrestrial life on Mars. The chapters in this dissertation investigate fluid compositions capable of precipitating primary and secondary silica phases and the extent to which microorganisms are preserved, specifically their morphology and chemistry, by early silicification. Twenty potential fluid compositions were modeled using PHREEQC, and the mineral phases capable of precipitating were compared to the mineralogies observed in thin sections from silicified microbial mats of the Angmaat Formation, Bylot Supergroup. This model indicates that silica phases were capable of precipitating as primary or secondary mineral phases over a wide range of fluid chemistries. However, only brine solutions were capable of precipitating each mineral phase observed in the Angmaat Formation samples, including amorphous silica and silica gel.

Hydrous silica phases permeate the sheaths of the organisms, which preserves the individual microorganisms and the complexity of microbial mats. Mat morphologies in the Angmaat Formation preserve a range of taphonomic states, including well-preserved mats that are interpreted to reflect the top layers of mats, to poorly-preserved mats that may reflect buried layers in the mat that were exposed to greater heterotrophic degradation. A taphonomic assessment of the individual microfossils reveals preserved complexity within the microbial mats and a new taphonomic assessment technique is introduced to account for the complexity. Regardless of taphonomic grade, coccoidal microfossils exhibit better preservation than filamentous mat-building organisms. Differential preservation may be related to the motility of the organisms.

Organic geochemical characterization of the silicified mats indicates that despite exceptional morphologic preservation, lipids are not preserved in early diagenetic chert. Lipids, specifically hopanes and steranes, could be used to elucidate microbial processes active at the time of silicification and paleoenvironmental conditions. The lack of lipid preservation suggests that silica-rich low-temperature deposits may not be ideal targets for the search of ancient extraterrestrial life.

TABLE OF CONTENTS

Introduction.....	1
Early Diagenetic Silicification.....	1
Overview of the Present Study	2
References.....	5
Chapter 1 Proterozoic microbial mats and their constraints on environments of silicification	8
Abstract.....	9
Introduction.....	10
Bylot Supergroup Chert	12
Geological setting and age of the Bylot Supergroup	12
Chert facies and their interpretation.....	13
Constraints on timing of silicification.....	14
Constraints on nature of silicification	16
Constraints on regional environments of silicification	17
Modeling Chemical Environments of Silicification	19
Constraints on Proterozoic seawater.....	20
PHREEQC modeling	21
Results and Interpretation of Geochemical Models.....	22
Group 1 solutions.....	23
Group 2 solutions.....	23
Group 3 solutions.....	24
Group 4 solutions.....	25
Discussion.....	25
Additional insight from geochemical models.....	28
Conclusions.....	31
Acknowledgements.....	32
References.....	33
Appendix.....	38
Chapter 2 Taphonomic variability in the 1.1 Ga microbial mats of the Angmaat Formation, Bylot Supergroup, Baffin Island.....	47
Abstract.....	48
Introduction.....	49
Geologic Setting and Age	52
Bylot Supergroup.....	52
Angmaat Formation chert	53
Microbial assemblages of the Angmaat Formation	54
Methods.....	55
Technique Development	55
Taphonomic classification and assessment.....	55
Taphonomic analysis using image mosaics	59
Quadrat sampling.....	60
Results.....	61
Taphonomic patterns: filamentous microfossils.....	61
Taphonomic patterns: coccoidal microfossils.....	62
Results of traditional point-counting	63

Results of quadrat sampling	64
Raman spectroscopy	67
Discussion	68
Taphonomic analyses using quadrat sampling on image mosaics	68
Mat fabrics and implications for biomarker preservation	69
Conclusions	73
References	75
Appendix	80
Chapter 3 Geochemical Characterization of Preserved Lipids within Silicified Microbial Mats of the Angmaat Formation	102
Abstract	103
Introduction	104
Geologic Framework	105
Bylot Supergroup	105
Angmaat Formation chert	107
Sample sets	109
Methods	110
Initial sample preparation	110
Bitumen I extraction	112
Bitumen II extractions	113
Carbon isotope ratios	115
Blanks	115
Results and Interpretation	116
Bitumen I extracts	116
Bitumen II extracts	118
Carbon isotope ratios	119
Discussion	120
Preservation of organic compounds in chert	120
Sources of contamination	123
Carbon isotopes	124
Silicification process	126
Conclusions	129
References	131
Appendix	139
Conclusions	154
References	159
Vita	161

LIST OF TABLES

Table 1.1 Results of fluid mixing models using $[Ca^{2+}] = 9$ mmol/kg (Spear et al., 2014).	45
Table 1.2 Results of fluid mixing models using $[Ca^{2+}] = 12$ mmol/kg (Spear et al., 2014).	46
Table 2.1. Taphonomic assessment of the microfossils preserved in the Angmaat Formation. Individual microfossils were classified as “good,” “fair,” and “poor.” Over 600 individual microfossils were counted using the quadrat method and the percent area of unrecognizable carbonaceous matter was calculated with ImageJ over the entire thin section.	90
Table 2.2 Raman Index Parameters for the Angmaat Formation are around 7. Values closer to 1 are considered more highly altered samples; whereas values closer to 9 indicate less thermal alteration (Schopf et al., 2005).	101
Table 3.1 Major sources of contamination identified throughout the 2017 samples. Phthalates, siloxanes, DEET, Pheols, and Fryol fr 2 are observed in chert samples. Whereas the Ergosterol, squalenes, dioloptene, and bute haydrocarbon occur in the carbonate sample.	150
Table 3.2 Carbon isotopes data for the 1994 sample suite and the 2017 suite. The data are sorted according to the lithology of the mat fabric.	151

LIST OF FIGURES

- Figure 1.1. Simplified geologic map of the Bylot Supergroup within the Milne Inlet graben (modified from Knoll et al., 2013), showing locations of strata of the Eqaulik (EQA), Uluksan, and Nunatsiaq (NUN) groups. The Iqqittuq and Angmaat formations range from Tay Sound (TS) in the east to just west of Tremblay Sound (TB) in the west. The Angmaat Formation west of Milne Inlet (MI) is dominated by oolitic-intraclastic shoal deposits. Black chert is most common between White Bay (WB) and Tay Sound (TS). Small black circles show localities from which early diagenetic chert samples were collected from the Angmaat Formation. 38
- Figure 1.2 Patterns of early diagenetic chert in the Angmaat Formation. (a) Lensoidal to bedded black chert within irregular, low-relief microbial facies. White laminae represent storm-deposited micrite drapes. (b) Nodular black chert within microlaminated carbonate precipitate facies. Within precipitate facies, chert is often centered around rare microbial facies that are marked by development of depositional relief on the substrate. (c) Early diagenetic chert within tufted microbial facies. Microbial tufts draped by white micrite are marked by black arrows. Alternation of black and white chert in the lower part of the image represents silicification of original organic material and primary void space (see Knoll et al., 2013). (d) Nodular black chert within tufted microbialite facies. Grey carbonate represents stacked microbial tufts (see Fig. 1.2C) and white represents the partial draping of surface topography by white micrite. Note that chert nodules track the primary morphology of mat laminae (dotted line). Scale bar is 10 cm in (a) and 2 cm in (b), (c), and (d). 39
- Figure 1.3. Common microbial mat fabrics within Angmaat Formation chert. (a) Coccoid-dominated mat showing concentrations of coccoidal sheaths surrounded by pale regions interpreted as pockets of EPS. (b) Coccoid-dominated mat in crossed-polars. (c) Tightly woven filament-dominated mat consisting primarily of *Siphonophycus inornatum* (thin filaments) and *Eomicrocoleus crassus* (thick filaments) (cf. Knoll et al., 2013); contact between adjacent filament sheaths suggest that the primary mat contained no mineral constituents. (d) Filament-dominated mat in crossed-polars. (e)..... 40
- Figure 1.4. Void structures in Angmaat Formation microbial mats. (a) Vertical filamentous microbial tuft (M) lining the edge of a constructional void. Void is lined with chalcedony (CHAL), and ultimately filled by late-stage, dolomite (DOLO) cement. (b) Mat-to-void fabrics viewed under crossed-polars. (c) Constructional voids within a filament-dominated microbial mat (M) that contain a combination of unsilicified to partially silicified carbonate microspar (CARB) and chalcedony (CHAL). Scale bar is 250 micrometers in (a) and (b), and 1 mm in (c). 41
- Figure 1.5. Associated mineral phases within early diagenetic chert. (a) Compacted filament-dominated mat interlaminated with detrital microbreccia. (b) Detail of microbreccia showing clasts that reflect transport of microbial mat elements (M). (c) Silicified carbonate precipitate facies (see Kah and Knoll, 1996; Knoll et al., 2014). (d) Silicified lenticular pseudomorphs after gypsum (arrows; see also Kah et al., 2001). Scale bar is 250 micrometers in (a), 100 micrometers in (b) and (c), and 25 micrometers in (d). 42
- Figure 1.6. Determination of pCO₂ and pH values used to model Proterozoic seawater fluids; modified from Grotzinger and Kasting (1993). White region indicates hypothesized range of pCO₂ and pH conditions for Paleoproterozoic to Archean seawater assuming that [HCO₃⁻] > 2[Ca²⁺] in marine systems, which would result in an evaporative mineral sequence (cf.

Warren, 2006) without gypsum. The same range of pCO₂ values were used in this manuscript, although because the Mesoproterozoic Angmaat Formation contains some of earliest extensive gypsum in the geologic record (Kah et al., 2001), so values (black dots) were chosen that fall along the line described by [HCO₃⁻] = 2[Ca²⁺]. After the appearance of calcium sulfate evaporate minerals in the rock record, all seawater compositions should have pH and pCO₂ values that plot within the green area. 43

Figure 1.7. Minimum and maximum concentrations of [Ca²⁺] from fluid inclusion data for the Proterozoic (Spear et al., 2014) was used to create two starting solutions. To model these solutions as open systems, compositions were modeled in equilibrium with five different pH and pCO₂ values (see Fig. 1.6) to create 10 potential solutions. These ten solutions were then used in two mixing models. Physical scenarios that drive these two mixing models are illustrated in Figure 1.8, and model results are discussed in the text and summarized in Tables 1.2 and 1.3. 44

Figure 1.8. Scenarios for silicification within the Angmaat Formations. Initiation of the Angmaat Formation is marked by development of a mid-ramp oolitic shoal complex. (a) During sea level highstands, open marine waters circulate freely across the inner platform, which may experience modification by freshwater influx. Model 1 (cf. Tables 1.2 and 1.3) examines the potential for marine and freshwater-modified marine fluids to satisfy constraints for silicification as determined from petrographic analysis of Angmaat chert. (b) During sea level lowstand, isolation of inner-ramp environments permits evaporation to gypsum salinity (cf. Kah et al., 2001). Model 2 (cf. Tables 1.2 and 1.3) examines the potential for marine brines and freshwater-modified brines to satisfy constraints for silicification as determined from petrographic analysis of Angmaat chert. 44

Figure 2.1 An idealized microbial mat adapted from Stolz, 2000. Microbial mats typically consist of five to six layers of various microbial communities that form differently colored laminae as a result of chemical and light gradients within the mat. 80

Figure 2.2 Samples used in this study were collected during a 1993-1994 field season to Baffin Island (A). All of the samples were collected from the Angmaat Formation (B) within the Bylot Supergroup (C). Here the sample localities are plotted here as black squares (B). 81

Figure 2.3 Early diagenetic black chert occurs as thin layers (A) to nodules and lenses (B) in the carbonate strata of the Angmaat Formation. Later diagenetic chert is also present in these strata, although they are typically yellow (C) or gray (D) in color. 82

Figure 2.4 Overall mat taphonomy was determined based on quick, petrographic observations. Uncompacted mat fabrics, with abundant microfossils in vertical and horizontal arrangements were given the classification of “good.” “Fair” mat fabrics exhibit more compaction and have obvious, compacted layers that are pigmented light- to dark-brown. Mats labelled as “poor” are often highly compacted, individual microfossils are not easily, or quickly, identified and compacted layers are dark-brown to black in color. 83

Figure 2.5 Taphonomic grades of “good,” “fair,” and “poor” were assigned to individual microfossils. These grades were determined based on the compaction of the microfossil, how pristine the sheath or cell wall appear (i.e. whether it was torn or collapsed). A subcategory of “poor” was used for samples that were too darkly pigmented and the organic matter was too homogenized to determine whether the microfossil had been filamentous or coccoidal. These samples were labelled as “unrecognizable.” 84

Figure 2.6 A quadrat system was overlain onto each mosaic. The mosaic was first divided into 25 partitions (A1-E5). Each partition was divided into 64 quadrats. For each partition, a

random number generator in Microsoft Excel was then used to determine which quadrat would be used in the assessment (1-64)..... 85

Figure 2.7 Two types of filamentous microfossils are observed in the Angmaat Formation mats. The larger, darker filaments are *Microcoleus* filaments and are highlighted with the black arrow in (A) and (B). The dark, compacted layers (B) observed in these mats, are often the result of bundling of these *Micorcoleus* sheaths. The white boxes highlight areas where the second filamentous organisms are easily seen (A and B). These are *Siphonophycus* filaments, which fade during mat decomposition and are not able to be counted for taphonomic analyses. 86

Figure 2.8 Coccoidal organisms preserved in a microbial mat that is visually identified as “fair.” Coccoidal microfossils commonly have a cell wall with a dark center, like the *Gloediniopsis* (Gds) microfossils preserved in the top right corner. This image also contains *Entophysalis* (En), which compose dark patchy areas within a mat and never preserve well. The small (2-3 μm) cells are identified as *Sphaerophycus* (Sph); however, these fossils are too small for an accurate description of their taphonomy. 87

Figure 2.9 Coccoidal microfossils within “good” or “fair” mats tend to accumulate into layers of coccoidal microfossils as they decay. When the coccoidal organisms reach the taphonomic grade of “poor” the organic matter becomes homogenized and forms patches that are almost opaque. 88

Figure 2.10 A taphonomic assessment was performed on a thin section using traditional point counting techniques on the microscope. The thin section was moved in 2 mm increments from right to left and then down and left to right. Results from this assessment were compared to point counting on an image mosaic with a grid overlay, where microfossils were counted when they were under the intersection point of two gridlines..... 89

Figure 2.11 A taphonomic assessment was performed on the same sample five times. The assessments were performed on different days to judge the consistency of the observer’s taphonomic assessment. Different quadrats were counted in each assessment to determine if using the quadrat sampling technique would provide a more representative assessment of the thin section. 91

Figure 2.12 Taphonomic variation is observed from one quadrat to another. Each triangle on this ternary plot represents all of the microfossils (filaments and coccoids) that were counted and scored in one quadrat. To obtain the desired 600 microfossil count, 40 quadrats were counted. Each number corresponds to the quadrat number. Data show is for a mat taphonomically identified as "good" (DAC-15). Microfossils in this sample exhibit a wide range of preservation and plot within several of the taphonomic fields of the ternary plot (Kowalewski et al., 1995). 92

Figure 2.13 Quadrat data for DAC-15, a “good” mat fabric, plotted by the taphonomy of coccoidal microfossils (A) and filamentous microfossils (B) per quadrat. Each of the data labels represents the number of the quadrat..... 93

Figure 2.14 Taphonomic assessment of sample DBG-42 by quadrat for a mat fabric that is taphonomically identified as "fair." Most of the microfossils (coccoidal and filamentous) preserve within the taphonomic range of “poor.” 94

Figure 2.15 Quadrat data for DBG-42 a “fair” mat fabric, plotted by the taphonomy of coccoidal microfossils (A) and filamentous microfossils (B) per quadrat. Each of the data labels represents the number of the quadrat. 95

Figure 2.16 Taphonomic assessment of sample DAC-16 by quadrat for a mat fabric that is taphonomically identified as "fair." Most of the microfossils (coccoidal and filamentous) preserve within the taphonomic range of "poor."	96
Figure 2.17 Quadrat data for DAC-16, which is identified as a "fair" mat fabric, plotted by the taphonomy of coccoidal microfossils (A) and filamentous microfossils (B) per quadrat. Each of the data labels represents the number of the quadrat.	97
Figure 2.18 Taphonomic assessment of sample DBN-4 by quadrat for a mat fabric that is visually identified as having a "poor" taphonomic grade. Most of the microfossils (coccoidal and filamentous) preserve within the taphonomic range of "fair-poor."	98
Figure 2.19 Quadrat data for DBN-4 a "fair" mat fabric, plotted by the taphonomy of coccoidal microfossils (A) and filamentous microfossils (B) per quadrat. Each of the data labels represents the number of the quadrat.	99
Figure 2.20 Quadrat data six samples with taphonomic grades ranging from "good" to "poor." The circles represent the coccoidal microfossil data, which generally have a wider range of taphonomic preservation. Whereas the square represents filamentous microfossil data. The filamentous data plots more consistently in the "poor" taphonomic range.	100
Figure 2.21 Filamentous microfossils are preserved in various taphonomic states within this figure. Each box represents a location where a Raman point spectrum was collected. The color of the Raman spectra correlate to the color box on the figure. Despite the taphonomic grade of the microfossil, the Raman spectra obtained for each box have similar patterns.	101
Figure 3.1 Map of Baffin Island (A). Samples were collected near White Bay (B) within the carbonate strata of the Angmaat Formation of the Bylot Supergroup (C). The squares represent sample localities for the 1994 samples used in this study, and the circles represent samples that were collected during the 2017 field season (B).....	139
Figure 3.2 Early diagenetic chert within the Angmaat Formation occurs as beds up to ~10 cm thick (A) or as nodules and lenses (B). Examples of late diagenetic chert nodules are also observed in the field area. Late diagenetic chert nodules were yellow in color (C) or gray (D) and the concentric rings were always within the nodules.	140
Figure 3.3 Two sample sets were used in this study. The first set was collected during a 1993-1994 field season and had been stored in the collections at Harvard University. The sample billets were used for geochemical analyses, which limited the amount of sample available. A second set of samples was collected in 2017. To minimize potential contamination, these samples were send immediately to JPL. The methods used for bitumen I and II, and isotopic analyses, were used on both sets of samples. The largest difference in sample prep were the steps taken to ensure that contaminants were not introduced to the 2017 samples.	141
Figure 3.4 Total Ion Chromatograms (TIC) are shown for several of the 1994 samples. Mass ion chromatograms provide evidence for the preservation of <i>n</i> -alkanes ($m/z=85$), hopanes ($m/z=191$), and steranes ($m/z=217$).	142
Figure 3.5 Detailed data for one of the 23 samples from the 1994 sample suite. In the m/z 85 ion chromatogram, <i>n</i> -alkanes are identified and exhibit an even-over-odd carbon preference. The T_s and T_m peaks are labeled on the m/z 191 ion chromatogram. Long-chain carbon hopanes are also identified on this ion chromatogram. Within the m/z 217 chromatogram, $C_{27} - C_{30}$ steranes are highlighted.	143
Figure 3.6 Chromatograms for chert samples (on top) and the chromatograms of the chert-associated carbonate samples below them. The chromatograms of the chert samples and their corresponding carbonate samples do not show the same peaks. A similar distribution	

of peaks would be expected for the chert and carbonate because the two phases were from the same samples and should therefore have the same lipids preserved..... 144

Figure 3.7 Two major contaminants are identified from the TIC of a 2017 sample. Siloxane contamination is seen in the early in the measurement. These compounds typically have a mass fragment of 74 and are therefore identified in the m/z 74 ion chromatogram. Siloxanes are seen in all of the TIC for the 2017 samples and are the result of contamination by the GC column. Other common contaminants in the 2017 samples are a group of phthalates that elude between 60 and 80 minutes in the chromatogram. These compounds are identified in the mass 85 ion chromatogram. 145

Figure 3.8 The most common contaminant in the 2017 samples was DEET. On the left, the TIC peak is highlighted and seen in the m/z 191 ion chromatogram directly below the TIC. The spectra associated with the DEET compound is shown on the right of this figure with the chemical structure. This was identified using the NIST standard library..... 146

Figure 3.9 Pristane was observed in one of the carbonate samples collected in 2017. The peak eludes immediately after the *n*-C₁₇ alkane..... 147

Figure 3.10 Fatty acid methyl esters were found in all of the bitumen II samples. These were the two most prominent peaks in the TICs. The top TIC is the entire TIC and the bottom graph is a zoomed-in view of the same TIC. 148

Figure 3.11 Cartoon showing the difference between bitumen I and bitumen II. Bitumen I is the solvent-soluble organic matter that is preserved between the crystals of the mineral phase and bitumen II is the soluble organic matter that is incorporated into the crystal of the mineral phase. 148

Figure 3.12 Bitumen I and II chromatograms were different for the 1994 and 2017 samples. A TIC is provided for each sample, as are the mass ion chromatograms 85 (*n*-alkanes), 191 (hopanes), and 217 (steranes). On the left is the comparison of a 1994 sample to the bitumen II data. No evidence for the presence of hopanes or steranes is observed in the bitumen II data. On the right, a sample from the 2017 sample collection. The bitumen II data look different from the bitumen I data for these samples as well. Bitumen II data do not preserve the same geolipids at the bitumen I data, which suggests that the bitumen I data are contaminants. 149

Figure 3.13 Several blanks were used throughout the method development. The granite acted as a procedural blank for the 2017 sample set. At various stages in the preparation method, blanks were analyzed if there was potential for contamination. Ashed sand was used to ensure that the puck-mill and ball-mill were clean while powdering the 1994 and 2017 samples. Teflon boiling stones were used as blanks during the bitumen II extractions. The chromatogram in each of these blanks indicate that contamination was not introduced by the methods. Siloxanes, where are present in the m/z 74 ion chromatograms, are likely the result of compounds from the column of the GC. 152

Figure 3.14 Carbon isotope samples of the mats are grouped by their assigned taphonomic grade. As samples become less well-preserved, and more unrecognizable, the samples become with more enriched ¹³C. More data are required to support this trend. 153

INTRODUCTION

Early Diagenetic Silicification

Chert commonly occurs as bedded and nodular features and as infillings of cavities in sedimentary rocks. The ways in which chert form have changed over geologic time (Hesse, 1988; Knauth, 1994; Perry and Leticariu, 2007). In modern settings, chert formation occurs in the deep-sea where siliceous tests are concentrated. Siliceous tests, like those made by diatoms, radiolarians, and sponges, are composed of an amorphous silica phase that ultimately recrystallizes to more stable micro- and megaquartz phases (Maliva et al., 1989; Knauth, 1994). However, in the absence of these biogenic silica phases, Proterozoic chert deposits, which occur as nodules and lenses in peritidal carbonate environments (Maliva and Siever, 1989), represent the precipitation of silica phases from seawater saturated with respect to silica phases (Siever, 1962; Maliva and Siever, 1989; Maliva et al., 2005).

Proterozoic chert deposits preserve some of Earth's earliest microfossil assemblages and commonly contain exceptionally well preserved microbial components (Schopf, 1968; Awramik and Barghoorn, 1977; Horodyski and Donaldson, 1983; Nyberg and Schopf, 1984; Knoll et al., 1986; Southgate, 1986; Knoll et al., 1988; Hofmann and Jackson, 1991; Sergeev et al., 1995). Such preservation has prompted the astrobiology community to consider sedimentary silica deposits on Mars as potential targets for finding evidence of ancient life on Mars (Cady et al., 2003; McMahon et al., 2018). Based on petrographic observations of preserved microfossils (Schopf, 1968; Knoll and Barghoorn, 1975; Knoll, 1985; Bartley et al., 2000), observations of modern microbial communities (Decho, 1990; Wacey et al., 2010), actualistic studies of microbial degradation (Bartley, 1996), and artificial fossilization experiments (Oehler, 1976;

Westall et al., 1995), rapid precipitation of silica is required to halt heterotrophic decomposition of the organisms and preserve the variation in microbial morphologies, caused by taphonomic alteration, observed in these deposits.

Morphology alone can provide only limited information about ancient ecosystems. Geochemical data, including lipid biomarkers (Summons et al., 1999; Brocks and Summons, 2003; French et al., 2015), isotopic values (Kilburn and Wacey, 2011; Williford et al., 2013; Peng et al., 2016; Williford et al., 2016), elemental concentrations and chemistry (Lemelle et al., 2008; DeGregorio et al., 2009; Qu et al., 2015) and mineral phases (Benzerara and Menguy, 2009) that are associated with preserved microbial assemblages, can provide insight into the microbial metabolisms that were active at the time of silicification. Paleoenvironmental conditions can then be inferred from this data (Brocks et al., 2005; Ricci et al., 2014; Brocks et al., 2017; Gold et al., 2017; Schinteie and Brocks, 2017). To fully understand the extent to which ancient organisms are preserved, taphonomic variation of microfossils needs to be examined.

Overview of the Present Study

The study outlined in the following chapters was performed to better understand and constrain environments in which early diagenetic chert was deposited and to investigate the extent to which microbial organisms and communities are preserved by silicification. Exceptional preservation of microbial morphologies can be used to place constraints on the timing of silicification. Sheaths of filamentous microorganisms, as well as coccoidal envelopes with collapsed cellular material, are commonly preserved in early diagenetic chert samples. The morphologies of these microbial elements show evidence of having been altered by biologic decomposition. Documented changes in morphology include the discoloration of envelopes and sheaths, shrinking of sheaths and envelopes, cell collapse, fragmentation of the filaments,

nucleation/granulation of cellular contents, empty sheaths, and the reduction of cellular envelopes to an amorphous mass (c.f. Bartley, 1996). Much of the morphologic changes occur within 12-15 weeks (Bartley, 1996). Although preserved morphologic data is useful, to fully understand the processes that were active within the microbial community, and within the depositional environment organic geochemical data is required.

Only approximately 1% of organic matter is preserved in the rock record (Hayes et al., 1983; Brocks and Summons, 2003). Organic compounds, including nucleic acids, carbohydrates, and proteins, are rapidly remineralized in the environment (Tegelaar et al., 1989; Brocks and Summons, 2003; Arndt et al., 2013) and if these compounds escape remineralization, they are rarely preserved in the rock record. Instead, recalcitrant molecules, like lipids, accumulate in sediments and are more likely to be preserved (Hayes et al., 1983; Brocks and Summons, 2003). The degradation products of lipids, which are used to strengthen the cell wall (prokaryotes have hopanoids and eukaryotes have sterols), are identifiable in ancient samples. Some of these lipids are specific to certain organisms and can thus be used to identify microbial processes that were possibly active within that community.

Chapter One: Proterozoic microbial mats and their constraints on environments of silicification

This chapter describes a geochemical model created using published compositions of Proterozoic seawater to better understand the environment of silicification for microfossiliferous, early diagenetic chert. The model indicates which mineral phases are capable of precipitating at various pH and CO₂ concentrations, under evaporative conditions, and with the introduction of fresh water. The petrographic fabrics, preserved microfossils, and associated mineral phases in the silicified microbial mats of the Mesoproterozoic Bylot Supergroup placed constraints on

which fluid chemistries best reflect the fluids responsible for the precipitation of early diagenetic chert phases.

Chapter Two: Taphonomic variability in the 1.1 Ga microbial mats of the Angmaat Formation, Bylot Supergroup, Baffin Island

This chapter describes the preservation of the individual microfossils within the microfossil assemblages and microbial mat fabrics preserved in the Angmaat Formation early diagenetic chert deposits. A taphonomic assessment of the microfossils and overall mat fabric was preserved to describe the range of microbial taphonomy preserved in these chert samples. This chapter attempts to determine whether the visual identification of the overall mat taphonomy is reflected in the individual microfossils that make up the mat fabric. A new method for taphonomic assessment of thin sections using high-resolution image mosaics is also described.

Chapter Three: Geochemical Characterization of Preserved Lipids within Silicified Microbial Mats of the Angmaat Formation

This chapter investigates the extent to which the organisms are preserved in the silicified mats of the Angmaat Formation. Organic geochemistry techniques were used to determine whether organic compounds, i.e. lipids, were preserved in organisms entombed by rapidly precipitating mineral phases like early diagenetic chert. Preservation of organic compounds within the organic matter could be used to elucidate the microbial physiology and processes that were active at the time of silicification. New methods for sample preparation, which are meant to address potential contamination concerns and ensure that the organic material analyzed is indigenous to the rock, are also presented in this chapter.

References

- Arndt, S., Jørgensen, B. B., LaRowe, D. E., Middelburg, J. J., Pancost, R. D., and Regnier, P., 2013, Quantifying the degradation of organic matter in marine sediments: A review and synthesis: *Earth-Science Reviews*, v. 123, no. 0, p. 53-86.
- Awramik, S. M., and Barghoorn, E. S., 1977, The Gunflint microbiota: *Precambrian Research*, v. 5, no. 2, p. 121-142.
- Bartley, J., Knoll, A., P Grotzinger, J., and Sergeev, V., 2000, Lithification and fabric genesis in precipitated stromatolites and associated peritidal carbonates, Mesoproterozoic Billyakh Group, Siberia.
- Bartley, J. K., 1996, Actualistic Taphonomy of Cyanobacteria: Implications for the Precambrian Fossil Record: *PALAIOS*, v. 11, no. 6, p. 571-586.
- Benzerara, K., and Menguy, N., 2009, Looking for traces of life in minerals: *Comptes Rendus Palevol*, v. 8, no. 7, p. 617-628.
- Brocks, J. J., Jarrett, A. J. M., Sirantoine, E., Hallmann, C., Hoshino, Y., and Liyanage, T., 2017, The rise of algae in Cryogenian oceans and the emergence of animals: *Nature*, v. 548, no. 7669, p. 578-581.
- Brocks, J. J., Love, G. D., Summons, R. E., Knoll, A. H., Logan, G. A., and Bowden, S. A., 2005, Biomarker evidence for green and purple sulphur bacteria in a stratified Palaeoproterozoic sea: *Nature*, v. 437, no. 7060, p. 866-870.
- Brocks, J. J., and Summons, R. E., 2003, 8.03 - Sedimentary Hydrocarbons, Biomarkers for Early Life, *in* Turekian, H. D. H. K., ed., *Treatise on Geochemistry*: Oxford, Pergamon, p. 63-115.
- Cady, S. L., Farmer, J. D., Grotzinger, J. P., Schopf, J. W., and Steele, A., 2003, Morphological biosignatures and the search for life on Mars: *Astrobiology*, v. 3, no. 2, p. 351-368.
- Decho, A. W., 1990, Microbial Exopolymer Secretions in Ocean Environments: Their Role (s) in Food Webs and Marine Processes: *Oceanogr. Mar. Biol. Annu. Rev.*, v. 28, p. 73-153.
- DeGregorio, B. T., Sharp, T. G., Flynn, G., Wirick, S., and Hervig, R., L., 2009, Biogenic origin for Earth's oldest putative microfossils: *Geology*, v. 37, no. 7, p. 631-634.
- French, K. L., Hallmann, C., Hope, J. M., Schoon, P. L., Zumberge, J. A., Hoshino, Y., Peters, C. A., George, S. C., Love, G. D., Brocks, J. J., Buick, R., and Summons, R. E., 2015, Reappraisal of hydrocarbon biomarkers in Archean rocks: *Proceedings of the National Academy of Sciences*, v. 112, no. 19, p. 5915-5920.
- Gold, D. A., Caron, A., Fournier, G. P., and Summons, R. E., 2017, Paleoproterozoic sterol biosynthesis and the rise of oxygen: *Nature*, v. 543, no. 7645, p. 420-423.
- Hayes, J. M., Kaplan, I. R., and Wedeking, K. W., 1983, Precambrian organic geochemistry, preservation of the record, *in* Schopf, J. W., ed., *Earth's earliest biosphere: Its origin and evolution*: Princeton, NJ, Princeton University Press, p. 93-134.
- Hesse, R., 1988, Diagenesis #13. Origin of chert: *Diagenesis of biogenic siliceous sediments*: 1988.
- Hofmann, H. J., and Jackson, G. D., 1991, Shelf-Facies Microfossils from the Uluksan Group (Proterozoic Bylot Supergroup), Baffin Island, Canada: *Journal of Paleontology*, v. 65, no. 3, p. 361-382.
- Horodyski, R. J., and Donaldson, J. A., 1983, Distribution and Significance of Microfossils in Cherts of the Middle Proterozoic Dismal Lakes Group, District of Mackenzie, Northwest Territories, Canada: *Journal of Paleontology*, v. 57, no. 2, p. 271-288.

- Kilburn, M. R., and Wacey, D., 2011, Elemental and Isotopic Analysis by NanoSIMS: Insights for the Study of Stromatolites and Early Life on Earth, *in* Tewari, V., and Seckbach, J., eds., *STROMATOLITES: Interaction of Microbes with Sediments*: Dordrecht, Springer Netherlands, p. 463-493.
- Knauth, L. P., 1994, Petrogenesis of chert: *Reviews in Mineralogy and Geochemistry*, v. 29, no. 1, p. 233-258.
- Knoll, A. H., 1985, Exceptional Preservation of Photosynthetic Organisms in Silicified Carbonates and Silicified Peats: *Philosophical Transactions of the Royal Society B: Biological Sciences*, v. 311, no. 1148, p. 111-122.
- Knoll, A. H., and Barghoorn, E. S., 1975, Precambrian Eukaryotic Organisms: A Reassessment of the Evidence: *Science*, v. 190, no. 4209, p. 52-54.
- Knoll, A. H., Hayes, J. M., Kaufman, A. J., Swett, K., and Lambert, I. B., 1986, Secular variation in carbon isotope ratios from Upper Proterozoic successions of Svalbard and East Greenland: *Nature*, v. 321, no. 6073, p. 832-838.
- Knoll, A. H., Strother, P. K., and Rossi, S., 1988, Distribution and diagenesis of microfossils from the lower proterozoic duck creek dolomite, Western Australia: *Precambrian Research*, v. 38, no. 3, p. 257-279.
- Lemelle, L., Labrot, P., Salomé, M., Simionovici, A., Viso, M., and Westall, F., 2008, In situ imaging of organic sulfur in 700–800 My-old Neoproterozoic microfossils using X-ray spectromicroscopy at the S K-edge: *Organic Geochemistry*, v. 39, no. 2, p. 188-202.
- Maliva, R. G., Knoll, A. H., and Siever, R., 1989, Secular Change in Chert Distribution: A Reflection of Evolving Biological Participation in the Silica Cycle: *PALAIOS*, v. 4, no. 6, p. 519-532.
- Maliva, R. G., Knoll, A. H., and Simonson, B. M., 2005, Secular change in the Precambrian silica cycle: Insights from chert petrology: *Geological Society of America Bulletin*, v. 117, no. 7-8, p. 835-845.
- Maliva, R. G., and Siever, R., 1989, Nodular Chert Formation in Carbonate Rocks: *The Journal of Geology*, v. 97, no. 4, p. 421-433.
- McMahon, S., Bosak, T., Grotzinger, J. P., Milliken, R. E., Summons, R. E., Daye, M., Newman, S. A., Fraeman, A., Williford, K. H., and Briggs, D. E. G., 2018, A Field Guide to Finding Fossils on Mars: *Journal of Geophysical Research: Planets*, v. 0, no. 0.
- Nyberg, A. V., and Schopf, J. W., 1984, Microfossils in Stromatolitic Cherts from the Upper Proterozoic Min'yar Formation, Southern Ural Mountains, USSR: *Journal of Paleontology*, v. 58, no. 3, p. 738-772.
- Oehler, J. H., 1976, Experimental studies in Precambrian paleontology: Structural and chemical changes in blue-green algae during simulated fossilization in synthetic chert: *Geological Society of America Bulletin*, v. 87, no. 1, p. 117-129.
- Peng, X. T., Guo, Z. X., House, C. H., Chen, S., and Ta, K. W., 2016, SIMS and NanoSIMS analyses of well-preserved microfossils imply oxygen-producing photosynthesis in the Mesoproterozoic anoxic ocean: *Chemical Geology*, v. 441, p. 24-34.
- Perry, E. C., and Lefticariu, L., 2007, Formation and Geochemistry of Precambrian Cherts *in* Holland, H. D., Turekian, Karl K., ed., *Treatise on Geochemistry*: Oxford, Pergamon, p. 1-21.
- Qu, Y., Engdahl, A., Zhu, S., Vajda, V., and McLoughlin, N., 2015, Ultrastructural Heterogeneity of Carbonaceous Material in Ancient Cherts: Investigating Biosignature Origin and Preservation: *Astrobiology*, v. 15, no. 10, p. 825-842.

- Ricci, J. N., Coleman, M. L., Welander, P. V., Sessions, A. L., Summons, R. E., Spear, J. R., and Newman, D. K., 2014, Diverse capacity for 2-methylhopanoid production correlates with a specific ecological niche: *Isme Journal*, v. 8, no. 3, p. 675-684.
- Schinteie, R., and Brocks, J. J., 2017, Paleoecology of Neoproterozoic hypersaline environments: Biomarker evidence for haloarchaea, methanogens, and cyanobacteria: *Geobiology*, v. 15, no. 5, p. 641-663.
- Schopf, J. W., 1968, Microflora of the Bitter Springs Formation, Late Precambrian, Central Australia: *Journal of Paleontology*, v. 42, no. 3, p. 651-688.
- Sergeev, V. N., Knoll, A. H., and Grotzinger, J. P., 1995, Paleobiology of the Mesoproterozoic Billyakh Group, Anabar Uplift, Northern Siberia: *Memoir (The Paleontological Society)*, v. 39, no. 1, p. 1-37.
- Siever, R., 1962, Silica Solubility, 0°-200° C., and the Diagenesis of Siliceous Sediments: *The Journal of Geology*, v. 70, no. 2, p. 127-150.
- Southgate, P. N., 1986, Depositional environment and mechanism of preservation of microfossils, upper Proterozoic Bitter Springs Formation, Australia: *Geology*, v. 14, no. 8, p. 683-686.
- Summons, R. E., Jahnke, L. L., Hope, J. M., and Logan, G. A., 1999, 2-Methylhopanoids as biomarkers for cyanobacterial oxygenic photosynthesis: *Nature*, v. 400, no. 6744, p. 554-557.
- Tegelaar, E. W., de Leeuw, J. W., Derenne, S., and Largeau, C., 1989, A reappraisal of kerogen formation: *Geochimica et Cosmochimica Acta*, v. 53, no. 11, p. 3103-3106.
- Wacey, D., Gleeson, D., and Kilburn, M. R., 2010, Microbialite taphonomy and biogenicity: new insights from NanoSIMS: *Geobiology*, v. 8, no. 5, p. 403-416.
- Westall, F., Boni, L., and Guerzoni, E., 1995, The experimental silicification of microorganisms: *Palaeontology*, v. 38, no. 3, p. 495-528.
- Williford, K. H., Ushikubo, T., Lepot, K., Kitajima, K., Hallmann, C., Spicuzza, M. J., Kozdon, R., Eigenbrode, J. L., Summons, R. E., and Valley, J. W., 2016, Carbon and sulfur isotopic signatures of ancient life and environment at the microbial scale: Neoproterozoic shales and carbonates: *Geobiology*, v. 14, no. 2, p. 105-128.
- Williford, K. H., Ushikubo, T., Schopf, J. W., Lepot, K., Kitajima, K., and Valley, J. W., 2013, Preservation and detection of microstructural and taxonomic correlations in the carbon isotopic compositions of individual Precambrian microfossils: *Geochimica Et Cosmochimica Acta*, v. 104, p. 165-182.

CHAPTER 1
PROTEROZOIC MICROBIAL MATS AND THEIR CONSTRAINTS ON
ENVIRONMENTS OF SILICIFICATION

A version of this chapter was originally published by Ashley R. Manning-Berg and Linda C. Kah:

Ashley Manning-Berg and Linda C. Kah. "Proterozoic microbial mats and their constraints on environments of silicification." *Geobiology* 15 (2017): 469-483.

Using a PHREEQ-C model, I used published ion concentrations to model Proterozoic seawater chemistry. Modeled seawater compositions and brines were introduced to a modeled freshwater composition to see which mineral phases were able to precipitate out of solution. This article was reviewed by 3 anonymous reviewers and the editor of a special issue of *Geobiology*. The article was written by me. The co-author collected the samples that were used to compare preserved fabrics and mineralogy to the model results. Therefore, she helped me write the geologic background and clarify the discussion section of the paper. She also edited the article prior to submission.

Abstract

The occurrence of microfossiliferous, early diagenetic chert in Proterozoic successions is broadly restricted to peritidal marine environments. Such coastal environments are amongst the most environmentally variable of marine environments, experiencing both enhanced evaporation and potential influx of terrestrial fresh waters. To better understand potential conditions under which silicification occurs, we focus on microfossiliferous early diagenetic chert from the Mesoproterozoic Bylot Supergroup, northern Baffin Island. Spectacular preservation of silicified microbial mats, their associated mineral phases, and the petrographic fabrics of the chert itself require that silicification occurred at the sediment-water interface, penecontemporaneously with mat growth. In some cases, silica is the primary precipitated mineral phase, and is not associated with replacement of precursor mineral phases. In other cases, silica deposition includes the mimetic replacement of carbonate, gypsum, and halite mineral phases. These petrographic constraints suggest that silicification potentially occurred under a range of fluid chemistries associated with environmental variability in nearshore peritidal environments. Here we provide the first direct thermodynamic modeling of hypothetical Proterozoic seawater solutions, seawater-derived brines, and mixed seawater-freshwater solutions and demonstrate that peritidal

environments are capable of providing a wide range of fluid chemistries under which early diagenetic silica can both precipitate and replace primary mineralogical phases. Despite the thermodynamic potential for silica deposition under a wide range of fluid compositions, chert is not ubiquitous in Proterozoic environments, suggesting that the kinetics of silica polymerization exert a primary control over deposition.

Introduction

Authigenic quartz is abundant in sedimentary rocks, where it occurs as bedded to nodular features and as infillings of cavities. The origins of authigenic chert, however, remain uncertain, in part because, over geologic time, such phases represent a range of formation conditions (*see reviews in* Hesse, 1989; Knauth, 1994; Bustillo, 2010). Cenozoic and younger chert results primarily from the remobilization of amorphous silica (opal-A) from tests of planktonic organisms and its recrystallization to more stable microcrystalline quartz. Such chert typically occurs in the deep-sea—often beneath the carbonate compensation depth—where siliceous tests are most concentrated. Prior to the major evolutionary expansion of siliceous diatoms in the late Cretaceous (Finkle & Kotrc, 2010), chert deposition in the deep-sea was restricted to scarce radiolarian oozes (e.g., Dec et al., 1992; Ogg et al., 1992; Aitchison, 1998; Tolmacheva et al., 2001). More commonly, Paleozoic and Mesozoic chert is linked to carbonate shelf environments where opal-A is produced and concentrated by siliceous sponges (Clayton, 1986; Maliva et al., 1989).

By contrast, most Proterozoic authigenic chert occurs as nodules, lenses, and discontinuous thin beds within peritidal carbonate environments (Maliva et al., 1989; Maliva et al., 2005; Perry & Lefticariu, 2007). Peritidal chert deposits mark a substantial change in the environment of chert deposition and suggest critical differences in the mode of deposition. Prior

to the late Neoproterozoic evolution of silica-secreting sponges (cf. Brasier et al., 1997; Li et al., 1998; Love et al., 2009; Sperling et al., 2010), dissolved silica concentrations in seawater are estimated to have been 1.25–1.45 mM (Siever, 1992). This value is in sharp contrast to concentrations of 0.07 mM today (Treguer et al., 1995) and potentially allowed the direct precipitation of authigenic silica from seawater (Maliva et al., 2005; Maliva et al., 1989). Elevated dissolved silica concentrations, however, appear to have been insufficient to produce widespread precipitation of silica in marine environments. Current models for silica precipitation have therefore focused primarily on highly evaporative environments, where increased silica saturation are hypothesized to overcome kinetic inhibition to precipitation (Maliva et al., 2005; Perry & Lefticariu, 2007). Alternative models have focused on coastal mixing zones, where an influx of meteoric waters and associated changes in pH could have driven both dissolution of precursor mineral phases and chert deposition (Knauth, 1979; Knauth, 1994). Similarly, others have suggested the importance of microenvironments with variable redox conditions, wherein oxidation of organic matter (Maliva & Siever, 1989) or H₂S gas (Clayton, 1986; Xiao et al., 2010) would drive a decrease in pH, and promote both carbonate dissolution and silica precipitation.

Despite a number of potential scenarios in which silicification could occur, details of the silicification process remain understudied. For instance, the most detailed analysis of Proterozoic chert (Maliva et al., 2005) relies, in part, on a compilation of data from numerous basins (e.g., Horodyski and Donaldson, 1983; Knoll and Swett, 1984) to define parameters for silicification, and does not provide details on potential fluid chemistries. To better understand environments of silicification, here we document early diagenetic chert from a single basin—the Mesoproterozoic Bylot Supergroup, northern Baffin Island, Nunavut, Canada (cf. Kah & Knoll, 1996; Knoll et al.,

2013). Spectacular preservation of both microbial mats and their associated mineral phases, along with petrographic fabrics of the chert itself, allow us to define specific constraints on the timing and environmental conditions of silicification. We then combine petrographic constraints with published constraints on the composition of Proterozoic seawater, and use a series of thermodynamic chemical models, run with PHREEQC, to determine the extent to which the silicification process may have require modification of local fluids, such as through evaporation or mixing with fresh water.

Bylot Supergroup Chert

Geological setting and age of the Bylot Supergroup

The Bylot Supergroup contains more than 6 km of unmetamorphosed, and relatively undeformed Proterozoic sedimentary rock exposed within the fault-bounded Borden basin of northern Baffin and Bylot islands (Fig. 1.1) (Jackson & Iannelli, 1981; Kah & Knoll, 1996; Kah et al., 1999; Turner, 2009). Three stratigraphic groups—the Eقالulik Group, the Uluksan Group, and the Nunatsiaq Group—reflect overall basin development. The basal Eقالulik Group is marked by eruptive tholeiitic basalt flows that reflect initial rifting of the basin. These volcanic deposits are overlain by a broadly westward-deepening and fining-upward succession of fluvial to shallow-marine quartz arenite and marine shale (Jackson & Iannelli, 1981; Turner, 2009). The Uluksan Group conformably overlies marine shale of the upper Eقالulik Group and consists of a laterally extensive, yet heterogeneous, package of carbonate-dominated facies. In the lower Uluksan Group, peritidal microbial- and precipitate-dominated cycles and an associated oolitic shoal complex of the Angmaat Formation (formerly Society Cliffs Formation of Kah & Knoll, 1996; Kah et al., 1999, 2001) locally interfinger with conglomeratic and coarse-grained arenite near graben-bounding faults (Fabricious Fjord Formation; Jackson & Iannelli, 1981), fault-

controlled carbonate seep deposits of the Ikpiarjuk Formation (Hahn et al., 2015), shallow marine carbonate to siliciclastic cycles of the Iqqittuq Formation (Turner, 2009), and subtidal carbonate of the Nanisivik Formation (Turner, 2009). Heterogeneous strata of the lower Uluksan Group are then overlain, with local unconformity, by subtidal carbonate and carbonate reef development of the Victor Bay Formation (Narbonne & James, 1996; Sherman et al., 2001). A tectonically-driven reversal of basin polarity during deposition of the Victor Bay Formation (Sherman et al., 2002) led to erosional exposure of the western basin prior to deposition of the fluvial to marine siliciclastic lithologies of the Nunatsiaq Group.

Timing of sedimentation within the Bylot Supergroup is broadly constrained by U-Pb baddeleyite ages on basalts that both pre- and post-date sediment deposition. Tholeiitic flows near the base of the Bylot succession provide a maximum depositional age of 1270 ± 4 Ga (Le Cheminant & Heaman, 1989), and Franklinian-aged dikes that crosscut Bylot Supergroup strata provide a maximum age of ~ 723 Ma (Pehrsson & Buchan, 1999). Micropaleontological data from the Uluksan Group (Hofmann & Jackson, 1991, 1994) suggest that deposition occurred primarily within the Mesoproterozoic. Inference of a late Mesoproterozoic age is consistent with both carbon isotope stratigraphy that independently suggests an age between ~ 1250 and 1100 for Uluksan Group strata (Kah et al., 1999, 2012), and geochronological data for the Uluksan Group (1199 ± 24 Ma, whole rock Pb-Pb on carbonate; unpublished data in Kah et al., 2001) and uppermost strata of the underlying Eqalulik Group (1092 ± 59 Ma, whole rock U-Th-Pb on black shale; Turner & Kamber, 2012).

Chert facies and their interpretation

Within the Bylot Supergroup, chert facies occur predominantly in the lower Uluksan Group, and are most abundant east of Milne Inlet (Jackson & Ianelli, 1981; Hofmann &

Jackson, 1991; Kah & Knoll, 1996) in the Iqqituq and Angmaat formations. Chert within the Angmaat Formation occurs in a variety of colors, from black to grey, blue, brown, red, green, and white (Jackson & Iannelli, 1981). Various colored chert occurs largely as ovoid nodules that are commonly discordant to bedding (Jackson & Iannelli, 1981) and rarely preserve primary petrographic features, although a few, poorly preserved microbial fossils have been documented (Hofmann & Jackson, 1991). These cherts have been inferred to represent a late diagenetic phase of silicification. By contrast, black chert, which represents the most abundant chert, is inferred to be of early diagenetic origin based on ubiquitous microfossil preservation (Hoffman & Jackson, 1991; Kah & Knoll, 1996; Knoll et al., 2013). Black chert (Fig. 1.2) occurs as cm-scale irregular lenses and nodules, as well as semi-continuous beds up to 10 cm in thickness. These nodules and beds are typically conformable to bedding and reflect the morphology of primary sedimentary textures. In the field, black chert appears to most commonly occur within microbial facies, including stratiform microbial laminae, tufted microbial mats, and small domal stromatolites, while only rarely replacing isopachously laminated fabrics associated with carbonate seafloor precipitates. Tufted microbial mats, in particular, commonly display an alternation of black-and-white chert (cf. Fig. 1.2C) that reflects silicification of microbial elements by black chert and infilling of primary void space by chalcedony (cf. Knoll et al., 2013).

Constraints on timing of silicification

Individual microorganisms and microbial mat fabrics that occur within Angmaat Formation chert have been well documented (Hofmann & Jackson, 1991; Kah & Knoll, 1996; Knoll et al., 2013). Angmaat chert preserves various microbial mat communities across a range of peritidal environments, wherein filamentous communities dominate persistently subaqueous

subtidal environments and lower intertidal environments, and coccoidal communities, often with abundant extracellular polymeric substances (EPS) dominate more frequently exposed intertidal to supratidal environments (cf. Kah & Knoll, 1996; Knoll et al., 2013). These distinct microbial communities also show wide differences in the taphonomic state (i.e. the preserved morphology) of the microbial elements (cf. Horodyski et al., 1992; Bartley, 1996). Best-preserved coccoid-dominated mats record a variety of sheath morphologies intermixed with billowy masses interpreted as pockets of EPS (Fig. 1.3A). Best-preserved filament-dominated mat fabrics contain well-preserved microfossils that lack evidence of tearing, folding, or collapse of the microbial sheaths (Fig. 1.3C). In other cases, particularly within filament-dominated communities, microbial sheaths reveal various degrees of flattening upon compaction, ultimately leading to the loss of morphologically distinct mat elements (Fig. 1.3E). Preservation of these microbial elements provides uniquely strong evidence for penecontemporaneous silicification, because preserved organic constituents such as filamentous sheaths, coccoidal envelopes, and EPS decompose over short time scales. Whereas EPS can lose 30 – 50% of its associated carbon in only days (Decho et al., 2005), more robust sheaths can take weeks to months to become unrecognizable (Bartley, 1996). Observations of various taphonomic states also indicate that silicification occurred at or near the sediment-water interface, wherein silicification captured both the photosynthetic growth surface of microbial mats and zones of compaction, decomposition, and heterotrophic activity that occur in the lower portions of active microbial mats (cf. Stal et al., 1985; Van Gemerden, 1993). An interpretation of penecontemporaneous silicification is consistent with both experimental fossilization models, which show permineralization of biofilms initiated in as little as 24 hours (Toporsky et al., 2002) and stabilization of mineralized coatings over weeks to months (Newman et al., 2016). Early

silicification associated with microbial mats is also consistent with observed (Bennett & Siegel, 1987) and experimental data (see review in Coradin & Lopez, 2003) that suggest that organic complexing of silica, particularly by long chain organic molecules, such as polyamines, polysilines, and polyargenines, or hydroxyl groups associated with microbial biofilms, may play a critical role in enhancing polymerization and deposition of silica.

Constraints on nature of silicification

Petrographic relationships within early diagenetic chert also provide constraint on the nature of the silicification process. Many well preserved microbial mat fabrics (e.g., Fig. 1.3A, C) contain intact pockets of EPS or tightly woven microbial elements, wherein filament sheaths are in direct contact with each other with no evidence of interfilament mineral phases, such as carbonate or clay. These uncompacted mat fabrics are typically preserved in uniform, microcrystalline chert (Figs. 1.3B, D). Compacted filamentous mats similarly show no evidence of interfilament mineral phases (Fig. 1.3E), although chert often shows differences in crystal size that broadly correlate to the density of incorporated organic matter (Fig. 1.3F). Differences in crystal size within chert are similar to that observed in carbonate mineralization outside of the chert nodules, indicating that both silica and carbonate mineralization occurred during various stages of mat compaction. Additionally, similar thickness of laminae within silicified and unsilicified portions of the mat suggest that precipitation of these phases was penecontemporaneous. In fact, many of the preserved mat fabrics within Angmaat formation chert can be directly identified in adjacent carbonate (Knoll et al., 2013). Constructional voids (i.e. voids that are inferred to represent primary features present during mat growth) are also common within preserved microbial mat fabrics, some of which may represent gas bubbles (Knoll et al., 2013; cf. Bosak et al., 2010). These voids are associated with infill of chalcedony

(Fig. 1.4A, B) and, in some samples, with a combination of micritic carbonate, silicified micritic carbonate, and chalcedony (Fig. 1.4C). Combined, these observations suggest that silica is, in many cases, the primary mineral phase within microbial mats. Minor silicification of carbonate contained within constructional voids suggest that environments of silicification were, at least at times, incapable of the wholesale dissolution and replacement of associated carbonate.

In addition to silica as a primary mineral phase, microbial mats within the Angmaat Formation chert commonly contain evidence for the mimetic replacement of associated mineral phases, including detrital carbonate laminae (often containing clasts of microbial mat and individual torn filament sheaths), microlaminated sea floor precipitated carbonate, and lenticular gypsum (Fig. 1.5). Samples from elsewhere in the Angmaat Formation also record silicification of individual halite crystals that occurred without dissolution of surrounding gypsum (Fig. 3F in Kah et al., 2001). Combined, these observations require that early diagenetic silicification in the Angmaat Formation reflects a chemical environment (or range of chemical environments) capable of penecontemporaneous (primary) silica and carbonate deposition, dissolution of carbonate and replacement by silica, dissolution of gypsum and replacement by silica, and dissolution of halite (without dissolution of gypsum) and replacement by silica.

Constraints on regional environments of silicification

The ubiquity of microfossiliferous black chert in the Iqqituq and Angmaat formations, and in particular within the Angmaat Formation, suggests a relationship between the depositional environment and chert formation. Petrographic evidence for a variety of marine to hypersaline lithologies is consistent with interpretations of the depositional setting (cf. Kah, 2000; Kah et al., 2001; Turner, 2009). The Iqqituq Formation marks flooding of the Borden basin and initiation of cyclic carbonate deposition. Carbonate facies are represented by

stromatolitic and microbially laminated dolostone produced in inner ramp environments under predominantly normal-marine (Kah et al., 2001; Turner, 2009) to potentially more alkaline (Hahn et al., 2015) fluids. Inner ramp environments were prone to evaporation, as evidenced by evaporate nodules within microbially laminated dolostone, rare bedded gypsum, and cataclastic deposits interpreted as evaporate collapse breccias. Evaporation was most extensive during sea level lowstands, as evidenced by the capping of bedded gypsum deposits by progradation of terrigenous red shale. Chert occurs most commonly in microbially laminated facies and, only rarely, as small nodules within gypsum beds.

The transition to the Angmaat Formation is marked by initiation of an oolitic-intraclastic shoal west of Milne Inlet (Fig. 1.1) and a landward retreat of terrigenous facies. Exposure of the oolitic shoal during sea level lowstands resulted in formation of an evaporative lagoon dominated by a mosaic of low-relief domal stromatolites, thinly laminated microbial carbonate (often associated with small gypsum nodules), tufted microbial mats, and microlaminated seafloor cements (Kah, 2000; Kah et al., 2001; Knoll et al., 2013). Mosaic distribution of facies and the absence of clear meter-scale cycles in inner ramp facies suggest that these environments may have remained at least partially submerged even when the oolitic shoal complex was emergent (Kah, 2000), resulting in the potential for a wide variety of marine, evaporative marine, and mixed marine-fresh water fluid chemistries. Chert abundance increases dramatically within the Angmaat Formation, although notably only in facies eastward of the oolitic-intraclastic shoal, suggesting that silicification was directly linked to variable water chemistries within the inner ramp lagoon.

Modeling Chemical Environments of Silicification

Geologic and petrographic evidence suggests that early diagenetic silicification occurred penecontemporaneously with mat growth, and that silica was commonly the primary mineral phase. This demands that the process of silicification occurred at or near the sediment-water interface from ambient surface waters. The presence of penecontemporaneous carbonate and silica mineralization within microbial mats further indicates that at least some fluids may have been capable of simultaneously precipitating both silica and carbonate phases. The presence of penecontemporaneous primary silica and carbonate phases places a critical constraint on the geochemistry of the precipitating fluid, because alkaline pH conditions that most favor carbonate precipitation promote silica dissolution, while more acidic pH conditions that favor silica precipitation promote carbonate dissolution. Petrographic evidence that early diagenetic silica *also* replaced carbonate (including microlaminated precipitates whose morphology indicates an aragonitic origin; Kah & Knoll, 1996), gypsum, and halite mineral phases demands that at least some silica-bearing fluids were also capable of dissolving these various mineral phases. Mimetic (i.e., fabric retentive) preservation of these disparate mineral phases further indicates that the dissolution process that occurred during silicification was rate-limited, which suggests that fluids may have been close to the saturation state for these various mineral phases. When taken together, these constraints suggest that early diagenetic silicification in the Angmaat Formation may potentially represent a range of fluid chemistries, rather than a single fluid. In the following sections, we use geochemical modeling to explore the extent of possible modification of seawater within nearshore peritidal environments, and the potential role of seawater modification in the silicification process.

Constraints on Proterozoic seawater

An obvious limitation to modeling Proterozoic silicification environments is the availability of data regarding solute concentrations in Proterozoic seawater. As noted previously, in the absence of silica-secreting organisms, the concentration of dissolved silica (H_4SiO_4) in the oceans may have been near 1.4 mM (Siever, 1992), which is near the saturation state for amorphous silica (Opal-A). Fluid inclusion data can provide additional evidence of the concentrations of other critical ions (Knauth, 2005; Spear et al., 2014), although these data are rare for the Precambrian. A hypothetical Proterozoic seawater (Table 1) can be modeled from fluid inclusion data published by Spear et al. (2014). Data from Spear et al. (2014) are derived from halite deposits that are approximately 830 million years old and are therefore younger than the Mesoproterozoic conditions modeled here. Sulfate concentrations of these Neoproterozoic fluid inclusions closely match predicted concentrations of ~3 mM for the Mesoproterozoic from Kah et al. (2004) and were thus used for the model solutions. Note that such low sulfate concentrations result in a mineral evaporation sequence in which gypsum salinities are not reached until >90% evaporation, which results in gypsum and halite reaching saturation at approximately the same point. This is consistent with prior observations that suggest greater than 80% evaporation of seawater was required prior to gypsum deposition (Kah et al., 2001).

Other unconstrained parameters include the partial pressure of dissolved gasses CO_2 and O_2 , the pH of the ocean, and the temperature and salinity of the Proterozoic ocean. Values of pCO_2 proposed by Grotzinger & Kasting (1993) for Archean to Proterozoic time were used to construct Proterozoic seawater solutions (Fig. 6). Key assumptions made by these authors include a maximum value of 10^{22} g/mol of total carbon in the biosphere, and elevated pCO_2 to account for the lower solar flux. Elevated pCO_2 further results in elevated marine $[\text{HCO}_3^-]$, which was considered favorable in this model. Under conditions where $[\text{HCO}_3^-] > 2 [\text{Ca}^{2+}]$, gypsum is

limited by the availability of calcium, which has been proposed as an explanation for the paucity of gypsum in the Paleoproterozoic and Archean. Based on these assumptions, limits on the composition of the Precambrian ocean suggest that the pH range was between 5.7 and 8.6, with CO₂ values ranging from 0.03 – 3 atm (Grotzinger & Kasting, 1993). These values are consistent with earlier estimates of pCO₂ suggested by Kasting (1987), as well as a variety of independent estimates of pCO₂ for the Proterozoic (see Kaufman & Xiao, 2003; Kah & Bartley, 2004; Sheldon, 2006; Kah & Riding, 2007).

PHREEQC modeling

In order to explore the consequences of potential seawater modification on the silicification process, estimated Proterozoic seawater solutions were manipulated in PHREEQC (Parkhurst & Appelo, 1999). Five different pH and pCO₂ values (Grotzinger & Kasting, 1993) were selected and combined with major ion concentrations constrained from fluid inclusions (Spear et al., 2014). Maximum and minimum concentrations of Ca²⁺ were used because fluid inclusion data had established a potential range of concentration, resulting in 10 starting compositions. Model solutions were held at a constant temperature of 25°C and all major ion concentrations were held constant except for calcium and bicarbonate. HCO₃⁻ was modeled as equal to two times the concentration of calcium ions in the water (i.e., [HCO₃⁻] = 2[Ca²⁺]; represented by the black line on Fig. 6). Because the Angmaat Formation contains gypsum deposits, which require that [HCO₃⁻] < 2 [Ca²⁺], HCO₃⁻ values used in the models represent a maximum estimate for Mesoproterozoic seawater.

Each starting seawater solution was speciated using the SOLUTIONS block and treated as an open system by setting the solutions in equilibrium with pCO₂ using EQUILIBRIUM_PHASES. These solutions were then mixed with a freshwater solution modeled

from ion concentrations published by Fontes and Matray (1993). Incremental mixtures of potential seawater fluids and freshwater were modeled, ranging from 100% seawater and 0% freshwater to 0% seawater and 100% freshwater. Speciation of the resulting solution was performed, and mineral saturation indices calculated by PHREEQC (based on pH and changes in pH of the solution with changes in $p\text{CO}_2$) were used as indicators of which minerals would be likely to precipitate or dissolve. In order to account for potential evaporation of primary depositional fluids, the ten seawater solutions were also evaporated to a point at which gypsum was capable of precipitating using a forward model. Low sulfate concentrations used in this model result in gypsum and halite precipitating simultaneously upon evaporation. Evaporative brines were then incrementally mixed with freshwater. Saturation indices were again used as indicators of whether a mineral would likely precipitate or dissolve in the resulting solutions. All reactions were performed in PHREEQC using the wateq4f database which uses the Truesdell-Jones, or the extended Debye-Hückel equation to calculate activities. This database can be used for ionic strengths ranging from 0.1 to 2, thereby avoiding issues of the Debye-Hückel equation use in high ionic strength fluids.

Results and Interpretation of Geochemical Models

A total of 20 waters (10 non-evaporated seawaters and 10 brines) were produced using the ion concentrations of seawater from a Proterozoic fluid inclusion and varying $p\text{CO}_2$ concentrations and pH (Fig. 7). The first model mixes potential seawater compositions with freshwater, as might be expected in nearshore peritidal environments. The second model takes into account evidence for evaporation in the Angmaat Formation (cf. Kah et al., 2001) and starts with evaporative brines and mixes these brines with freshwater (Fig. 8). Results of these mixing

models are divided into four groups based on salinity and initial calcium concentrations and tabulated in Tables 1.2 and 1.3.

Group 1 solutions

Group 1 solutions (solutions 1, 3, 5, 7, 9) consist of unevaporated seawater solutions containing initial calcium concentrations of 9 mmol/kg (Table 1.2). For Group 1 solutions, carbonate phases (aragonite, calcite, and dolomite) did not precipitate in seawater solutions with a pH of <6.5 (solutions 1, 3). Even in solutions at pH 6.5 (solution 5), most carbonate phases did not precipitate. In seawater solutions with pH > 7 (solutions 7, 9), all carbonate phases were saturated in the initial solution. Aragonite was capable of precipitating until the model reached >30% freshwater, calcite saturation state was maintained until the model reached >40% input of freshwater, and the precipitation of dolomite was possible until the solution reached >20% freshwater. Three silica phases (chalcedony, opal-C, and quartz) were capable of precipitating in all mixing models, up to 100% freshwater. Solutions remained saturated with respect to silica gel until the solution was composed of 60% freshwater. Magadiite was able to precipitate in all Group 1 solutions until freshwater was introduced to the model. For all of the mixing models, amorphous silica (opal-A) remained undersaturated. Solution 3, which had an initial pCO₂ of 0.3 and pH of 6, was the only solution to become undersaturated with respect to amorphous silica when at a 30:70 seawater:freshwater ratio. As expected, the saturation indices for evaporite minerals (anhydrite, gypsum, and halite) were negative for initial unevaporated seawater solutions and their mixture with a freshwater solution.

Group 2 solutions

Group 2 solutions (solutions 2, 4, 6, 8, 10) consist of unevaporated seawater with initial calcium concentrations of 12 mmol/kg (Table 1.3). Potential seawater solutions with an initial pH

below 6.5 were unable to precipitate carbonate phases at any stage of mixing. These solutions were undersaturated with respect to carbonate phases but were saturated with respect to silica phases. Chalcedony, opal-C, and quartz saturation indices were positive in all solutions and mixing ratios. Solutions became undersaturated with respect to magadiite with >10% freshwater input; amorphous silica remained undersaturated in all solutions until models (as with Group 1 models); and silica gel remained saturated until mixtures reached >50% freshwater.

Group 3 solutions

Group 3 solutions (solutions 1, 3, 5, 7, 9) consist of seawater solutions containing initial calcium concentrations of 9 mmol/kg that were evaporated by forward modeling until gypsum saturation was reached, then incrementally mixed with freshwater (Table 1.2). Evaporation to gypsum saturation required removal of approximately 93% of the water volume, at which point all evaporate phases (anhydrite, gypsum, and halite) had positive saturation indices. With the addition any freshwater, however, all of the solutions become undersaturated with respect to evaporite phases. With the exception of solution 1, which was undersaturated with respect to aragonite in all mixing models, all Group 3 solutions were saturated with respect to carbonate phases, as well as chalcedony, opal-C, quartz, silica gel, magadiite, and amorphous silica, prior to freshwater mixing. With evaporation, all solutions are able to precipitate amorphous silica. Depending on the initial pH of the solution, aragonite was capable of precipitating until >10–60% freshwater input, calcite was capable of precipitating until >10–60% freshwater input, and dolomite was capable of precipitating until freshwater input of >30–70%. The saturation indices of chalcedony, opal-C, and quartz remained positive throughout the mixing models. Solutions were saturated with respect to silica gel until the addition of 70% freshwater.

Amorphous silica was capable of precipitating until 50% of the solution was composed of freshwater.

Group 4 solutions

Group 4 solutions (solutions 1, 3, 5, 7, 9) consist of seawater solutions containing initial calcium concentrations of 12 mmol/kg that were evaporated by forward modeling until gypsum saturation was reached, then incrementally mixed with freshwater (Table 1.3). Approximately 92% of the water in the modeled system was removed to reach gypsum salinity, at which point all evaporate phases (anhydrite, gypsum, and halite) were capable of precipitating. As with Group 3 solutions, the addition of any freshwater to the system causes the solution to become undersaturated with respect to evaporite. In terms of silica phases, magadiite becomes undersaturated when freshwater comprises 50–70% of the solution. For all initial solutions, fluids become undersaturated with respect to amorphous silica once seawater to freshwater ratios reach 50:50. Silica gel, however, remains saturated in all solutions until 70% freshwater compositions are reached.

Discussion

Fluid inclusion data for Proterozoic seawater and other published estimates of Proterozoic $p\text{CO}_2$, $p\text{O}_2$, and pH permit a detailed investigation of potential fluid compositions capable of the silicification of microbial mats and their associated mineral phases. By mixing several potential seawater solutions and seawater-derived brines with a freshwater solution to model mineral precipitation at the sediment-water interface, saturation indices of a variety of mineral phases can be compared to both extant and inferred mineralogies observed within Angmaat Formation chert. The pH and the initial amount of silica used in the model control the saturation indices for silica phases. Saturation of carbonate phases are controlled by the pH, and

the initial pCO₂ of the solution. A positive saturation index simply means that the phase is thermodynamically capable of precipitating; it does not guarantee precipitation of that mineral.

Fluids that best match petrographic constraints from Angmaat Formation chert should initially be saturated with respect to evaporite, carbonate, and silica phases. Constraints documented here are consistent with earlier descriptions of Meso- and Neoproterozoic chert fabrics that infer hypersalinity in environments of early diagenetic silicification (Horodyski & Donaldson, 1980; Knoll, 1985; Butterfield, 2001; Kah et al., 2001; Maliva et al., 2005; Knoll et al., 2013). The ubiquity of these interpretations lends support to arguments that conditions present in peritidal environments were required for silica deposition. Similarly, the broad restriction of early diagenetic chert to evaporative peritidal environments, and comparative absence in even open marine shallow water environments (cf. Hofmann & Jackson, 1981) suggests mixing of evaporative brines with freshwater as a critical precursor to silicification. Models presented here infer addition of fresh water as a mechanism for driving the pH changes necessary for dissolution of associated mineral phases (see also Knauth, 1994). A fresh water component is consistent, however with observations of silicified akinetes in a number of Mesoproterozoic successions (Sergeev et al., 1995; Tomitani et al., 2006; Sharma, 2006). Akinetes are resting cysts of cyanobacteria that are produced as a result of environmental stressors, like desiccation and fluctuating salinity, and are common in brackish water environments (Golubic et al., 1995; Sergeev et al., 1995; Tomitani et al., 2006).

Replication of the mineral phases and petrographic fabrics observed in early diagenetic chert of the Angmaat Formation further require a solution capable of (1) precipitation of silica as a primary depositional phase, (2) penecontemporaneous precipitation of primary carbonate and silica phases (or, similarly, precipitation of silica without dissolution of associated carbonate

phases), (3) replacement of halite by silica without dissolution of associated gypsum, (4) mimetic replacement of gypsum by silica, and (5) mimetic replacement of carbonate by silica. Changes in both saturation state and pH are key drivers in these modeled solutions. Introduction of freshwater into the system immediately promotes the dissolution of evaporite phases, and open-system re-equilibration of fluids under potentially elevated $p\text{CO}_2$ provides ample opportunity for fluctuation in pH. The elevated pH required to promote silica dissolution, however, was not reached in these models, which allowed all solutions to be saturated with respect to certain silica phases. Overall, model results indicate that chemical environments inherent to the Proterozoic (e.g., elevated silica concentrations, and elevated $p\text{CO}_2$), when combined with a model that requires silicification to occur at the sediment-water interface, offer a wide range of solutions capable of producing the mineralogy and textures observed within early diagenetic chert.

It must also be noted that solutions with high initial calcium concentrations also indicate the potential for magnesite as a primary carbonate phase. Although magnesite was not likely a common primary phase in the Angmaat Formation, earlier studies have demonstrated that dolomitization occurred very early in the depositional history of the Angmaat Formation (Kah, 2000). Mg/Ca ratios of 0.54–0.58 in the Angmaat Formation indicate that dolomitization was near-stoichiometric. Elevated Mg/Ca ratios of 0.68–0.78 in coeval strata of the Hunting Formation (Kah et al., 1999), however, may indicate the presence of a Mg-rich carbonate phase such as magnesite.

Ultimately, results of this model are in broad agreement with previous inferences regarding environments of silicification (Knauth, 1979; 1994; Maliva et al., 2005), and demonstrates that a wide range of initial seawater solutions are capable of the penecontemporaneous silicification. It is, however, unlikely that a single solution was

responsible for all of the variation observed in early diagenetic chert. The wide range of fluid chemistries capable of reproducing mineralogical phases observed in Angmaat Formation chert supports origination of early diagenetic chert as a continuum process within these environments.

Additional insight from geochemical models

Initial brine solutions best fit the conditions required to form penecontemporaneous carbonate and silica phases. Across nearly all pH values, seawater-derived brines were able to produce primary carbonate, evaporite (gypsum and halite) and silica phases. Furthermore, brines modeled were also capable of precipitating a range of initial silica phases, including chalcedony, quartz, amorphous silica (opal-A), opal-C, silica gel, and even Magadiite. Brine models were the only solutions capable of precipitating opal-A, remained saturated with respect to opal-C despite the addition of freshwater, and the saturation indices for silica gel remained positive until solutions are represented by as much as 70% freshwater.

The most soluble phases should always be the first to precipitate from solution; although Knauth (1979, 1994) suggests the potential of direct precipitation of microquartz from solutions that exceed 0.06 mM. Precipitation of amorphous and hydrated silica phases is also considered critical for the exceptional preservation of microfossils (Knoll, 1985). There remains, however, considerable difficulty in determining the primary phase of precipitated silica because post-depositional recrystallization (Williams et al., 1985) inhibits retention of primary depositional fabrics. The original phase of sedimentary-hosted authigenic chert has been variably inferred to be a silica gel (Oehler, 1976), opal-A or opal-CT (Wise et al., 1972), opal-CT (Maliva & Siever, 1988), or even Magadiite (Schubel & Simonson, 1990). Both the abundance of preserved microfossils in the Angmaat Formation and their preservation state is unusual (Knoll et al., 2013), and indicate that chert likely precipitated as either an amorphous silica phase or silica gel.

Under the alkaline conditions that characterize marine waters, silica is also capable of being incorporated into magnesium-silicate phases. Modeled mixtures with an initial pH >6.5, as well as all of the initial brine models were saturated with respect to sepiolite prior to freshwater mixing, with the exact percentage of fresh water mixing varying between 10–60% for each starting solution. Sepiolite, a hydrous magnesium silicate clay, is generally considered to be diagnostic of arid, alkaline environments, and is thus common in many restricted environments that also precipitate carbonate and sulfate phases (Wollast, 1968; Weaver, 1984; Singer, 1989). Precipitation of sepiolite is inhibited by the presence of aluminum, which further restricts the environment of formation to one with minimal siliciclastic influx (Wollast, 1968; Singer, 1989). It is reasonable to expect that model fluids would be supersaturated with respect to sepiolite as the model inputs do not consider aluminum. Brine mixtures are also saturated with respect to talc. Although talc is not common as a sedimentary mineral, it has been previously documented in Neoproterozoic carbonates (Tosca et al., 2011), and experimental data shows that a hydrated, talc-like mineral can precipitate from a silica- and magnesium-rich, low aluminum, saline solution with a pH of >8.7 (Tosca et al., 2011). Upon freshwater influx, however, these phases readily dissipate. Although Mg-silicate phases are capable of precipitating from model fluids, clay minerals have not been observed in Angmaat Formation peritidal chert. It is possible that sepiolite precipitated within the Angmaat Formation and was lost during fresh-water mixing.

Interestingly, our models also suggest magadiite as a possible silica phase. Magadiite, an amorphous sodium silicate phase, commonly precipitates in alkaline playa lakes (Hesse, 1989, Schubel & Simonson, 1990). While magadiite is commonly a precursor to chert (Eugster, 1969), and alkaline water chemistries have been suggested for the Borden Basin by Hahn et al. (2015),

the reticulate (Hay, 1968) and “toothpaste” (Eugster, 1969) textures associated with magadiite chert are inconsistent with preserved chert morphologies.

Despite the elevated silica saturation of the Proterozoic oceans that results in a range of potential crystalline and amorphous silica phases, early diagenetic chert is not ubiquitous in Proterozoic peritidal environments. This fundamental observation requires consideration of additional parameters that may have exerted control over polymerization of silica and its ultimate deposition. At low temperatures, rates of silica polymerization and deposition are generally slow (Krauskopf, 1956; Coradin & Lopez, 2003). Silica polymerization, wherein silica monomers link together to form a siloxane (Si-O-Si) bond, is additionally strongly pH dependent, and is generally greatest at a pH between 6 and 9 (Rothbaum & Rohde, 1979; Coradin & Lopez, 2003). As polymerization continues, silica gels develop. Rate of gel formation also increases with elevated salinities (Rothbaum & Rohde, 1979). Together, these observations suggest that enhanced evaporation in peritidal environments may, by themselves, promote polymerization of silica.

Polymerization of silica in peritidal environments may also be enhanced by biological activity within mat substrates. Experimental investigation of microbes common in siliceous hot springs (cf. Phoenix et al., 2002; Yee et al., 2003; Lalonde et al., 2005) suggest that the activation energy that inhibits silica precipitation can be reduced in the presence of microbial surfaces. Reactive sites on the microbial surface, specifically associated with the amine (Kuno et al., 2011), hydroxyl (Lalonde et al., 2005), and carboxyl functional groups (Westall, 1995; Renaut & Jones, 2000) create charged surfaces that decrease the energy barrier to silica precipitation. Precipitation in these cases, however, is restricted to external coatings on microorganisms. It is not apparent to what extent such charged surfaces contribute to the

through-going permineralization observed in many Proterozoic microfossiliferous cherts. By contrast to the direct binding of silica to organic surfaces, organic acids associated with microbial decomposition have been shown to complex silica (Bennet & Siegel, 1987). The range of microbial taphonomy preserved within Angmaat Formation chert indicates that organic acids would have been present within environments of silicification. Concentration of silica through organic acid complexes may have played a critical role in promoting polymerization of silica in these environments.

Conclusions

Petrographic relationships within early diagenetic chert provide constraint on the silicification process. Well-preserved microbial mat fabrics generally lack evidence of interfilament carbonate, and associated voids are infilled by chalcedony, indicating that silica is the primary mineral phase responsible for the preservation of the microbial mats. Elements of microbial fabrics can also be identified in adjacent primary carbonate phases. Detrital carbonate laminae, microlaminated sea floor carbonate precipitates, lenticular gypsum, and silicified halite crystals are also mimetically preserved within early diagenetic chert of the Angmaat Formation. These observations require that early diagenetic chert formed in a range of chemical environments that were able to precipitate primary silica and carbonate phases, dissolve and replace carbonate phases with silica, and replace gypsum and halite without dissolving all of the gypsum.

Constraints placed on Proterozoic seawater, including major ion composition, pH, and $p\text{CO}_2$, were used to produce a geochemical model of potential seawater solutions for the Meso- and Neoproterozoic. These seawater solutions, and associated seawater-derived brines were mixed with a model freshwater within an open-system surface environment to determine which

mineral phases were thermodynamically able to precipitate. The geochemical model presented here, tests the hypothesis of Maliva et al. (2005) that Proterozoic peritidal chert precipitated directly from seawater in marginal marine environments where evaporation was likely to occur. All models were able to precipitate the amorphous silica phase opal-C and silica gel, evaporation, however, was required to produce solutions that were saturated with respect to sulfate and carbonate phases. Evaporative brines were also able to precipitate opal-A as an additional amorphous phase. Model solutions were further constrained by mineralogy and textures preserved within early diagenetic chert. Results suggests that silicification cannot be constrained to a single fluid type, and that silicification likely represents a continuum of processes in chemically variable, peritidal environments. Furthermore, despite the thermodynamic potential for silica deposition, the general scarcity of chert in Proterozoic environments suggests that the kinetics of silica polymerization—potentially driven by organic productivity and decomposition—exert a primary control over chert deposition.

Acknowledgements

Field work was supported by a National Geographic Society Grant 5304-94 (to LCK) and logistical support from the Polar Continental Shelf Project. The authors would like to thank A.S. Engel at the University of Tennessee for initial review of this project and for helpful discussions. We would also like to thank J.D. Schiffbauer and the three anonymous reviewers for their thoughtful reviews that greatly improved the clarity of this manuscript.

References

- Aitchison, J. C., Flood, P. G., and Malpas, J., (1998), Lowermost Ordovician (basal Tremadoc) radiolarians from the Little Port Complex, western Newfoundland: *Geological Magazine*, v. 135, no. 03, p. 413-419.
- Bennett, P., and Siegel, D., (1987), Increased solubility of quartz in water due to complexing by organic compounds
- Bartley JK (1996) Actualistic taphonomy of cyanobacteria: implications for the Precambrian fossil record. *Palaios*, **11**, 571-586.
- Bosak, T., Bush, J., Flynn, M., Liang, B., Ono, S., Petroff, A., and Sim, M., (2010), Formation and stability of oxygen-rich bubbles that shape photosynthetic mats: *Geobiology*, v. 8, no. 1, p. 45-55.
- Brasier, M., Green, O., and Shields, G., (1997), Ediacarian sponge spicule clusters from southwestern Mongolia and the origins of the Cambrian fauna: *Geology*, v. 25, no. 4, p. 303-306.
- Bustillo MA (2010) Silicification of continental carbonates. *Developments in Sedimentology*, **62**, 153-178.
- Butterfield NJ (2001) Paleobiology of the late Mesoproterozoic (ca. 1200 Ma) hunting formation, Somerset Island, arctic Canada. *Precambrian Research*, **111**, 235-256.
- Clayton CJ (1986) *The Chemical environment of flint formation in Upper Cretaceous chalks*, Cambridge University Press.
- Coradin, T., and Lopez, P. J., (2003), Biogenic silica patterning: simple chemistry or subtle biology?: *ChemBioChem*, v. 4, no. 4, p. 251-259.
- Dec, T., Swinden, H., and Floyd, J., (1992), Sedimentological, geochemical, and sediment provenance constraints on stratigraphy and depositional setting of the Strong Island Chert (Exploits Subzone, Notre Dame Bay): *Curt. Res. Newf. Dep. Mines Energy, Geol. Surv. Branch, Rep*, p. 92-91.
- Decho AW, Visscher PT, Reid RP (2005) Production and cycling of natural microbial exopolymers (EPS) within a marine stromatolite. *Palaeogeography, Palaeoclimatology, Palaeoecology*, **219**, 71-86.
- Eugster H (1969) Inorganic bedded cherts from the Magadi area, Kenya. *Contributions to Mineralogy and Petrology*, **22**, 1-31.
- Finkel, Z. V., and Kotrc, B., (2010), Silica use through time: macroevolutionary change in the morphology of the diatom fustule: *Geomicrobiology Journal*, v. 27, no. 6-7, p. 596-608.
- Fontes JC, Matray JM (1993) Geochemistry and origin of formation brines from the Paris Basin, France: Brines associated with Triassic Salts. *Chemical Geology*, **109**, 149-175.
- Golubic, S., Sergeev, V. N., and Knoll, A. H., (1995), Mesoproterozoic Archaeoellipsoides: akinetes of heterocystous cyanobacteria: *Lethaia*, v. 28, no. 4, p. 285-298.
- Grotzinger JP, Kasting JF (1993) New constraints on Precambrian ocean composition. *The Journal of Geology*, 235-243.
- Hahn KE, Turner EC, Babechuk MG, Kamber BS (2015) Deep-water seep-related carbonate mounds in a Mesoproterozoic alkaline lake, Borden Basin (Nunavut, Canada). *Precambrian Research*, **271**, 173-197.
- Hay RL (1968) Chert and its sodium-silicate precursors in sodium-carbonate lakes of East Africa. *Contributions to Mineralogy and Petrology*, **17**, 255-274.

- Hesse R (1989) Silica diagenesis: origin of inorganic and replacement cherts. *Earth-Science Reviews*, **26**, 253-284.
- Hofmann HJ, Jackson GD (1991) Shelf-facies microfossils from the Uluksan Group (Proterozoic Bylot Supergroup), Baffin Island, Canada. *Journal of Paleontology*, **65**, 361-381.
- Hofmann HJ, Jackson GD (1994) Shale-facies microfossils from the Proterozoic Bylot Supergroup, Baffin Island, Canada. *Journal of Paleontology*, **68**, S1-S39.
- Horodyski RJ, Donaldson JA (1983) Distribution and significance of microfossils in cherts of the middle Proterozoic Dismal Lakes Group, District of Mackenzie, Northwest Territories, Canada. *Journal of Paleontology*, 271-288.
- Jackson G, Iannelli T (1981) Rift-related cyclic sedimentation in the Neohelikian Borden Basin, northern Baffin Island. *Geological Survey of Canada, Paper*, 81-10.
- Horodyski R, Bauld J, Lipps J, Mendelson C (1992) Preservation of prokaryotes and organic-walled and calcareous and siliceous protists. *The Proterozoic Biosphere*, 185-192.
- Horodyski RJ, Donaldson JA (1980) Microfossils from the Middle Proterozoic Dismal Lakes Groups, Arctic Canada. *Precambrian Research*, **11**, 125-159.
- Kah LC (2000) Depositional $\delta^{18}\text{O}$ signatures in Proterozoic dolostones: constraints on seawater chemistry and early diagenesis. *SEPM Special Publication*, **67**, 345-360.
- Kah, L. C., Bartley, J. K., and Teal, D. A., (2012), Chemostratigraphy of the Late Mesoproterozoic Atar Group, Taoudeni Basin, Mauritania: Muted isotopic variability, facies correlation, and global isotopic trends: *Precambrian Research*, v. 200–203, no. 0, p. 82-103.
- Kah LC, Knoll AH (1996) Microbenthic distribution of Proterozoic tidal flats: Environmental and taphonomic considerations. *Geology*, **24**, 79-82.
- Kah LC, Sherman AG, Narbonne GM, Knoll AH, Kaufman AJ (1999) $\delta^{13}\text{C}$ stratigraphy of the Proterozoic Bylot Supergroup, Baffin Island, Canada: implications for regional lithostratigraphic correlations. *Canadian Journal of Earth Sciences*, **36**, 313-332.
- Kah LC, Lyons TW, Chesley JT (2001) Geochemistry of a 1.2 Ga carbonate-evaporite succession, northern Baffin and Bylot Islands: implications for Mesoproterozoic marine evolution. *Precambrian Research*, **111**, 203-234.
- Kah LC, Lyons TW, Frank TD (2004) Low marine sulphate and protracted oxygenation of the Proterozoic biosphere. *Nature*, **431**, 834-838.
- Kah LC, Riding R (2007) Mesoproterozoic carbon dioxide levels inferred from calcified cyanobacteria. *Geology*, **35**, 799-802.
- Kasting JF (1987) Theoretical constraints on oxygen and carbon dioxide concentrations in the Precambrian atmosphere. *Precambrian Research*, **34**, 205-229.
- Kaufman AJ, Xiao S (2003) High CO₂ levels in the Proterozoic atmosphere estimated from analyses of individual microfossils. *Nature*, **425**, 279-282.
- Knauth LP (1979) A model for the origin of chert in limestone. *Geology*, **7**, 274-277.
- Knauth LP (1994) Petrogenesis of chert. *Reviews in Mineralogy and Geochemistry*, **29**, 233-258.
- Knauth LP (2005) Temperature and salinity history of the Precambrian ocean: implications for the course of microbial evolution. *Palaeogeography, Palaeoclimatology, Palaeoecology*, **219**, 53-69.
- Knoll A, Swett K (1989) Carbonate deposition during the late Proterozoic Era: an example from Spitsbergen. *American Journal of Science*, **290**, 104-132.

- Knoll AH (1985) Exceptional Preservation of Photosynthetic Organisms in Silicified Carbonates and Silicified Peats. *Philosophical Transactions of the Royal Society, Biological Sciences*, **311**, 111-122.
- Knoll AH, Wörndle S, Kah LC (2013) Covariance of microfossil assemblages and microbialite textures across an upper Mesoproterozoic carbonate platform. *Palaios*, **28**, 453-470.
- Krauskopf KB (1956) Dissolution and precipitation of silica at low temperatures. *Geochimica et Cosmochimica Acta*, **10**, 1-26.
- Kuno T, Nonoyama T, Hirao K, Kato K (2011) Influence of the charge relay effect on the silanol condensation reaction as a model for silica biomineralization. *Langmuir*, **27**, 13154-13158.
- Lalonde SV, Konhauser KO, Reysenbach AL, Ferris FG (2005) The experimental silicification of Aquificales and their role in hot spring sinter formation. *Geobiology*, **3**, 41-52.
- LeCheminant AN, Heaman LM (1989) Mackenzie igneous events, Canada: Middle Proterozoic hotspot magmatism associated with ocean opening. *Earth and Planetary Science Letters*, **96**, 38-48.
- Li C-W, Chen J-Y, Hua T-E (1998) Precambrian Sponges with Cellular Structures. *Science*, **279**, 879-882.
- Love GD, Grosjean E, Stalvies C, Fike DA, Grotzinger JP, Bradley AS, Kelly AE, Bhatia M, Meredith W, Snape CE (2009) Fossil steroids record the appearance of Demospongiae during the Cryogenian period. *Nature*, **457**, 718-721.
- Maliva RG, Siever R (1989) Nodular Chert Formation in Carbonate Rocks. *The Journal of Geology*, **97**, 421-433.
- Maliva RG, Knoll AH, Siever R (1989) Secular Change in Chert Distribution: A Reflection of Evolving Biological Participation in the Silica Cycle. *PALAIOS*, **4**, 519-532.
- Maliva RG, Knoll AH, Simonson BM (2005) Secular change in the Precambrian silica cycle: Insights from chert petrology. *Geological Society of America Bulletin*, **117**, 835-845.
- Narbonne GM, James NP (1996) Mesoproterozoic deep-water reefs from Borden Peninsula, Arctic Canada. *Sedimentology*, **43**, 827-848.
- Oehler JH (1976) Experimental studies in Precambrian paleontology: Structural and chemical changes in blue-green algae during simulated fossilization in synthetic chert. *Geological Society of America Bulletin*, **87**, 117-129
- Ogg JG, Karl SM, Behl RJ (1992) 32. Jurassic through Early Cretaceous sedimentation history of the Central Equatorial Pacific and of Sites 800 and 801. In: *Proceedings of the Ocean Drilling Program, Scientific Results*, pp. 571-613.
- Parkhurst DL, Appelo C (1999) User's guide to PHREEQC (Version 2): A computer program for speciation, batch-reaction, one-dimensional transport, and inverse geochemical calculations.
- Pehrsson SJ, Buchan KL (1999) Borden dykes of Baffin Island, NWT: A Franklin U-Pb Baddeleyite age and a paleomagnetic interpretation. *Canadian Journal of Earth Sciences*, **36**, 65-73.
- Perry EC, Leticariu L (2007) Formation and Geochemistry of Precambrian Cherts. In: *Treatise on Geochemistry*, pp. V. 7, p. 1-21.
- Phoenix VR, Adams DG, Konhauser KO (2000) Cyanobacterial viability during hydrothermal biomineralisation. *Chemical Geology*, **169**, 329-338.
- Renaut RW, Jones B (2000) Microbial precipitates around continental hot springs and geysers. In: *Microbial sediments*. Springer, pp. 187-195.

- Rothbaum H, Rohde A (1979) Kinetics of silica polymerization and deposition from dilute solutions between 5 and 180 C. *Journal of Colloid and Interface Science*, **71**, 533-559.
- Sergeev VN, Knoll AH, Grotzinger JP (1995) Paleobiology of the Mesoproterozoic Billyakh Group, Anabar Uplift, Northern Siberia. *Memoir (The Paleontological Society)*, 1-37.
- Sharma M (2006) Small-sized akinetes from the Mesoproterozoic Salkhan Limestone, Semri Group, Bihar, India. *J. Palaeontol. Soc. India*, **51**, 109-118.
- Schubel KA, Simonson BM (1990) Petrography and diagenesis of cherts from Lake Magadi, Kenya. *Journal of Sedimentary Research*, **60**.
- Sheldon ND (2006) Precambrian paleosols and atmospheric CO₂ levels. *Precambrian Research*, **147**, 148-155.
- Sherman AG, Narbonne GM, James JP (2001) Anatomy of a cyclically packaged Mesoproterozoic carbonate ramp in northern Canada. *Sedimentary Geology*, **139**, 171-203.
- Sherman AG, Hames NP, Narbonne GM (2002) Evidence for reversal of basin polarity during carbonate ramp development in the Mesoproterozoic Borden Basin, Baffin Island. *Canadian Journal of Earth Sciences*, **39**, 519-538.
- Siever R (1992) The silica cycle in the Precambrian. *Geochimica et Cosmochimica Acta*, **56**, 3265-3272.
- Singer A (1989) Palygorskite and sepiolite group minerals. *Minerals in soil environments*, 829-872.
- Spear N, Holland H, Garcia-Veigas J, Lowenstein T, Giegegack R, Peters H (2014) Analyses of fluid inclusions in Neoproterozoic marine halite provide oldest measurement of seawater chemistry. *Geology*, **42**, 103-106.
- Sperling E, Robinson J, Pisani D, Peterson K (2010) Where's the glass? Biomarkers, molecular clocks, and microRNAs suggest a 200-Myr missing Precambrian fossil record of siliceous sponge spicules. *Geobiology*, **8**, 24-36.
- Stal LJ, van Gemerden H, Krumbein WE (1985) Structure and development of a benthic microbial mat. *FEMS Microbiology Ecology*, **31**, 111-125.
- Tolmacheva TJ, Danelian T, Popov LE (2001) Evidence for 15 my of continuous deep-sea biogenic siliceous sedimentation in early Paleozoic oceans. *Geology*, **29**, 755-758.
- Tomitani A, Knoll AH, Cavanaugh CM, Ohno T (2006) The evolutionary diversification of cyanobacteria: Molecular-phylogenetic and paleontological perspectives. *Proceedings of the National Academy of Sciences*, **103**, 5442-5447.
- Toporski JK, Steele A, Westall F, Thomas-Keprta KL, McKay DS (2002) The simulated silicification of bacteria-New clues to the modes and timing of bacterial preservation and implications for the search for extraterrestrial microfossils. *Astrobiology*, **2**, 1-26.
- Tosca NJ, Macdonald FA, Strauss JV, Johnston DT, Knoll AH (2011) Sedimentary talc in Neoproterozoic carbonate successions. *Earth and Planetary Science Letters*, **306**, 11-22.
- Treguer P, Demaster DJ, Leynaert A, Queguiner B (1995) The silica balance in the world ocean: a reestimate. *Science*, **268**, 375-379.
- Turner EC (2009) Mesoproterozoic carbonate systems in the Borden Basin, Nunavut. *Canadian Journal of Earth Sciences*, **46**, 915-938.
- Turner EC, Kamber BS (2012). Arctic Bay Formation, Borden Basin, Nunavut (Canada): Basin evolution, black shale, and dissolved metal systematics in the Mesoproterozoic ocean. *Precambrian Research*, **208**, 1-18.
- Van Gemerden H (1993) Microbial mats: a joint venture. *Marine Geology*, **113**, 3-25.

- Weaver CE (1984) Origin and geologic implications of the palygorskite deposits of the SE United States. *Palygorskite-Sepiolite: Occurrences, Genesis, and Uses*, **37**, 39-58.
- Westall F, Boni L, Guerzoni E (1995) The experimental silicification of microorganisms. *Palaeontology*, **38**, 495-528.
- Williams LA, Parks GA, Crerar DA (1985) Silica diagenesis; I, Solubility controls. *Journal of Sedimentary Research*, **55**, 301-311.
- Wise SW, Buie BF, Weaver FM (1972) Chemically precipitated sedimentary cristobalite and the origin of chert. *Eclogae Geol. Helv*, **65**, 157-163.
- Wollast R, Mackenzie, F.T., Bricker, O.P. (1968) Experimental precipitation and genesis of sepiolite at Earth-surface conditions. *American Mineralogist*, **53**, 1645-1662.
- Xiao, S., Schiffbauer, J.D., McFadden, K.A., Hunter, J. (2010) Petrographic and SIMS pyrite sulfur isotope analyses of Ediacaran chert nodules: Implications for microbial processes in pyrite rim formation, silicification, and exceptional fossil preservation. *Earth and Planetary Science Letters*, **297**, 481-495.
- Yee N, Phoenix VR, Konhauser KO, Benning LG, Ferris FG (2003) The effect of cyanobacteria on silica precipitation at neutral pH: implications for bacterial silicification in geothermal hot springs. *Chemical Geology*, **199**, 83-90.

Appendix

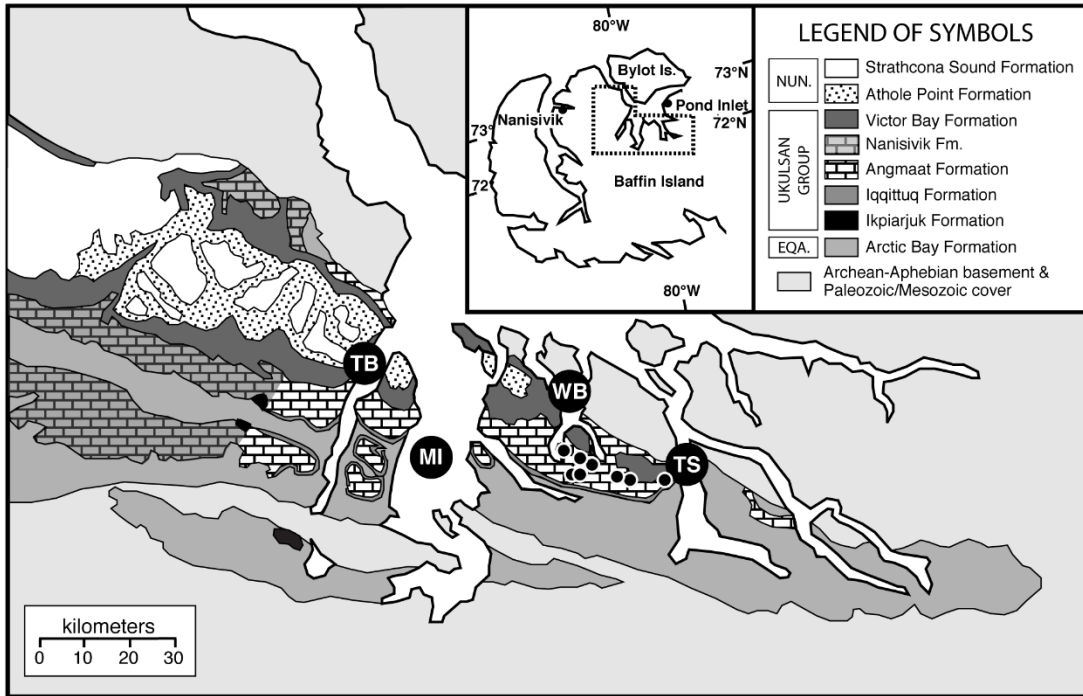


Figure 1.1. Simplified geologic map of the Bylot Supergroup within the Milne Inlet graben (modified from Knoll et al., 2013), showing locations of strata of the Eqalulik (EQA), Uluksan, and Nunatsiaq (NUN) groups. The Iqqittuq and Angmaat formations range from Tay Sound (TS) in the east to just west of Tremblay Sound (TB) in the west. The Angmaat Formation west of Milne Inlet (MI) is dominated by oolitic-intraclastic shoal deposits. Black chert is most common between White Bay (WB) and Tay Sound (TS). Small black circles show localities from which early diagenetic chert samples were collected from the Angmaat Formation.

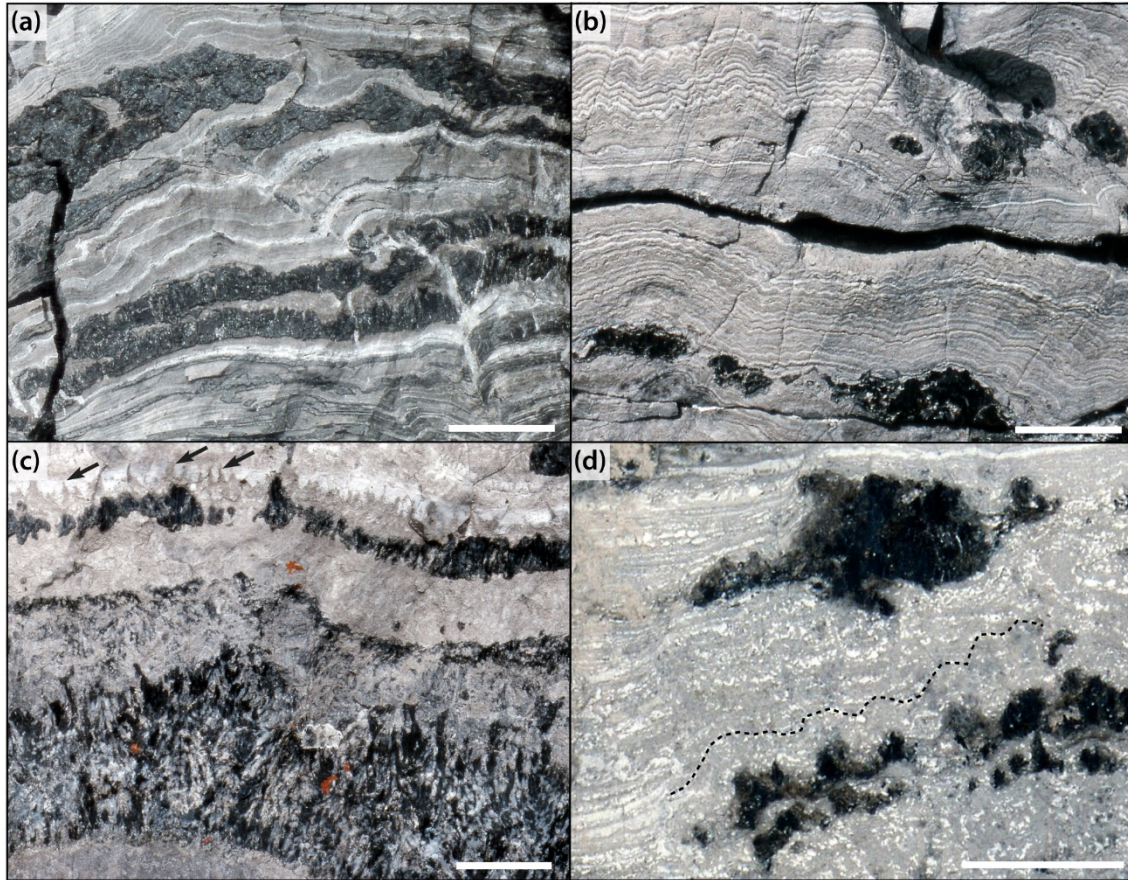


Figure 1.2 Patterns of early diagenetic chert in the Angmaat Formation. (a) Lensoidal to bedded black chert within irregular, low-relief microbial facies. White laminae represent storm-deposited micrite drapes. (b) Nodular black chert within microlaminated carbonate precipitate facies. Within precipitate facies, chert is often centered around rare microbial facies that are marked by development of depositional relief on the substrate. (c) Early diagenetic chert within tufted microbial facies. Microbial tufts draped by white micrite are marked by black arrows. Alternation of black and white chert in the lower part of the image represents silicification of original organic material and primary void space (*see* Knoll et al., 2013). (d) Nodular black chert within tufted microbialite facies. Grey carbonate represents stacked microbial tufts (*see* Fig. 1.2C) and white represents the partial draping of surface topography by white micrite. Note that chert nodules track the primary morphology of mat laminae (dotted line). Scale bar is 10 cm in (a) and 2 cm in (b), (c), and (d).

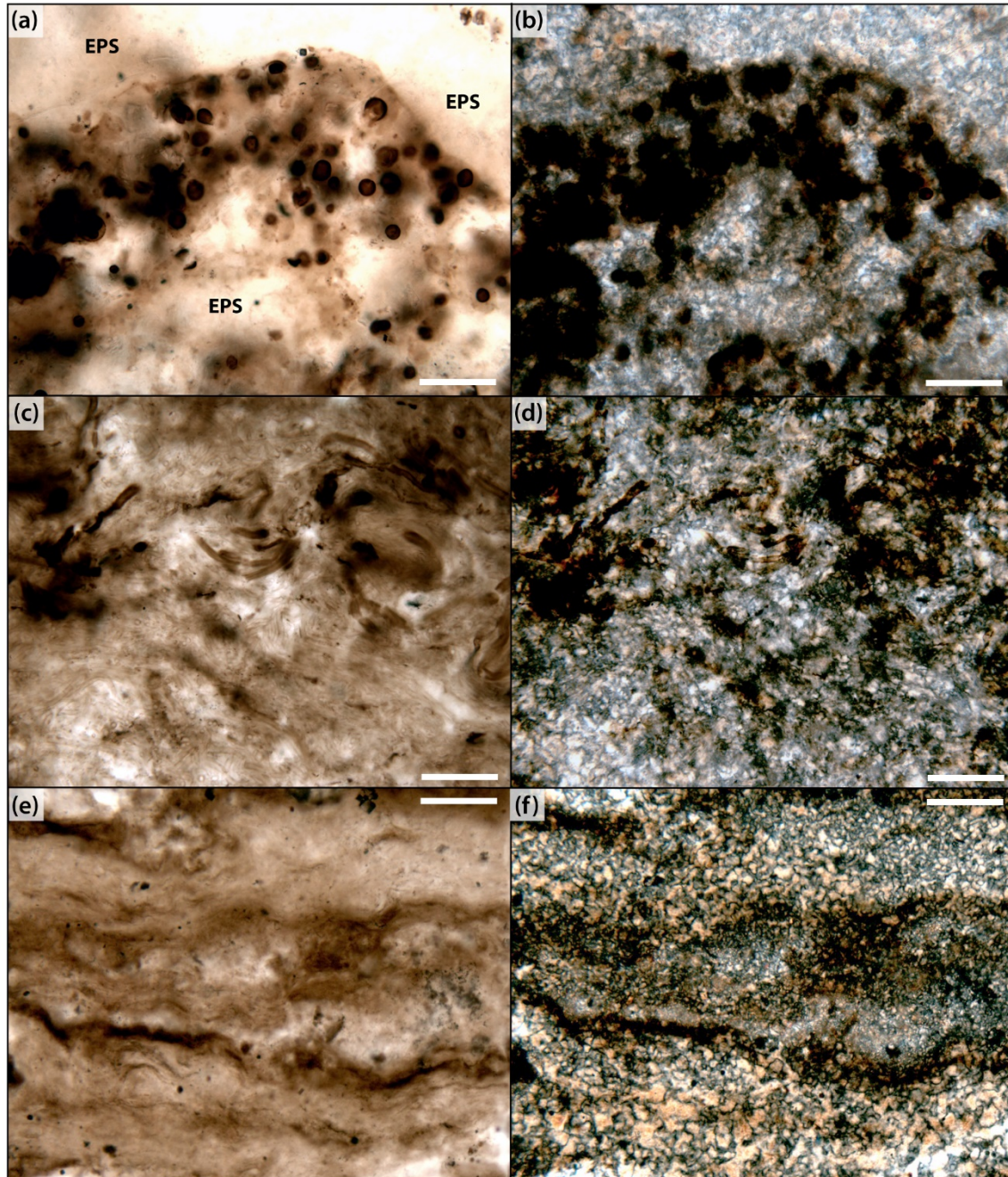


Figure 1.3. Common microbial mat fabrics within Angmaat Formation chert. (a) Coccoid-dominated mat showing concentrations of coccoidal sheaths surrounded by pale regions interpreted as pockets of EPS. (b) Coccoid-dominated mat in crossed-polars. (c) Tightly woven filament-dominated mat consisting primarily of *Siphonophycus inornatum* (thin filaments) and *Eomicrocoleus crassus* (thick filaments) (cf. Knoll et al., 2013); contact between adjacent filament sheaths suggest that the primary mat contained no mineral constituents. (d) Filament-dominated mat in crossed-polars. (e)

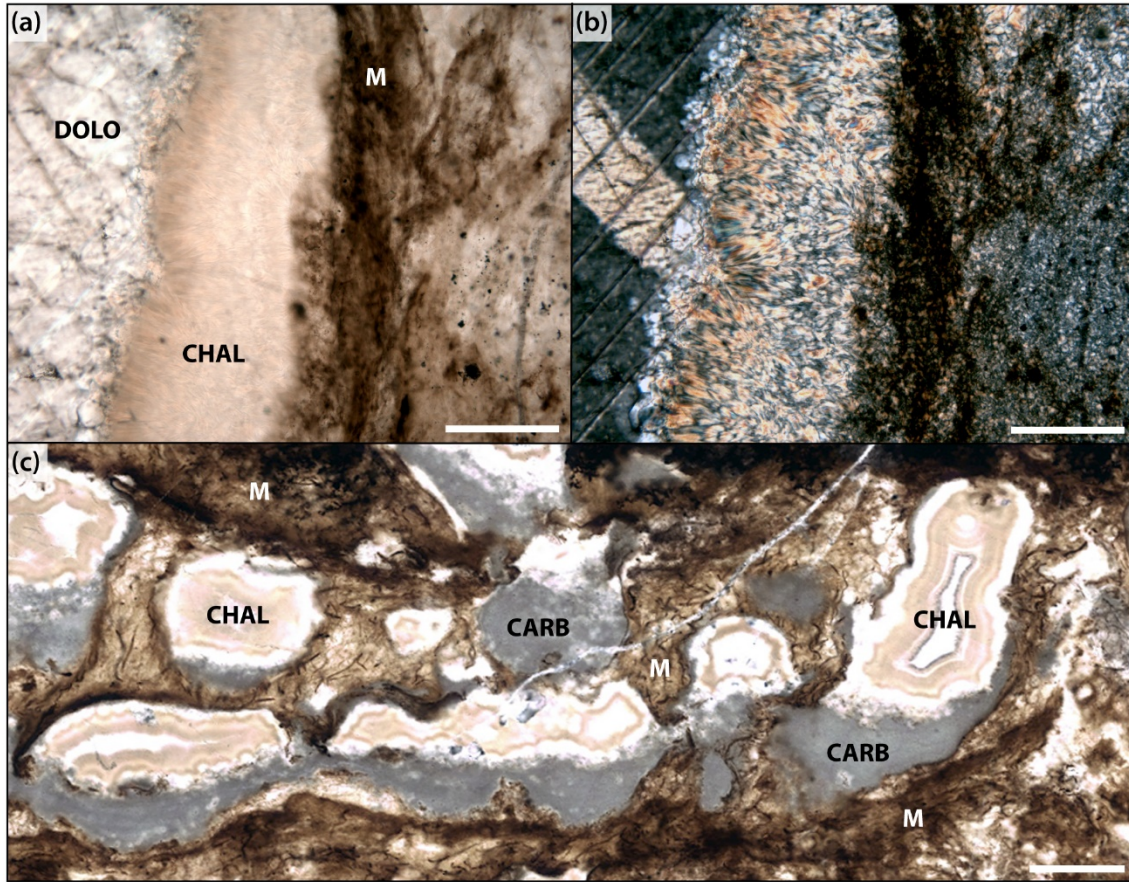


Figure 1.4. Void structures in Angmaat Formation microbial mats. (a) Vertical filamentous microbial tuft (M) lining the edge of a constructional void. Void is lined with chalcedony (CHAL), and ultimately filled by late-stage, dolomite (DOLO) cement. (b) Mat-to-void fabrics viewed under crossed-polars. (c) Constructional voids within a filament-dominated microbial mat (M) that contain a combination of unsilicified to partially silicified carbonate microspar (CARB) and chalcedony (CHAL). Scale bar is 250 micrometers in (a) and (b), and 1 mm in (c).

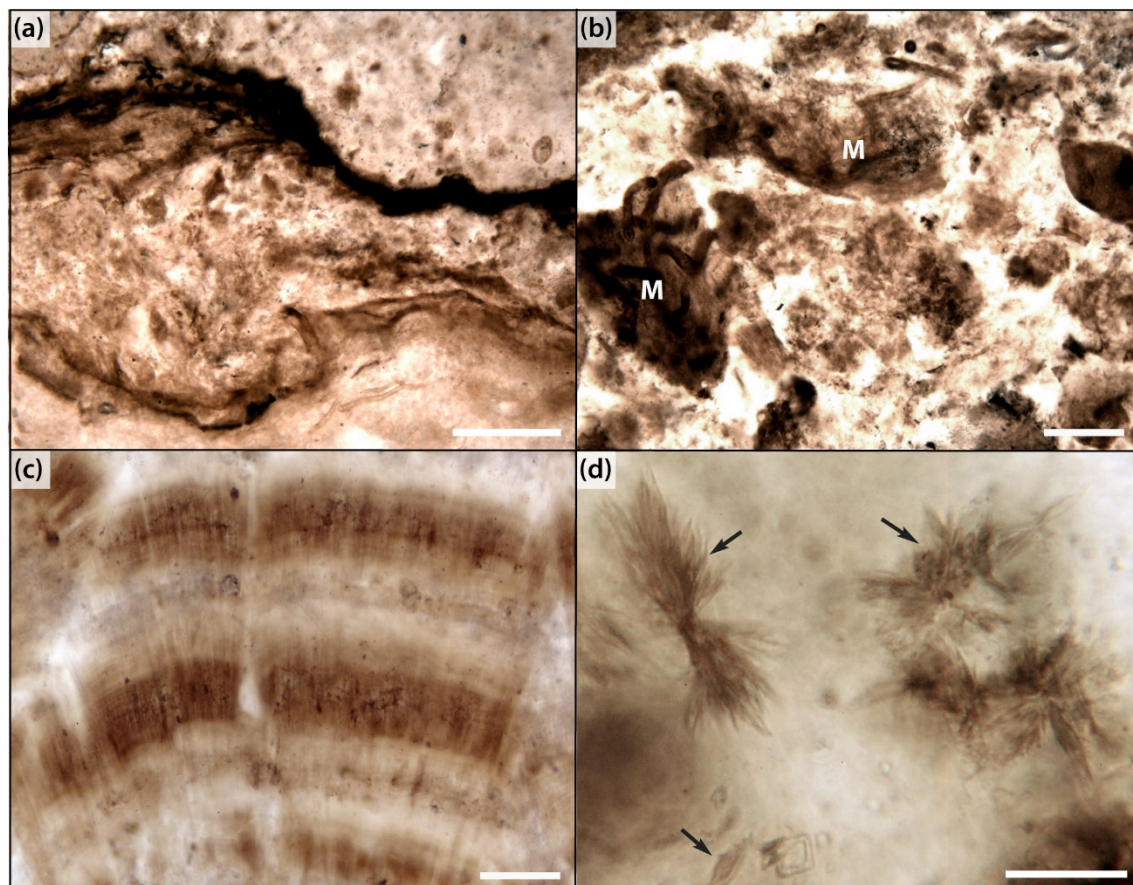


Figure 1.5. Associated mineral phases within early diagenetic chert. (a) Compacted filament-dominated mat interlaminated with detrital microbreccia. (b) Detail of microbreccia showing clasts that reflect transport of microbial mat elements (M). (c) Silicified carbonate precipitate facies (see Kah and Knoll, 1996; Knoll et al., 2014). (d) Silicified lenticular pseudomorphs after gypsum (arrows; see also Kah et al., 2001). Scale bar is 250 micrometers in (a), 100 micrometers in (b) and (c), and 25 micrometers in (d).

Table 1. Major ion concentrations for Proterozoic seawater and freshwater used in this study.

Element	Seawater* (mmol/kg)	Freshwater** (mmol/kg)
Na	456	0.27
K	1	0.05
Mg	50	0.50
SO ₄	3	0.12
Ca	9-12	0.65
Cl	565	0.23
Si	2	0.54

*from Holland (1974) and Spear et al. (2014) **from Fontes & Matray (1993)

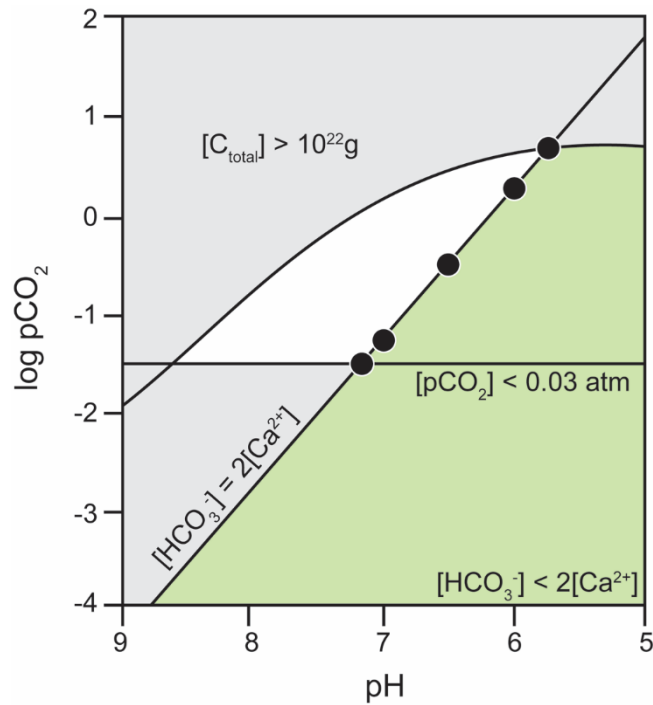


Figure 1.6. Determination of $p\text{CO}_2$ and pH values used to model Proterozoic seawater fluids; modified from Grotzinger and Kasting (1993). White region indicates hypothesized range of $p\text{CO}_2$ and pH conditions for Paleoproterozoic to Archean seawater assuming that $[\text{HCO}_3^-] > 2[\text{Ca}^{2+}]$ in marine systems, which would result in an evaporative mineral sequence (cf. Warren, 2006) without gypsum. The same range of $p\text{CO}_2$ values were used in this manuscript, although because the Mesoproterozoic Angmaat Formation contains some of earliest extensive gypsum in the geologic record (Kah et al., 2001), so values (black dots) were chosen that fall along the line described by $[\text{HCO}_3^-] = 2[\text{Ca}^{2+}]$. After the appearance of calcium sulfate evaporate minerals in the rock record, all seawater compositions should have pH and $p\text{CO}_2$ values that plot within the green area.

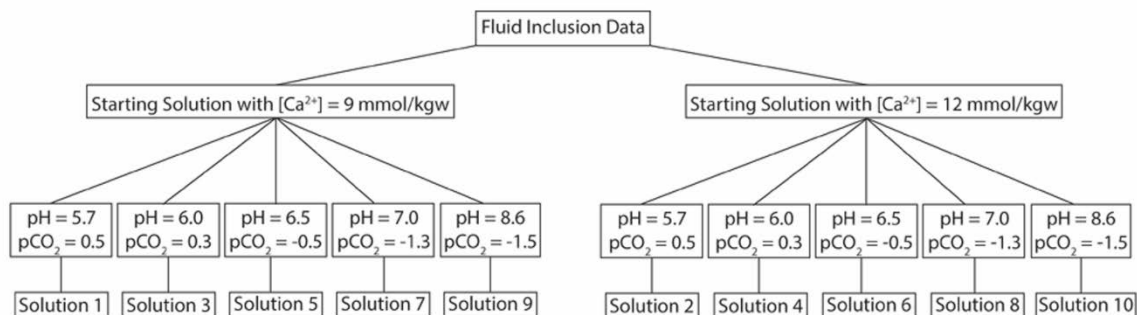
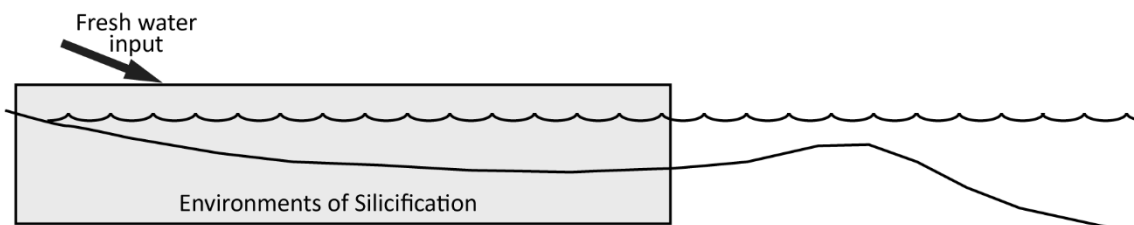


Figure 1.7. Minimum and maximum concentrations of $[Ca^{2+}]$ from fluid inclusion data for the Proterozoic (Spear et al., 2014) was used to create two starting solutions. To model these solutions as open systems, compositions were modeled in equilibrium with five different pH and pCO_2 values (see Fig. 1.6) to create 10 potential solutions. These ten solutions were then used in two mixing models. Physical scenarios that drive these two mixing models are illustrated in Figure 1.8, and model results are discussed in the text and summarized in Tables 1.2 and 1.3.

(a) Model 1 – Sealevel highstand



(b) Model 2 – Sealevel lowstand

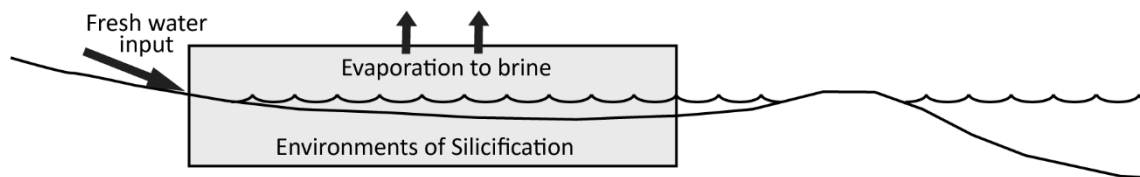


Figure 1.8. Scenarios for silicification within the Angmaat Formations. Initiation of the Angmaat Formation is marked by development of a mid-ramp oolitic shoal complex. (a) During sea level highstands, open marine waters circulate freely across the inner platform, which may experience modification by freshwater influx. Model 1 (cf. Tables 1.2 and 1.3) examines the potential for marine and freshwater-modified marine fluids to satisfy constraints for silicification as determined from petrographic analysis of Angmaat chert. (b) During sea level lowstand, isolation of inner-ramp environments permits evaporation to gypsum salinity (cf. Kah et al., 2001). Model 2 (cf. Tables 1.2 and 1.3) examines the potential for marine brines and freshwater-modified brines to satisfy constraints for silicification as determined from petrographic analysis of Angmaat chert.

Table 1.1 Results of fluid mixing models using $[Ca^{2+}] = 9$ mmol/kg (Spear et al., 2014).

Potential seawater solutions mixed with freshwater*						
Fluid #	Carbonate Phases			Evaporite Phases		
	Aragonite	Calcite	Dolomite	Anhydrite	Gypsum	Halite
1	–	–	–	–	–	–
3	–	–	–	–	–	–
5	–	–	80:20	–	–	–
7	70:30	60:40	40:60	–	–	–
9	60:40	50:50	30:70	–	–	–
Potential seawater brines mixed with freshwater*						
Fluid #	Silica Phases					
	Chalcedony	Quartz	Opal C	Opal A	Silica Gel	Magadiite
1	0:100	0:100	0:100	–	40:60	100:0
3	0:100	0:100	0:100	–	40:60	100:0
5	0:100	0:100	0:100	–	40:60	80:20
7	0:100	0:100	0:100	–	40:60	60:40
9	0:100	0:100	0:100	–	40:60	60:40
Potential seawater brines mixed with freshwater*						
Fluid #	Carbonate Phases			Evaporite Phases		
	Aragonite	Calcite	Dolomite	Anhydrite	Gypsum	Halite
1	–	90:10	70:30	100:0	100:0	100:0
3	90:10	90:10	70:30	100:0	100:0	100:0
5	70:30	60:40	50:50	100:0	100:0	100:0
7	50:50	40:60	30:70	100:0	100:0	100:0
9	40:60	40:60	30:70	100:0	100:0	100:0
Potential seawater brines mixed with freshwater*						
Fluid #	Silica Phases					
	Chalcedony	Quartz	Opal C	Opal A	Silica Gel	Magadiite
1	0:100	0:100	0:100	50:50	30:70	50:50
3	0:100	0:100	0:100	50:50	30:70	50:50
5	0:100	0:100	0:100	50:50	30:70	40:60
7	0:100	0:100	0:100	50:50	30:70	40:60
9	0:100	0:100	0:100	50:50	30:70	30:70

*values depict the greatest degree of mixing (SW:FW) at which a mineral phase has a positive saturation index; N/A indicates that the mineral phase does not reach saturation in the model.

Table 1.2 Results of fluid mixing models using $[Ca^{2+}] = 12$ mmol/kg (Spear et al., 2014).

Potential seawater solutions mixed with freshwater*						
Fluid #	Carbonate Phases			Evaporite Phases		
	Aragonite	Calcite	Dolomite	Anhydrite	Gypsum	Halite
2	–	–	–	–	–	–
4	–	–	–	–	–	–
6	100:0	80:20	–	–	–	–
8	50:50	40:60	30:70	–	–	–
10	40:60	30:70	30:70	–	–	–
Fluid #	Silica Phases					
	Chalcedony	Quartz	Opal C	Opal A	Silica Gel	Magadiite
2	0:100	0:100	0:100	–	40:60	–
4	0:100	0:100	0:100	–	40:60	90:10
6	0:100	0:100	0:100	–	50:50	80:20
8	0:100	0:100	0:100	–	40:60	60:40
10	0:100	0:100	0:100	–	40:60	50:50
Potential seawater brines mixed with freshwater*						
Fluid #	Carbonate Phases			Evaporite Phases		
	Aragonite	Calcite	Dolomite	Anhydrite	Gypsum	Halite
2	90:10	80:20	70:30	100:0	100:0	100:0
4	70:30	70:30	60:40	100:0	100:0	100:0
6	60:40	50:50	40:60	100:0	100:0	100:0
8	40:60	30:70	30:70	100:0	100:0	100:0
10	30:70	30:70	20:80	100:0	100:0	100:0
Fluid #	Silica Phases					
	Chalcedony	Quartz	Opal C	Opal A	Silica Gel	Magadiite
2	0:100	0:100	0:100	50:50	30:70	50:50
4	0:100	0:100	0:100	50:50	30:70	50:50
6	0:100	0:100	0:100	50:50	30:70	40:60
8	0:100	0:100	0:100	50:50	30:70	40:60
10	0:100	0:100	0:100	50:50	30:70	30:70

*values depict the greatest degree of mixing (SW:FW) at which a mineral phase has a positive saturation index; N/A indicates that the mineral phase does not reach saturation in the model.

CHAPTER 2
TAPHONOMIC VARIABILITY IN THE 1.1 GA MICROBIAL MATS OF
THE ANGMAAT FORMATION, BYLOT SUPERGROUP, BAFFIN
ISLAND

Abstract

The complex nature of growth and decomposition in microbial mats results in a broad range in the quality of microbial preservation. Such taphonomic variability complicates both taxonomic classification of preserved materials and the interpretation of microbial biomarkers. This study provides a taphonomic assessment of the silicified microbial mats of the late Mesoproterozoic (~1.0 Ga) Angmaat Formation, Bylot Supergroup, Baffin Island. The Angmaat Formation records unmetamorphosed and essentially undeformed, intertidal to supratidal deposition within an evaporative microbial flat. Early diagenetic silicification records microbial growth and decomposition across a range of environments from episodically exposed to more persistently submerged. Here we present the development of a new methodology involving the use of high-resolution image mosaics to investigate the taphonomy of the microfossils preserved in these mats. Taphonomic grade is assigned using a classification scheme, modified from that used in actualistic experiments, that accounts for both the taphonomic preservation state (good, fair, poor) of individual microfossils as well as the degree of compaction of the overall mat. We show that various taphonomic states are preserved within the silicified samples, from well preserved mats interpreted to have silicified during active growth, to highly degraded and compacted mats that are interpreted to represent preservation during later stages of biological decomposition. These data indicate that even small changes in the timing of silicification may have substantial implications for our identification of microbial biomarkers and, therefore, our interpretation of early Earth ecosystems.

Introduction

Microbial mats are highly resilient organosedimentary systems (van Gernerden, 1993a; Sprachta et al., 2001; Dupraz et al., 2009; Franks and Stolz, 2009) in which mat communities reflect complex microbial ecosystems comprised of photoautotrophic, photoheterotrophic, chemoautotrophic, and heterotrophic populations (Canfield and Des Marais, 1993; Franks and Stolz, 2009). These varied populations typically occur in a laminated structure that reflect a combination of physical and chemical gradients—on the laminae-scale, as well as within individual laminae (Van Gernerden 1993; Dupraz et al. 2009)—such as temperature and light availability, as well as oxygen concentration, pH, and salinity (Dupraz and Visscher, 2005). In addition to the micro-scale complexity of microbial mats, mats also preserve larger scale taphonomic differences that reflect the difference in biologic activity between surficial mats (i.e., regions of active mat accretion that are dominated by photosynthetic production of organic carbon) and buried mats (i.e., subsurface mat communities that are dominated by heterotrophic microbial activity).

The taphonomy of both living (Wacey et al., 2010) and ancient (Bartley, 1996; Bartley et al., 2000; Wacey et al., 2010) microbial mats is, therefore, also related to biogeochemical interactions within the microbial mats. Vertical stratification observed in microbial mats results from the occurrence of functionally different groups of organisms, that reflect changes in geochemical gradients (Stolz, 2000; Dupraz et al., 2009) and ultimately make up a dynamic ecosystem (Stal, 2002; Franks and Stolz, 2009). However, an idealized microbial mat (Fig. 2.1) can be envisioned as having approximately five to six layers (de Wit et al., 1995; Stolz, 2000; Stal, 2002; Herman and Kump, 2005; Franks and Stolz, 2009). Organisms at the upper surface of a mat, tend to be associated with dense pigmentation as protection from UV radiation; enhanced

production of EPS (extracellular polymeric substances) also aids in protection of microbes from environmental variability, such as changes in salinity or exposure (Stolz, 2000; Stal, 2002). This grades downward into a broader region dominated by cyanobacteria. Here, oxygen concentration can be supersaturated as a result of photosynthesis (Franks and Stolz, 2009). Organic matter produced in these surficial regions provide a ready carbon source for heterotrophic organisms at deeper levels of the mat (Stal, 2002). In the lower regions of the cyanobacteria-dominated mat, decomposition depletes oxygen and cyanobacteria are replaced by purple sulfur bacteria and anoxygenic phototrophic bacteria (Stal, 2002; Franks and Stolz, 2009). Below the purple sulfur bacteria, where light intensities are insufficient to support photosynthesis, the microbial mat becomes dominated by green sulfur bacteria. Finally, the lower portion of the mat become dominated by heterotrophic organisms, which survive off of the transfer of organic carbon provided by the various microbial species present throughout the layers of a mat (Stolz, 2000). These regions can be dominated by populations of sulfate reducers, metal reducing microbes, or methanogens, depending on the composition of pore fluids. With this view in mind, it is easy to envision that the biological and geochemical gradients within a microbial mat should be reflected in both the taphonomy of mat components and, potentially, in chemical signatures associated with preserved materials.

Earth's earliest microfossil assemblages are commonly preserved by silicification. Although substantial controversy exists over the biogenicity of the oldest examples (Schopf, 1993; Brasier et al., 2004; Brasier et al., 2005; Schopf and Kudryavtsev, 2012; Wacey et al., 2016), many Proterozoic cherts contain exceptional preservation of microbial components (Barghoorn and Tyler, 1965; Schopf, 1968; Awramik and Barghoorn, 1977; Horodyski and Donaldson, 1980; Horodyski and Donaldson, 1983; Knoll et al., 1988; Knoll et al., 1991;

Sergeev et al., 1995; Wacey et al., 2012). Because decomposition of cyanobacteria occurs on the time-scale of days to weeks (Bartley, 1996), the exceptional morphological preservation requires the rapid cessation of heterotrophic activity, exceptional morphological indicates that silicification occurred penecontemporaneously with deposition and prior to the neomorphic recrystallization of mineral phases that can physically destroy organic structures. Determining preservation state is, therefore, critical to our understanding of the extent to which biologic history of materials is accurately preserved. Such understanding is particularly important in light of efforts to develop unique chemical markers, such as the presence of molecular biomarkers (French et al. 2015; Manning-Berg et al. *in prep.*), the microanalytical identification of carbon sources (cf. Schopf et al. 2008; DeGregorio et al. 2009; Igisu et al., 2009; Qu et al. 2015; Hickman-Lewis et al. 2017; Guo et al. 2018), and the identification of chemical (Lemelle et al., 2008; Oehler et al. 2009; Thomen et al. 2014) and mineral phases (Benzerara and Menguy 2009; Wacey et al., 2012; Che et al. 2013) associated with microbial activity, to identify microbial life in geological ancient samples.

Here we describe variation in preserved morphology of silicified microbial mats of the Angmaat Formation, Bylot Supergroup, northern Baffin Island in order to understand the range of preservation of ancient microbial mats and the mechanisms that drive differences in preservation. We describe fundamental differences in the taphonomic response mat constituents and use high-resolution image mosaics of thin sections as a new way to explore the morphology of these mat fabrics on multiple scales.

Geologic Setting and Age

Bylot Supergroup

The Bylot Supergroup contains ~6 km of unmetamorphosed and relatively undeformed sedimentary rock within the fault-bounded Borden basins of northern Baffin and Bylot islands (Jackson and Iannelli, 1981; Kah and Knoll, 1996; Kah et al., 1999; Turner, 2009). Three stratigraphic groups, the Eqalulik Group, the Uluksan Group, and the Nunatsiaq Group, record overall basin development (Fig. 2.2). The Eqalulik Group is marked at its base by extrusion of tholeiitic basalts that reflect the initial rifting of the basin. These deposits are overlain by a westward-deepening and fining-upward succession of fluvial to shallow-marine sandstone and marine shale of the Adams Sound and Arctic Bay formations (Jackson & Iannelli 1981), and initiation of shallow marine carbonate deposition in the Iqqituq Formation (Turner 2009).

The Eqalulik Group is overlain by the Uluksan Group, which consists of a series of distinct carbonate successions. Initiation of the Uluksan Group is marked by sea level rise, restriction of terrigenous input into the basin, and the formation of several discrete, deep-water carbonate build-ups associated with fault-derived fluids (Hahn et al., 2015). Primary deposition of the Uluksan Group is represented by carbonate rocks of the laterally adjacent Angmaat and Nanisivik formations, and the overlying Victor Bay Formation (Kah, 1997; Sherman et al., 2002; Turner, 2009; Hahn et al., 2015). The Angmaat Formation, part of the formerly termed Society Cliffs Formation, is represented by a broad microbial flat bounded to the west by an oolitic shoal. Periodic subaerial exposure of the oolitic shoal resulted in restriction and evaporation of associated nearshore environments (Kah 1997). These deposits are dominated by microbial dolostones, sea floor precipitates (Kah and Knoll 1996; Kah et al. 2011), and abundant early diagenetic chert (Knoll et al. 2013; Manning-Berg and Kah 2017). Northwest of the oolitic shoal, offshore deposits consist predominantly of finely laminated microbial dolostone and are referred

to as the Nanisivik Formation (Turner, 2009). The upper Uluksan Group is represented by carbonate ramp (Sherman et al. 2001) and offshore reef (Narbonne and James 1998) deposits of the Victor Bay Formation. These deposits record evidence of tectonic reactivation of the Bylot Basin (Sherman et al. 2002), leading to thick, lithologically variable sandstone deposits of the Nunatsiaq Group.

The age of the Bylot supergroup is broadly constrained to within the late Mesoproterozoic. Tholeiitic basalts at the base of the Eqaulik Group provide a maximum depositional age of 1270 ± 4 Ma, indicating their emplacement as part of the widespread Mackenzie igneous event (LeCheminant and Heaman, 1989). Re-Os dating performed on shale of the Arctic Bay Formation (upper Uluksan Group) and the Victor Bay formation (upper Uluksan Group) yield ages of 1.048 ± 0.012 Ga and 1.046 ± 0.016 Ga, respectively (Gibson et al. 2017), confirming a late Mesoproterozoic age for carbonate-bearing strata of the Uluksan Group that has previously been inferred from chemostratigraphic analysis (Kah et al. 1999; Kah et al. 2012). Although the age of the uppermost Nunatsiaq Group is poorly constrained, crosscutting dikes that were part of the ~723 Ma Franklin Igneous Event (Pehrsson and Buchan, 1999) suggest that deposition ended prior to the late Neoproterozoic.

Angmaat Formation chert

Carbonate strata of the Angmaat Formation preserve peritidal microbial- and precipitate-dominated cycles that grade into an associated oolitic shoal complex (Turner, 2009). Black chert occurs throughout the Angmaat Formation as cm-scale irregular lenses and nodules, and as semi-continuous beds up to 10 cm in thickness (Jackson & Iannelli, 1981; Kah and Knoll, 1996; Manning-Berg and Kah, 2017). Chert typically conforms to bedding planes and reflects the morphology of primary sedimentary textures (Fig. 2.3) Black chert deposits are interpreted to be

primarily of early diagenetic origin based on ubiquitous microfossil preservation (Hoffman & Jackson, 1991; Kah & Knoll, 1996; Knoll et al., 2013). Late diagenetic chert is also present as gray to yellow chert nodules that cross-cut bedding (Fig 3).

Microbial assemblages of the Angmaat Formation

Microbial mat communities of the Angmaat chert are preserved across a range of peritidal environments, wherein subaqueous subtidal environments and lower intertidal environments are dominated by filamentous communities, and more frequently exposed intertidal to supratidal environments are record more abundant coccoidal communities and low-diversity filamentous communities (Kah and Knoll 1996; Knoll et al. 2013). Mat-building and mat-dwelling microbial communities are recorded in four distinct microfossil assemblages (Knoll et al. 2013). Mat building communities consist predominantly of filamentous microbial sheaths. Small diameter (6-12 μm) filaments have been interpreted as the extracellular polysaccharide sheaths of *Lyngbya*- or *Phormidium*-type cyanobacteria and classified as *Siphonophycus* sp. (Hofmann and Jackson, 1991; Kah and Knoll, 1996; Kah et al., 1999). Larger diameter (20-50 μm) filamentous sheaths have been assigned to *Eomicrocoleus* sp. (cf. Horodyski and Donaldson 1980) and interpreted to be analogous to the extant cyanobacteria *Microcoleus chthonoplastes* (Knoll et al. 2013) Coccoidal populations occur as small mat-dwelling populations and occasionally as primary mat builders. Preserved coccoids are varied in their composition (Knoll et al. 2013) but consist predominantly of populations of *Gloeocapsid*-like cyanobacterial assigned to *Eogloeocapsa* sp., which consists of multiple coccoids floating within a single external envelope; and simple, undefined coccoidal populations assigned to *Myxococcoides* sp. Additional coccoidal populations can be assigned to *Eoentophysalis* sp., *Gloeodiniopsis* sp., and *Polybessurus* sp., all of which have been compared to modern

cyanobacteria (Knoll et al. 2013). Eukaryotic algae, such as the red alga *Bangiomorpha pubescens* (Butterfield, 2000), also occur in several samples.

Methods

Traditional light microscopy was used to investigate the microbial mat fabrics and individual microfossils preserved in the Angmaat Formation. An Olympus B60 microscope was used to describe the fabrics of the microbial mats, and to do a preliminary taphonomic assessment of individual microfossils. Later analyses used image mosaics for taphonomic assessment (see Technique Development below). A first-order assessment of the preservation of organic material was then conducted using Raman spectroscopy. Raman spectroscopy was performed using a Horiba T64000 Raman microscope at the University of Cincinnati. The laser was set at 458 nm and no filter used during acquisition of the spectra. For each analysis, thirty spectra were acquired, each for one second, and averaged together. Prior to each analysis the Raman microscope was calibrated using a silicon chip.

Technique Development

Taphonomic classification and assessment

Taphonomic studies seek to understand how organic remains are incorporated into the rock record (Behrensmeyer and Kidwell, 1985). Taphonomic studies are used to inform biases present in the fossil record; to provide constraints on timing for paleoecologic, biostratigraphic, and evolution studies; and to understand differential preservation of organisms within fossil assemblages (Behrensmeyer and Kidwell, 1985). Although the data are qualitative, taphonomic schemes are built on systematic observations used to create descriptive categories into which organisms are categorized (Behrensmeyer 1978; Bartley 1996). Great care is taken into creating descriptions to ensure that data can be reproduced.

The classification scheme used in the current study to assess individual microfossil morphology is modified from the taphonomic grading scale developed by Bartley (1996). This taphonomic scale was developed using actualistic taphonomy experiments to specifically describe changes to cyanobacteria during decomposition. Taphonomic stages in Bartley (1996) broadly follow divisions outlined by Behrensmeyer (1978) that represent stages of decomposition that range from immediately post-mortem (i.e. containing evidence of rapidly degrading tissues), to nearly unrecognizable materials.

The grading scheme developed by Bartley (1996) focused on changes to cell morphology, trichome articulation, sheath morphology and terminal cell morphology. These characters were selected for observation based on observations made by Golubic and Hofmann (1976), Oehler (1976), Hofmann (1976), Knoll and Golubic (1979), and Knoll and Barghoorn (1975). Five grades were described for each character, with “one” being pristine and “five” being severely degraded, and one-hundred filaments were scored for each character using a light microscope. Of these characteristics, however, sheath morphology is the predominant character applicable to silicified microfossils preserved in the Angmaat Formation. Preferential preservation of sheaths relative to cellular material is common in both modern (Horodyski et al. 1977; Boon et al. 1981; Bartley 1996) and ancient (Golubic and Hofmann 1976; Hofmann 1976) assemblages. In the Angmaat chert, preservation of individual trichomes, in or out of sheaths, is exceedingly rare. Most of the cell morphology observed in the Angmaat Formation mats would therefore be given a grade of 5 in a taphonomic scheme that includes morphological detail of cellular trichomes.

To adequately describe the preserved microbial mats of the Angmaat Formation samples, we applied taphonomic grading schemes at two different scales: at the mesoscale, which defines

taphonomy on the scale of a thin section and represents the overall taphonomy of a preserved microbial mat, and at the microscale, which defines the taphonomy of individual microfossils.

At the mesoscale, the prominent taphonomic changes are reflected in a loss of structure driven by compaction of the microbial mat. Mesoscale fabrics were classified as “good,” “fair,” or “poor,” based on visual inspection of the thin sections (Fig. 2.4). Thin sections classified as “good” contain microfossils that are readily visible with only quick visual inspection. These samples also frequently contain irregularities in lamina thickness that are attributed to differential growth within the microbial mat and, frequently, contain chalcedony-lined voids that represent constructional voids (cf. Knoll et al. 2013) within the microbial mat. By contrast, upon a quick visual inspection, most of the microfossils observed in mesoscale fabrics defined as “fair” were concentrated in laminae. Individual microfossils could be identified but seemed to exhibit less variation in morphologies. “Fair” fabrics contain obvious, often differentially pigmented lamination. Laminae are typically smooth, suggesting a variable degree of compaction of mat fabrics. Finally, mesoscale fabrics defined as “poor” are typified by an absence of rapidly identifiable microfossils, highly compacted laminae, and homogenization of organic matter. When such samples are so strongly pigmented, making them appear nearly opaque in thin section, they may be referred to as “unrecognizable”.

Taphonomic grades for an individual microfossil are used to describe both filamentous sheaths and coccoidal microfossils. Microfossils with pristine sheath preservation that exhibit no compaction, were classified as a taphonomic grade of “good.” Filamentous sheaths classified as “good” had morphologies without tearing, bulging, or compaction. Coccoidal microfossils classified as “good” commonly have an outer sheath with a rounded cell wall preserved within the sheath (Fig 2.5). A grade of “fair” was given to microfossils that showed signs of

compaction. Commonly, these fossils had collapsed or folded sheaths that include tearing or bulging. In coccoidal organisms, a grade of “fair” is also indicated by collapse of the cell wall inside the outer sheath (Fig 2.5). Finally, a grade of “poor” was given to microfossils that have been heavily distorted by compaction, have lost the morphology of the sheath, and for those fossils in which the organic matter was homogenized and unrecognizable. In several samples, homogenized organic matter is present in the thin sections. This material can occur as clumps of organic material or dispersed throughout a sample. To describe this type of organic matter, the percent area of unrecognizable organic matter was determined using ImageJ. These taphonomic grades are commonly used in taphonomic assessments because they allow an entire sample to be characterized by the proportion of organisms characterized by three categories and are easily visualized on ternary taphograms (Kowalewski et al., 1995). However, some of the organic matter is degraded to the point that the original morphology of the microfossils was not able to be recognized.

Individual microfossils were scored using traditional point counting techniques (Howarth, 1998; Weltje, 2002). The thin sections were moved on the stage in 2 mm increments from right to left, and from top to bottom of the thin section. At each step, microfossils observed under the ocular cross-hair were scored as “good,” “fair,” or “poor,” and added to the overall count. In order to assess the taphonomy of individual microbial mat samples, 600 microfossils were counted from each sample. A sample size of 600 microfossils provides a 95% confidence level with a 4% confidence interval (Bartlett et al., 2001). Obtaining 600 counts, however, was not always feasible. For smaller sample sizes, such as those closer to 150 microfossils, the 95% confidence level is 8% of the value measured (Bartlett et al., 2001). Using such traditional point counting techniques, despite the inherent subjectivity in defining taphonomic categories, results

generally fell within 5% when comparing counts performed on the same thin section on different days, and counts performed by different people.

During this process, several deficiencies were noted in this traditional point-count method. First, this method was time-consuming, and it was often difficult to obtain the 600 counts desired in one sitting. Identification of a single microfossil under the ocular cross-hairs often required adjustment of the focal plane, making it difficult to maintain a uniform focal plane through the investigation. Finally, it was unclear whether a traditional point-count method accurately produced a representative picture of the overall fabric of the microbial mat. Any potential variation within a microbial mat, such as the spatially variable occurrence or preservation of different mat constituents, may not be recognized with traditional point counting.

Taphonomic analysis using image mosaics

To alleviate difficulties imparted by traditional point-counting, we developed a method of taphonomic assessment using image mosaics. Image mosaics taken produced on a Leica DFC400 camera attached to a Leica DM6000B microscope in the Astrobiogeochemistry Laboratory (abcLab) at NASA's Jet Propulsion Laboratory. For each thin section, 3000-4000 individual images were taken using a 20X objective. Prior to image acquisition, the borders of each thin section were delineated in the software, and predictive focus points were set up across the thin section. White balance was set using a frosted thin section. Image acquisition was performed by Leica Acquisition Software and images were stitched using the same software. An example of one of these image mosaics has been uploaded to the GigaPan website and is publicly viewable (<http://gigapan.com/gigapans/52663df35ba394d3cb7110452f8ebce0>). Such mosaics allow the user to view a thin section from a mesoscopic view (e.g. the entire thin section, which allows for the visualization of the relative amount of silica phases to carbonate phases, the color of the mats in

the thin section, identification of general lamina structure, constructional voids, etc.) and then to rapidly zoom to specific regions to identify whether laminae characteristics reflect a fundamental compositional difference within the fabric. For this study, image mosaics were manipulated within Photoshop to produce a reproducible method of taphonomic evaluation.

Quadrat sampling

Upon recognizing the difficulties that natural variation within microbial mats introduced to classifying microfossils, we sought to describe the mat taphonomy in a way that was more representative of the overall mat fabric. Quadrat sampling is a technique commonly used in ecological studies to produce an unbiased assessment of populations (Weaver, 1918; Heslehurst, 1971; Kenkel et al., 1989). Specifically, quadrat sampling involves dividing the study area into discrete regions and collecting data on all components within the quadrat. Such sampling permits investigation of the common or visually obvious components (e.g. here, either the mat building constituents, or the most easily recognized components) as well as the rare components.

Because individual image mosaics (~2 GB file sizes) are unwieldy for most imaging software, mosaics were split into 25 partitions using the photo editing software Gimp 2.8 (www.gimp.org). Each partition is of equal size—20% of the length of the image and 20% of the width of the image—and represents 4% of the total image. Because images varied in size, a percentage value is used to define the size of a quadrat instead of using a pixel count. Partitions were then saved as discrete TIFF files to prevent image compression. Each partition was then opened in Adobe Photoshop and divided into 64 quadrats by overlaying an 8x8 grid (Fig. 2.6) using the GuideGuide extension (<http://guideguide.me>). This method produced a total of 1,600 quadrats per thin section, with an average area of 0.0625%, the area of an individual quadrat.

A sampling template, created in Microsoft Excel, was used to determine which quadrats would be analyzed and to track results of taphonomic assessment. Within this file, a random number generator provided 25 values that correspond to a single quadrat in each of the partitions to be analyzed, providing a random assessment of the entire thin section. For each quadrat, the taphonomic state of every microfossil was assessed. Microfossils were noted as filament or coccooid, and assigned an assessment of good, fair, or poor. If needed, this process could be repeated, providing assessment of a second or third quadrat in each partition. Subsequent rounds permitted assessment of variability—with low total counts, one quadrant with extremely well-preserved microfossils can skew the assessment of the thin section toward better preservation. A greater number of counts therefore provides an assessment of both individual quadrants and the preserved microbial mat as a whole. Assessment of individual quadrats continued until at least 600 microfossils were assessed. Once the goal of counting 600 individual microfossils was reached, the assessment continued until that quadrat was completed.

Results

Taphonomic patterns: filamentous microfossils

Two species of filamentous organisms represent the dominant mat-forming constituents within Angmaat chert (Knoll et al., 2013) (Fig. 2.7). Small-diameter (6-12 μm) filament sheaths assigned to *Siphonophycus* sp. are robust and thick-walled, and, when well-preserved, occur as tightly woven mats and as vertical arrays of filaments that outline constructional voids within the mat. These simple forms rarely show evidence of either sheath degradation or compaction. Instead, the primary taphonomic pathway appears to be the gradual loss of pigmentation, which ultimately inhibits identification of distinct sheaths. This progressive loss of pigmentation from *Siphonophycus*-dominated regions correlated to poorly-pigmented regions of the laminated mats

at the mesoscale (Fig. 2.8). By contrast, large-diameter (20-60 μm) filamentous sheaths assigned to *Eomicrocoleus* sp. consist of heavily pigmented, thin-walled sheaths. *Eomicrocoleus* occurs either sparsely within Siphonophysuc-dominated mat regions, or in concentrated laminae. *Eomicrocoleus* –dominated regions undergo substantial compaction prior to any visible taphonomic alteration of *Siphonophysuc*-dominated regions, resulting in interlamination of thick, lightly pigmented regions (often containing little-deformed sheaths of *Eomicrocoleus* sp.) alternating with thin, heavily pigmented laminae of compacted sheaths of *Eomicrocoleus* sp.

Taphonomic patterns: coccoidal microfossils

Several coccoidal species are present in the Angmaat Formation mats. Pockets of thin-walled, ~ 10 μm -sized coccoids interpreted to be *Myxocoides* are seen in some filamentous mats. These microfossils tend to be well-preserved and maintain a circular to oval shape. In all cases, specific taxa were only able to be identified as “good” or “fair,” all of the organisms classified as “poor” can only be recognized as coccoidal or filamentous morphologies (also observed in Bartley et al., 2000). *Eogloeocapsa* sp. is also present in coccoidal mats. Well-preserved examples have 2-4 cells preserved within an envelope. Envelopes commonly rupture and examples of “fair” microfossils tend to preserve a couple of cells within a remnant of the envelope, or cells are preserved just outside of the ruptured envelope. Organisms with an envelope surrounding a cell wall, or dark centers (Fig. 2.8), which is likely the remnant organic matter from a collapsed cell wall (Bartley, 1996; Toporski et al., 2002) belong to the genus *Gloediniopsis*. Well-preserved *Gloediniopsis* are circular to oval-shaped with a dark circle in the center of the envelope. When compacted, these fossils are arranged in layers and lose their round shape with the discrete envelope and dark center pattern. In a poor section of the mat, discrete individual fossils cannot be identified, and their shape is lost (Fig. 2.9). Coccoidal mats contain a

lot of lightly-pigmented, structureless regions that surround them; these regions are interpreted as EPS. Within compacted mat fabrics, *Eogloecapsa* behave similarly to *Gloeodiniopsis* and compact into layers as the envelopes and cells become more oval in shape. Microfossils are more compacted and individual cells or envelopes are not identifiable in mats containing *Eogloecapsa* classified as “poor.” Other coccoidal organisms, like *Entophysalis belcherensis* (2-5 μm in diameter) occur in dark patches and are never well preserved (Fig. 2.8). These mats are often classified as unrecognizable and were assigned a percent area using Image J. Smaller coccoidal organisms, identified as *Sphaerophycus parvum* (2-3 μm), are abundant in many of the silicified microbial mats (Fig. 2.8). However, the size of their cell is approximately the size of one to two pixels on the image mosaics. Ultimately, these coccoids were unable to be included in a taphonomic account because of their small size. In many of the samples, clusters of these microfossils were distributed throughout the samples. These fossils seem to keep their spherical shape during each stage of taphonomy, but little can be determined regarding the ultrastructure of these organisms from light microscopy.

Results of traditional point-counting

Traditional point-counting methods were first used while developing the methodology to perform a taphonomic assessment on image mosaics. Results of point counting were then compared to an assessment of the same sample performed on the mosaic, using the intersection of gridlines as a proxy for ocular cross-hairs. The results of this comparison are shown in figure 2.10. More microfossils were able to be counted on the mosaic (n=400) than on the thin section (n= 300). In this analysis, 7% of the microfossils counted and scored using the microscopy were classified as “good,” while 25% and 68% were classified as “fair,” and “poor” respectively. These percentages were close to those obtained using a point-counting method on an image

mosaic of the same sample. In this case, 3% of the fossils were characterized as “good,” 28% were classified as “fair,” and 69% were classified as “poor.” These data indicate that the point-counting methods are repeatable, and can be translated to image mosaics, although we posit that such methods are insufficient to address spatial variability within a preserved mat.

Results of quadrat sampling

Data from samples analyzed via the quadrat system are presented on ternary plots (Figures 2.12-2.19). The average composition was then compared to the preliminary, mesoscale visual assessment of the sample. Approximately 600 microfossils were classified for seven samples that represented a range of mesoscale mat fabrics (Table 2.1). To ensure that the quadrat technique permitted an assessment of variability and was reproducible analyses were first performed on a single sample, and then a second analysis was performed on the same sample several weeks later. Additionally, in order to determine the potential counts needed to accurately assess spatial variability within the mat, a complete assessment, that is, assessing a single quadrat in each of the 25 partitions, was performed a total of five times. If the random number generator selected a quadrat from within a partition that had been previously assessed, a new quadrat was selected by the random number generator. Each round was plotted on a ternary plot to assess the degree to which spatial heterogeneity affected taphonomic assessment of the entire thin section (Fig 2.11).

The assessment of individual microfossils was collected in an Excel spreadsheet. Within this spreadsheet, data are presented as both the number of filaments and the total percentage of filaments, the number of coccoids and the total percentage of coccoids, and the percentages of the total microfossil count. Recording data in this way allowed for visualization of the complexity of the microbial mats at various scales. For example, figure 2.12 shows data for a

sample (DAC-15) that was visually identified on the mesoscopic scale as taphonomically “good” prior to the taphonomic assessment. To obtain 609 microfossil counts—here a total of 553 filaments and 56 coccoids—a total of 40 quadrats were included in the classification. Spatial variability in the taphonomy of the mat is readily noted by plotting individual quadrats on a ternary plot. In this sample, coccoids within one quadrat is assessed as taphonomically “good”, coccoids in six quadrats are assessed as taphonomically “poor”, and the other 37 quadrats preserve coccoidal morphologies that plot within the “good-fair,” “mixed,” and “fair-poor” regions of the ternary plot (Kowalewski et al. 1995). Filament morphologies for this sample span the same taphonomic range on the ternary plot, with the average filament classification plotting within the “fair-poor” region of the ternary plot. The coccoidal organisms in this sample have values that are influence by more “good” preserved morphologies, and thus most plot within the “mixed” portion of the ternary plot, as does the average coccoid data (Fig. 2.13).

Samples that were identified as taphonomically “fair” based on mesoscale visual inspection showed the greatest amount of variability when assessed via individual microfossil counts. Figure 2.14 shows the results of (DBG-42), which only required that 25 quadrats be counted in order to obtain the desired 600 microfossils. A total of 659 microfossils were counted; 283 of these were represented by filamentous sheaths, and 376 by coccoids. The microfossil counts, which includes the number of filaments and coccoids in each quadrat, result in most data plotting as taphonomically “poor”, with only 2 of the 25 quadrats plotting in the taphonomic range of “fair-poor”. When focusing on the filamentous data alone, the data plot within the “poor” taphonomic range (Fig. 2.15a). Coccoid-only data (Fig. 2.15b), range from “fair” to “fair-poor” preservation. The average taphonomy of all microfossils counts from DBG-42, however, plots within the “fair-poor” range. Similarly, a second sample (DAC-16) required counting 30

quadrats to obtain a count of 634 microfossils, including 614 filament sheaths and 20 coccoids. The total microfossil counts (number of filaments and coccoids) per each quadrat, result in most data plotting as taphonomically “poor” (Fig. 2.16). When looking at the filamentous data alone (Fig. 2.17a), all but one plot as “poor.” All but two of the quadrats, displaying the coccoid-only data for DAC-16, plot in the “fair” and “fair-poor” regions of the ternary plot (Fig. 2.17b)

A sample (DBN-4) that was identified as taphonomically “poor” *via* mesoscale visual inspection also shows variation at several scales. A total of 643 microfossils were counted from 25 quadrats. Of the microfossils, 113 were filaments and 510 were coccoids. Total microfossil assessments per quadrat (Fig. 2.18) vary between taphonomically “fair” to “poor”. The filament classification plots along the “fair” to “poor” line of the ternary plot (Fig. 2.19a). The coccoids, however, exhibit more variation, with some of the coccoidal microfossils plot in the “good-fair,” “mixed,” and the “uneven” range (Fig. 2.19b).

Together data indicate that coccoids exhibit more variability in taphonomic range than the filamentous sheaths. Coccoidal fossils span taphonomic ranges from “good-fair,” to “fair,” to “poor”. By contrast, filamentous sheaths plot in a narrower range of preservation, typically plotting within “fair-poor” and “poor” regions. These trends are observed regardless of the taphonomic grade assigned to the mesoscale mat. In general, the mesoscale taphonomic grade correspond well to the data collected on individual microfossils (Fig. 2.20: all overall fabrics and the filaments + coccoid averages). Mat fabrics classified as “good” had a higher percentage of “good” individual microfossils for both coccoidal and filamentous mats. Variation between the quadrats within one sample plot across the entire taphonomic continuum in the ternary plot (Fig. 2.12: DAC-15 quadrats). The trend of data plotting as “good,” through “good-fair” and “fair-

poor,” and ultimately to “poor” is the decomposition pattern observed in actualistic experiments (Bartley, 1996).

Raman spectroscopy

Raman spectra were collected on ~144 microfossils from a total of 12 mat samples, that were visually determined to span the taphonomic grades of “good” to “unrecognizable.” When possible, a “good,” “fair,” and “poor,” example of the microfossils within one mat sample were chosen for analysis. In some cases, like in mat fabrics identified as “unrecognizable,” the range of taphonomic preservation did not allow for “good,” or even “fair,” microfossils to be analyzed. Despite taphonomic variation in mat fabrics from the 12 samples and the individual microfossils analyzed, the shape and pattern of the Raman spectra were relatively similar (Fig. 2.21). Spectra show peaks centered around 467.93 cm^{-1} , 1331.8 cm^{-1} , 1612.74 cm^{-1} , and 2937.78 cm^{-1} . The peak around 467 cm^{-1} is a quartz peak (Lazzeri and Mauri, 2003), which is expected because the chert matrix is quartz. Peaks at 1331.8 cm^{-1} , 1612.74 cm^{-1} represent primary kerogen peaks. The D-band, or the disordered peak, forms at 1331.8 cm^{-1} and the G-band, or the graphite peak, is represented by the peak at 1612.74 cm^{-1} (Schopf et al., 2005). The D- and G-bands form when the crystal lattice is disordered. As temperature increases, thermal alteration of kerogen occurs, which causes the total area below the combined D- and G-bands to decrease as the D-band becomes sharper and narrower, and the G-band shifts to lower wave numbers (Schopf et al., 2005; Wacey, 2009). Peaks centered around these Raman shifts, however, minor variation in the shape of the peaks was observed based on the taphonomic classification of the individual fossil being analyzed. Fossils classified as “good” or “fair” tend to have D- and G-bands that are rounded or humped, whereas fossils classified as “fair” or “poor” tend to have slightly sharper peaks at these Raman shifts with a shoulder to the right of the peak. Raman Index Parameter

(RIP) values (Schopf et al., 2005) are a measurement of thermal maturity, and were calculated for all measurement. Angmaat Formation samples all provide a RIP of about 7 (Table 2.2), where a value of 9 indicates that the preserved organic matter is immature and has not experienced thermal alteration, and a value of 1 indicates that the organic matter has experienced substantial thermal alteration (Schopf et al., 2007).

Discussion

Taphonomic analyses using quadrat sampling on image mosaics

Here we present a new sampling methodology for the taphonomic assessment of microbial mats preserved in early diagenetic chert. Performing an assessment using image mosaics provides the ability to move rapidly between various scales to better understand the relationship between primary constituents and the overall fabrics, permits a more discrete exploration of complex mat fabrics. Several studies have realized the influence of taphonomy and the importance of understanding variation of chemistry to the preserved morphology for studies applicable to early life on Earth and extraterrestrial bodies (Williford et al., 2013; Wacey, 2014; Peng et al., 2016; Guo et al., 2018). Image mosaics can provide a detailed framework within which to explore the relationship between taphonomy and trends in isotopic, elemental, or molecular geochemistry.

High resolution images also provide the opportunity to rapidly investigate thin sections at multiple scales, which provides a holistic view of microfossils and the relationship of an individual fossil to the overall mat morphology. The ability to partition large mosaics, and to overlay grids for quadrat analysis greatly simplified taphonomic analysis and provides multiple possibilities for displaying data, depending on the question being addressed. The system is also modular, making it easy to go back to a sample if assessment of additional quadrats is necessary.

Finally, image mosaics can be easily shared among research groups with different expertise and interests.

The greatest difficulty with image mosaics was the size of the raw files, which overwhelmed standard image processing software. For this reason, the images needed to be divided into partitions to be accessible using standard software. Other drawbacks include the fixed focal plane, and limited depth of field for the image. Taphonomic studies performed using light microscopy often utilize changes the focal plane to determine the three-dimensional character of a microfossil. With a fixed focal plane, it must be assumed that the portion of the microfossil that can be seen in the image is representative of the rest of the 3-dimensional microfossil.

Mat fabrics and implications for biomarker preservation

Microbial mats are complex ecosystems that grow by accretion, with new mat growth occurring on top of old mat material (Van Gernerden, 1993b; Reid et al., 2000; Stal, 2002), resulting in the preservation of characteristic laminated textures. As mats grow, the organic matter produced by photosynthesizing organisms is recycled by heterotrophic bacteria, which may prevent the preservation of laminations (Stal, 1994, 2002). However, mats are also capable of precipitating and/or accreting sediment (Reid et al., 2000; Dupraz et al., 2009) which may halt heterotrophic degradation of organic matter and may ultimately preserve lamination (Canfield and Des Marais, 1993; Stal, 2002). This highlights the differences that microbial reworking of organic matter imparts on the taphonomic state of microbial mats, wherein incomplete degradation of organic matter would produce variation in both the condition of individual microfossils and overall mat fabrics. Therefore, taphonomy is a crucial component of Precambrian paleobiology studies and taphonomic processes largely affect the ultimate

preservation state of a fossil or microbial mat in the fossil record (Schopf, 1975; Knoll et al., 1988; Bartley, 1996; Bartley et al., 2000; Altermann and Kazmierczak, 2003). In the case of Angmaat cherts, all samples, despite differences in mesoscale and microscale taphonomic state, contain individual microfossils that record thermally immature organic matter. This suggests that taphonomy must be able to be explained by natural processes of microbial growth and degradation relative to the timing of silicification and not a reflection of post-depositional thermal alteration.

Filamentous sheaths or coccoidal envelopes are preserved, commonly 3-dimensionally (Schopf, 1968; Horodyski and Donaldson, 1980; Knoll, 1985; Knoll et al., 2013), in ancient samples. Cells tend to shrink prior to preservation and coccoid forms shrink to form a mass within the cell that could be mistaken for an organelle or nucleus (Golubic and Hofmann, 1976; Horodyski et al., 1977; Francis et al., 1978). These may be referred to as “spot cells” (Toporski et al., 2002). In filamentous communities, cellular trichomes readily exit, leaving empty sheaths. It is these empty sheaths that are most commonly preserved in ancient samples (Golubic and Hofmann, 1976; Hofmann, 1976; Horodyski et al., 1977; Bartley, 1996; Peng et al., 2016). Horodyski et al. (1977) noted that even in modern microbial mats, less than 0.5% of sheaths preserved in the lower layers of the mats contained trichomes. In laboratory experiments involving the silicification of microorganisms, trichomes are also rarely preserved, and if they are preserved, the trichome is usually found outside of its sheath and severely deformed (Oehler, 1976; Toporski et al., 2002). Cellular decomposition and the loss of cellular material in coccoidal organisms is also seen in laboratory experiments involving the silicification of bacteria (Toporski et al., 2002). In both actualistic experiments and ancient samples, accumulations of decomposed and homogenized organic matter are commonly observed. These accumulations are

unrecognizable in terms of individual mat constituents. The microbial fabrics observed in the Angmaat Formation are consistent with these earlier studies.

Overall mat textures of the Angmaat Formation reflect taphonomic processes that acted differentially on the various microbial constituents. Coccoidal organisms tend to be preserved across a wider range of taphonomic state, with more examples retaining markers of “good” preservation. By contrast, filamentous sheaths exhibit a narrower range in preservation, and are most often classified as “poor” (Fig. 2.4: overall mat morphologies). Within filament-dominated mats, this trend may result from a bias in taphonomic assessment, where more darkly pigmented materials are easier to identify and assess. We suggest however, such a bias reflects a fundamental difference in the taphonomic pathway experienced by *Eomicricoleus* sp. and *Siphonophycus* sp. communities. *Eomicrocoleus* filaments are often large and very heavily pigmented, which makes the microfossils easily identified in these mats. *Eomicrocoleus* sheaths, however, are relatively thin and readily undergo compaction. Even when the sheaths are compacted, the strong pigmentation often highlights the sheath boundaries, making it easier to identify discrete microfossils. By contrast, filamentous sheaths of *Siphonophycus* sp. readily lose pigmentation prior to discernable compaction of sheaths. As a result, even though sheaths of *Siphonophycus* sp. are the dominant mat-building organism in these samples, they are commonly not able to be counted because they cannot be clearly identified.

A taphonomic bias also appears to exist between the filamentous sheaths and coccoidal envelopes. Observations here suggest that the robustness (i.e. the ability to withstand compaction) of filament sheaths plays a primary role in determining the taphonomic state of these microfossils. Coccoids may experience a different degradational pathway. Coccoids here are associated with substantially more EPS than filament-dominated communities. Extracellular

polymer substances exist as a gel, colloid, or can be present in a dissolved state (Decho, 2000), having high water contents (Decho, 2010), and are primarily made up of polysaccharides (Braissant et al., 2009). The role of EPS is to stabilize the microenvironment, promote chemical gradients to help the microorganisms survive, and protect organisms from dramatic changes in their environment (Decho, 2000). Regions where EPS is abundant, particularly in the coccoidal mats, may be more resistant to compaction because of the higher water content, which may allow coccoidal communities to repair and retain their envelopes even as silicification begins. The EPS is also able to interact with, and bind ions important during mineral precipitation (Decho, 2010), and may be more easily permeated during silicification, which would also reduce the potential for compaction of the coccoidal mat communities. Another potential explanation for the observed taphonomic variation may reflect the relative motility of the microorganisms within the silicifying mats. Filamentous communities are highly mobile, migrating upward on diurnal cycles (Stolz, 2000; Dupraz and Visscher, 2005) and in response to chemical gradients and changes in light quality and quantity (Stolz, 2000). Furthermore, with mat accretion, trichomes naturally abandon their sheaths to form new ones at the mat surface (Ortega-Calvo et al., 1991). Modern mats, as a result, consist primarily of abandoned sheaths (Abed Raeid et al., 2003). We suggest, as well, that environmental changes and the introduction of environmental stresses—like the formation of a silica gel around microorganisms—may also force trichomes to abandon their sheaths. Once the sheaths are empty, they are no longer maintained and are thus more susceptible to taphonomic alteration (Krylov et al., 1989; Sergeev et al., 2002). Coccoidal organisms, however, are not motile and do not have the opportunity to leave portions of the mat that become entombed in silica. Instead, these organisms likely maintain their cellular components until the silicification process reduces nutrient supply below that necessary for

maintaining active metabolism, potentially resulting in a broader range of taphonomic states. EPS production within coccoid-dominated regions may enhance the ability for coccoids to maintain active metabolism during silicification (Krylov et al. 1989).

Conclusions

The taphonomic assessment of silicified microbial mats within the Angmaat Formation, Baffin Island demonstrate the preserved complexity of microbial mats in the fossil record. Variation in preservation was observed at both the mesoscale (thin-section scale) and the microscale (individual microfossils), across the various taxa of organisms preserved, and between the morphologies of the individual microfossils. Mat fabrics were visually identified as “good,” “fair,” or “poor;” these classifications were then compared to the taphonomic assessment of individual microfossils within the mat. In general, the visual identification of the mesoscale mat fabric reflected the average composition of the individual microfossil morphologies. Coccoidal organisms consistently exhibit a wider range of preservation than their filamentous counterparts, which typically exhibit a narrow range of preservation in the “poor” taphonomic category. This observation may reflect differences in diagenetic pathways for filamentous organisms, which are motile and able to abandon their sheaths, and coccoidal organisms that are non-motile and insulated from changes in their environment by EPS.

Within this study, we also describe a new method for taphonomic assessment of microfossils using a quadrat template on image mosaics. Despite some issues regarding sample size and the inability to move through a sample to better identify discrete microfossils, the image mosaics provide a more holistic view of the relationship of microfossils to overall mat morphologies. Image mosaics can also provide a template, or base map, for investigation of in-situ geochemical preservation with taphonomic variation inherent to microbial mats. Such a use

has far-reaching implications for improving our understanding of preservation in ancient samples crucial for understanding early ecosystems or even environments on Mars.

References

- Abed Raeid, M. M., Golubic, S., Garcia-Pichel, F., Camoin, G. F., and Sprachta, S., 2003, Characterization of microbialite-forming cyanobacteria in a tropical lagoon: Tikehau Atoll, Tuamotu, French Polynesia: *Journal of Phycology*, v. 39, no. 5, p. 862-873.
- Altermann, W., and Kazmierczak, J., 2003, Archean microfossils: a reappraisal of early life on Earth: *Research in Microbiology*, v. 154, no. 9, p. 611-617.
- Awramik, S. M., and Barghoorn, E. S., 1977, The Gunflint microbiota: *Precambrian Research*, v. 5, no. 2, p. 121-142.
- Barghoorn, E. S., and Tyler, S. A., 1965, Microorganisms from the Gunflint Chert: *Science*, v. 147, no. 3658, p. 563-577.
- Bartlett, J. E., Kotrlik, J. W., and Higgins, C. C., 2001, Organizational research: Determining appropriate sample size in survey research: *Information technology, learning, and performance journal*, v. 19, no. 1, p. 43.
- Bartley, J., Knoll, A., P Grotzinger, J., and Sergeev, V., 2000, Lithification and fabric genesis in precipitated stromatolites and associated peritidal carbonates, Mesoproterozoic Billyakh Group, Siberia.
- Bartley, J. K., 1996, Actualistic Taphonomy of Cyanobacteria: Implications for the Precambrian Fossil Record: *PALAIOS*, v. 11, no. 6, p. 571-586.
- Behrensmeyer, A. K., 1978, Taphonomic and Ecologic Information from Bone Weathering: *Paleobiology*, v. 4, no. 2, p. 150-162.
- Behrensmeyer, A. K., and Kidwell, S. M., 1985, Taphonomy's contributions to paleobiology: *Paleobiology*, v. 11, no. 1, p. 105-119.
- Braissant, O., Decho, A. W., Przekop, K. M., Gallagher, K. L., Glunk, C., Dupraz, C., and Visscher, P. T., 2009, Characteristics and turnover of exopolymeric substances in a hypersaline microbial mat: *FEMS Microbiology Ecology*, v. 67, no. 2, p. 293-307.
- Brasier, M., Green, O., Lindsay, J., and Steele, A., 2004, Earth's Oldest (~ 3.5 Ga) Fossils and the 'Early Eden Hypothesis': Questioning the Evidence: *Origins of life and evolution of the biosphere*, v. 34, no. 1, p. 257-269.
- Brasier, M. D., Green, O. R., Lindsay, J. F., McLoughlin, N., Steele, A., and Stoakes, C., 2005, Critical testing of Earth's oldest putative fossil assemblage from the ~3.5Ga Apex chert, Chinaman Creek, Western Australia: *Precambrian Research*, v. 140, no. 1, p. 55-102.
- Butterfield, N. J., 2000, *Bangiomorpha pubescens* n. gen., n. sp.: implications for the evolution of sex, multicellularity, and the Mesoproterozoic/Neoproterozoic radiation of eukaryotes: *Paleobiology*, v. 26, no. 03, p. 386-404.
- Canfield, D. E., and Des Marais, D. J., 1993, Biogeochemical cycles of carbon, sulfur, and free oxygen in a microbial mat: *Geochimica et Cosmochimica Acta*, v. 57, no. 16, p. 3971-3984.
- de Wit, R., van den Ende, F. P., and van Gernerden, H., 1995, Mathematical simulation of the interactions among cyanobacteria, purple sulfur bacteria and chemotrophic sulfur bacteria in microbial mat communities: *FEMS Microbiology Ecology*, v. 17, no. 2, p. 117-135.
- Decho, A. W., 2000, Microbial biofilms in intertidal systems: an overview: *Continental Shelf Research*, v. 20, no. 10-11, p. 1257-1273.
- Decho, A. W., 2010, Overview of biopolymer-induced mineralization: What goes on in biofilms?: *Ecological Engineering*, v. 36, no. 2, p. 137-144.

- DeGregorio, B. T., Sharp, T. G., Flynn, G., Wirick, S., and Hervig, R., L., 2009, Biogenic origin for Earth's oldest putative microfossils: *Geology*, v. 37, no. 7, p. 631-634.
- Dupraz, C., Reid, R. P., Braissant, O., Decho, A. W., Norman, R. S., and Visscher, P. T., 2009, Processes of carbonate precipitation in modern microbial mats: *Earth-Science Reviews*, v. 96, no. 3, p. 141-162.
- Dupraz, C., and Visscher, P. T., 2005, Microbial lithification in marine stromatolites and hypersaline mats: *Trends in microbiology*, v. 13, no. 9, p. 429-438.
- Francis, S., Barghoorn, E. S., and Margulis, L., 1978, On the experimental silicification of microorganisms. III. Implications of the preservation of the green prokaryotic alga prochloron and other coccoids for interpretation of the microbial fossil record: *Precambrian Research*, v. 7, no. 4, p. 377-383.
- Franks, J., and Stolz, J. F., 2009, Flat laminated microbial mat communities: *Earth-Science Reviews*, v. 96, no. 3, p. 163-172.
- French, K. L., Hallmann, C., Hope, J. M., Schoon, P. L., Zumberge, J. A., Hoshino, Y., Peters, C. A., George, S. C., Love, G. D., Brocks, J. J., Buick, R., and Summons, R. E., 2015, Reappraisal of hydrocarbon biomarkers in Archean rocks: *Proceedings of the National Academy of Sciences*, v. 112, no. 19, p. 5915-5920.
- Golovenok, V., and Belova, M. Y., 1984, Rifeyskiye mikrobioty v kremnyakh iz billyakhskoy serii Anabarskogo podniatiya [Riphean microbiotas in cherts of the Billyakh Group on the Anabar Uplift] *Paleontol: Zh*, v. 4, p. 23-32.
- Golubic, S., and Hofmann, H. J., 1976, Comparison of Holocene and Mid-Precambrian Entophysalidaceae (Cyanophyta) in Stromatolitic Algal Mats: Cell Division and Degradation: *Journal of Paleontology*, v. 50, no. 6, p. 1074-1082.
- Green, J. W., Knoll, A. H., Golubi, x, S., and Swett, K., 1987, Paleobiology of Distinctive Benthic Microfossils from the Upper Proterozoic Limestone-Dolomite "Series," Central East Greenland: *American Journal of Botany*, v. 74, no. 6, p. 928-940.
- Guo, Z., Peng, X., Czaja, A. D., Chen, S., and Ta, K., 2018, Cellular taphonomy of well-preserved Gaoyuzhuang microfossils: A window into the preservation of ancient cyanobacteria: *Precambrian Research*, v. 304, no. Supplement C, p. 88-98.
- Hahn, K. E., Turner, E. C., Babechuk, M. G., and Kamber, B. S., 2015, Deep-water seep-related carbonate mounds in a Mesoproterozoic alkaline lake, Borden Basin (Nunavut, Canada): *Precambrian Research*, v. 271, p. 173-197.
- Herman, E. K., and Kump, L. R., 2005, Biogeochemistry of microbial mats under Precambrian environmental conditions: a modelling study: *Geobiology*, v. 3, no. 2, p. 77-92.
- Heslehurst, M., 1971, The point quadrat method of vegetation analysis: A review.
- Hickman-Lewis, K., Garwood, R. J., Withers, P. J., and Wacey, D., 2017, X-ray microtomography as a tool for investigating the petrological context of Precambrian cellular remains: *Geological Society, London, Special Publications*, v. 448, no. 1, p. 33-56.
- Hofmann, H. J., 1976, Precambrian Microflora, Belcher Islands, Canada: Significance and Systematics: *Journal of Paleontology*, v. 50, no. 6, p. 1040-1073.
- Hofmann, H. J., and Jackson, G. D., 1991, Shelf-Facies Microfossils from the Uluksan Group (Proterozoic Bylot Supergroup), Baffin Island, Canada: *Journal of Paleontology*, v. 65, no. 3, p. 361-382.

- Horodyski, R. J., Bloeser, B., and Haar, S. V., 1977, Laminated algal mats from a coastal lagoon, Laguna Mormona, Baja California, Mexico: *Journal of Sedimentary Research*, v. 47, no. 2.
- Horodyski, R. J., and Donaldson, J. A., 1980, Microfossils from the Middle Proterozoic Dismal Lakes Groups, Arctic Canada: *Precambrian Research*, v. 11, no. 2, p. 125-159.
- Horodyski, R. J., and Donaldson, J. A., 1983, Distribution and Significance of Microfossils in Cherts of the Middle Proterozoic Dismal Lakes Group, District of Mackenzie, Northwest Territories, Canada: *Journal of Paleontology*, v. 57, no. 2, p. 271-288.
- Howarth, R. J., 1998, Improved estimators of uncertainty in proportions, point-counting, and pass-fail test results: *American Journal of Science*, v. 298, no. 7, p. 594-607.
- Igisu, M., Ueno, Y., Shimojima, M., Nakashima, S., Awramik, S. M., Ohta, H., and Maruyama, S., 2009, Micro-FTIR spectroscopic signatures of Bacterial lipids in Proterozoic microfossils: *Precambrian Research*, v. 173, no. 1-4, p. 19-26.
- Jackson, G., and Iannelli, T., 1981, Rift-related cyclic sedimentation in the Neohelikian Borden Basin, northern Baffin Island: *Geological Survey of Canada, Paper 81-10*, p. 269-302.
- Kah, L. C., 1997, Sedimentological, geochemical, and paleobiological interactions on a Mesoproterozoic carbonate platform: Society Cliffs Formation, northern Baffin Island, Arctic Canada.
- Kah, L. C., and Knoll, A. H., 1996, Microbenthic distribution of Proterozoic tidal flats: Environmental and taphonomic considerations: *Geology*, v. 24, no. 1, p. 79-82.
- Kah, L. C., Sherman, A. G., Narbonne, G. M., Knoll, A. H., and Kaufman, A. J., 1999, $\delta^{13}\text{C}$ stratigraphy of the Proterozoic Bylot Supergroup, Baffin Island, Canada: implications for regional lithostratigraphic correlations: *Canadian Journal of Earth Sciences*, v. 36, no. 3, p. 313-332.
- Kenkel, N. C., Juhász-Nagy, P., and Podani, J., 1989, On sampling procedures in population and community ecology: *Vegetatio*, v. 83, no. 1, p. 195-207.
- Knoll, A. H., 1985, Exceptional Preservation of Photosynthetic Organisms in Silicified Carbonates and Silicified Peats: *Philosophical Transactions of the Royal Society B: Biological Sciences*, v. 311, no. 1148, p. 111-122.
- Knoll, A. H., and Barghoorn, E. S., 1975, Precambrian Eukaryotic Organisms: A Reassessment of the Evidence: *Science*, v. 190, no. 4209, p. 52-54.
- Knoll, A. H., and Golubic, S., 1979, Anatomy and taphonomy of a precambrian algal stromatolite: *Precambrian Research*, v. 10, no. 1-2, p. 115-151.
- Knoll, A. H., Strother, P. K., and Rossi, S., 1988, Distribution and diagenesis of microfossils from the lower proterozoic duck creek dolomite, Western Australia: *Precambrian Research*, v. 38, no. 3, p. 257-279.
- Knoll, A. H., Swett, K., and Mark, J., 1991, Paleobiology of a Neoproterozoic Tidal Flat/Lagoonal Complex: The Draken Conglomerate Formation, Spitsbergen: *Journal of Paleontology*, v. 65, no. 4, p. 531-570.
- Knoll, A. H., Wörndle, S., and Kah, L. C., 2013, Covariance of microfossil assemblages and microbialite textures across an upper Mesoproterozoic carbonate platform: *Palaios*, v. 28, no. 7, p. 453-470.
- Kowalewski, M., Flessa, K. W., and Hallman, D. P., 1995, Ternary Taphograms: Triangular Diagrams Applied to Taphonomic Analysis: *PALAIOS*, v. 10, no. 5, p. 478-483.
- Krylov, I., Orleanskii, V., and Tikhomirova, N., 1989, Chertification: Secular Preparations: *Priroda*, no. 4, p. 73-78.

- Lazzeri, M., and Mauri, F., 2003, First-Principles Calculation of Vibrational Raman Spectra in Large Systems: Signature of Small Rings in Crystalline $\text{S}_{i\text{O}}_2$: *Physical Review Letters*, v. 90, no. 3, p. 036401.
- LeCheminant, A. N., and Heaman, L. M., 1989, Mackenzie igneous events, Canada: Middle Proterozoic hotspot magmatism associated with ocean opening: *Earth and Planetary Science Letters*, v. 96, no. 1–2, p. 38-48.
- Oehler, J. H., 1976, Experimental studies in Precambrian paleontology: Structural and chemical changes in blue-green algae during simulated fossilization in synthetic chert: *Geological Society of America Bulletin*, v. 87, no. 1, p. 117-129.
- Ortega-Calvo, J. J., Hernandez-Marine, M., and Saiz-Jimenez, C., 1991, Biodeterioration of building materials by cyanobacteria and algae: *International Biodeterioration*, v. 28, no. 1, p. 165-185.
- Pehrsson, S. J., and Buchan, K. L., 1999, Borden dykes of Baffin Island, Northwest Territories: a Franklin U-Pb baddeleyite age and a paleomagnetic reinterpretation: *Canadian Journal of Earth Sciences*, v. 36, no. 1, p. 65-73.
- Peng, X. T., Guo, Z. X., House, C. H., Chen, S., and Ta, K. W., 2016, SIMS and NanoSIMS analyses of well-preserved microfossils imply oxygen-producing photosynthesis in the Mesoproterozoic anoxic ocean: *Chemical Geology*, v. 441, p. 24-34.
- Qu, Y., Engdahl, A., Zhu, S., Vajda, V., and McLoughlin, N., 2015, Ultrastructural Heterogeneity of Carbonaceous Material in Ancient Cherts: Investigating Biosignature Origin and Preservation: *Astrobiology*, v. 15, no. 10, p. 825-842.
- Reid, R. P., Visscher, P. T., Decho, A. W., Stolz, J. F., Bebout, B. M., Dupraz, C., Macintyre, I. G., Paerl, H. W., Pinckney, J. L., Prufert-Bebout, L., Steppe, T. F., and DesMarais, D. J., 2000, The role of microbes in accretion, lamination and early lithification of modern marine stromatolites: *Nature*, v. 406, p. 989.
- Schopf, J. W., 1968, Microflora of the Bitter Springs Formation, Late Precambrian, Central Australia: *Journal of Paleontology*, v. 42, no. 3, p. 651-688.
- Schopf, J. W., 1975, Precambrian paleobiology: problems and perspectives: *Annual Review of Earth and Planetary Sciences*, v. 3, no. 1, p. 213-249.
- Schopf, J. W., 1993, Microfossils of the Early Archean Apex Chert: New Evidence of the Antiquity of Life: *Science*, v. 260, no. 5108, p. 640-646.
- Schopf, J. W., and Kudryavtsev, A. B., 2012, Biogenicity of Earth's earliest fossils: A resolution of the controversy: *Gondwana Research*, v. 22, no. 3-4, p. 761-771.
- Schopf, J. W., Kudryavtsev, A. B., Agresti, D. G., Czaja, A. D., and Wdowiak, T. J., 2005, Raman imagery: a new approach to assess the geochemical maturity and biogenicity of permineralized Precambrian fossils: *Astrobiology*, v. 5, no. 3, p. 333-371.
- Schopf, J. W., Kudryavtsev, A. B., Czaja, A. D., and Tripathi, A. B., 2007, Evidence of Archean life: Stromatolites and microfossils: *Precambrian Research*, v. 158, no. 3–4, p. 141-155.
- Sergeev, V. N., Gerasimenko, L. M., and Zavarzin, G. A., 2002, The Proterozoic History and Present State of Cyanobacteria: *Microbiology*, v. 71, no. 6, p. 623-637.
- Sergeev, V. N., Knoll, A. H., and Grotzinger, J. P., 1995, Paleobiology of the Mesoproterozoic Billyakh Group, Anabar Uplift, Northern Siberia: *Memoir (The Paleontological Society)*, v. 39, no. 1, p. 1-37.

- Sherman, A. G., James, N. P., and Narbonne, G. M., 2002, Evidence for reversal of basin polarity during carbonate ramp development in the Mesoproterozoic Borden Basin, Baffin Island: *Canadian Journal of Earth Sciences*, v. 39, no. 4, p. 519-538.
- Sprachta, S., Camoin, G., Golubic, S., and Le Campion, T., 2001, Microbialites in a modern lagoonal environment: nature and distribution, Tikehau atoll (French Polynesia): *Palaeogeography, Palaeoclimatology, Palaeoecology*, v. 175, no. 1, p. 103-124.
- Stal, L. J., *Microbial mats in coastal environments*, Berlin, Heidelberg, 1994, Springer Berlin Heidelberg, p. 21-32.
- , 2002, Cyanobacterial Mats and Stromatolites, *in* Whitton, B. A., and Potts, M., eds., *The Ecology of Cyanobacteria: Their Diversity in Time and Space*: Dordrecht, Springer Netherlands, p. 61-120.
- Stolz, J. F., 2000, Structure of Microbial Mats and Biofilms, *in* Riding, R. E., and Awramik, S. M., eds., *Microbial Sediments*: Berlin, Heidelberg, Springer Berlin Heidelberg, p. 1-8.
- Toporski, J. K., Steele, A., Westall, F., Thomas-Keprta, K. L., and McKay, D. S., 2002, The simulated silicification of bacteria-New clues to the modes and timing of bacterial preservation and implications for the search for extraterrestrial microfossils: *Astrobiology*, v. 2, no. 1, p. 1-26.
- Turner, E. C., 2009, Mesoproterozoic carbonate systems in the Borden Basin, Nunavut: *Canadian Journal of Earth Sciences*, v. 46, no. 12, p. 915-938.
- van Gernerden, H., 1993a, Marine Sediments, Burial, Pore Water Chemistry, Microbiology and Diagenesis Microbial mats: A joint venture: *Marine Geology*, v. 113, no. 1, p. 3-25.
- , 1993b, Microbial mats: a joint venture: *Marine Geology*, v. 113, no. 1, p. 3-25.
- Wacey, D., 2009, Techniques for Investigating Early Life on Earth, *Early Life on Earth: A Practical Guide*, Springer Netherlands, p. 87 - 123.
- Wacey, D., 2014, In situ Morphologic, Elemental and Isotopic Analysis of Archean Life, *in* Dilek, Y., and Furnes, H., eds., *Evolution of Archean Crust and Early Life*: Dordrecht, Springer Netherlands, p. 351-365.
- Wacey, D., Gleeson, D., and Kilburn, M. R., 2010, Microbialite taphonomy and biogenicity: new insights from NanoSIMS: *Geobiology*, v. 8, no. 5, p. 403-416.
- Wacey, D., Menon, S., Green, L., Gerstmann, D., Kong, C., McLoughlin, N., Saunders, M., and Brasier, M., 2012, Taphonomy of very ancient microfossils from the ~3400Ma Strelley Pool Formation and ~1900Ma Gunflint Formation: New insights using a focused ion beam: *Precambrian Research*, v. 220-221, p. 234-250.
- Wacey, D., Saunders, M., Kong, C., Brasier, A., and Brasier, M., 2016, 3.46 Ga Apex chert 'microfossils' reinterpreted as mineral artefacts produced during phyllosilicate exfoliation: *Gondwana Research*, v. 36, p. 296-313.
- Weaver, J. E., 1918, The Quadrat Method in Teaching Ecology: *The Plant World*, v. 21, no. 11, p. 267-283.
- Weltje, G. J., 2002, Quantitative analysis of detrital modes: statistically rigorous confidence regions in ternary diagrams and their use in sedimentary petrology: *Earth-Science Reviews*, v. 57, no. 3, p. 211-253.
- Williford, K. H., Ushikubo, T., Schopf, J. W., Lepot, K., Kitajima, K., and Valley, J. W., 2013, Preservation and detection of microstructural and taxonomic correlations in the carbon isotopic compositions of individual Precambrian microfossils: *Geochimica Et Cosmochimica Acta*, v. 104, p. 165-182.

Appendix

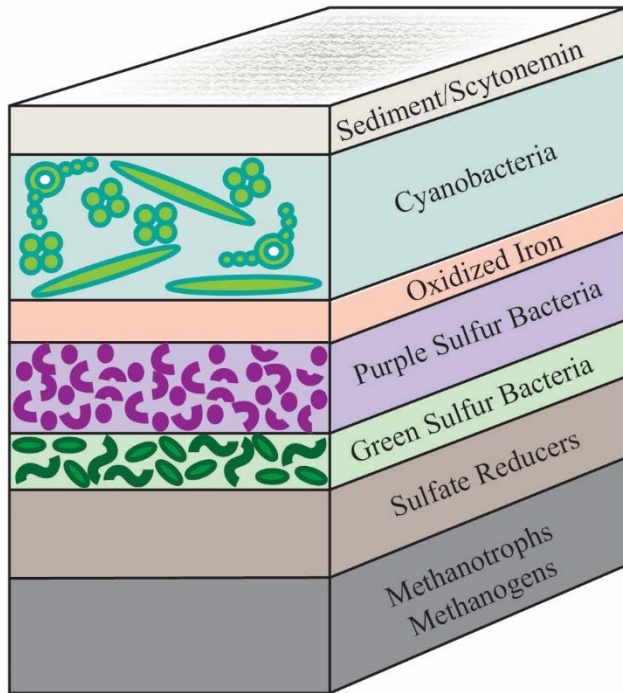


Figure 2.1 An idealized microbial mat adapted from Stolz, 2000. Microbial mats typically consist of five to six layers of various microbial communities that form differently colored laminae as a result of chemical and light gradients within the mat.

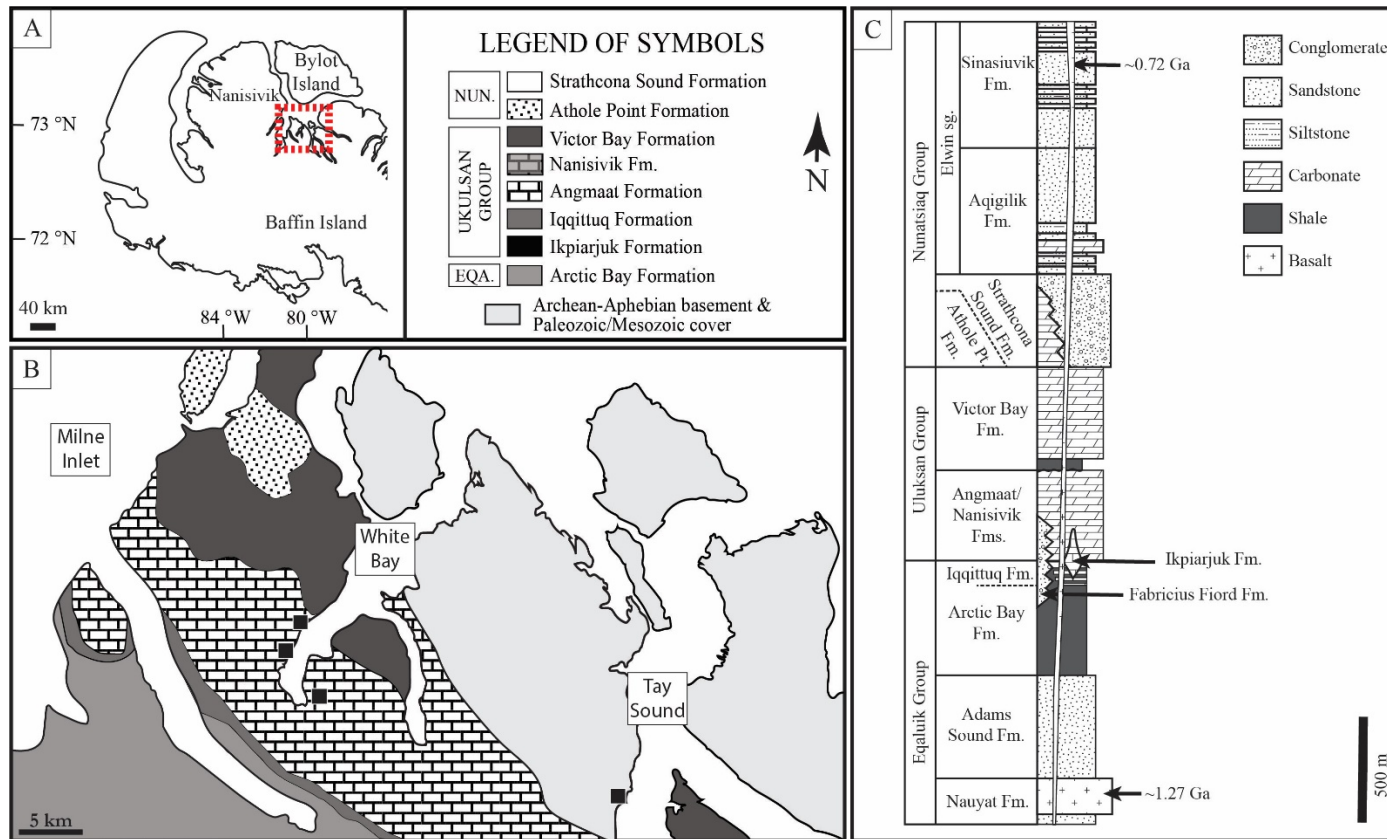


Figure 2.2 Samples used in this study were collected during a 1993-1994 field season to Baffin Island (A). All of the samples were collected from the Angmaat Formation (B) within the Bylot Supergroup (C). Here the sample localities are plotted here as black squares (B).

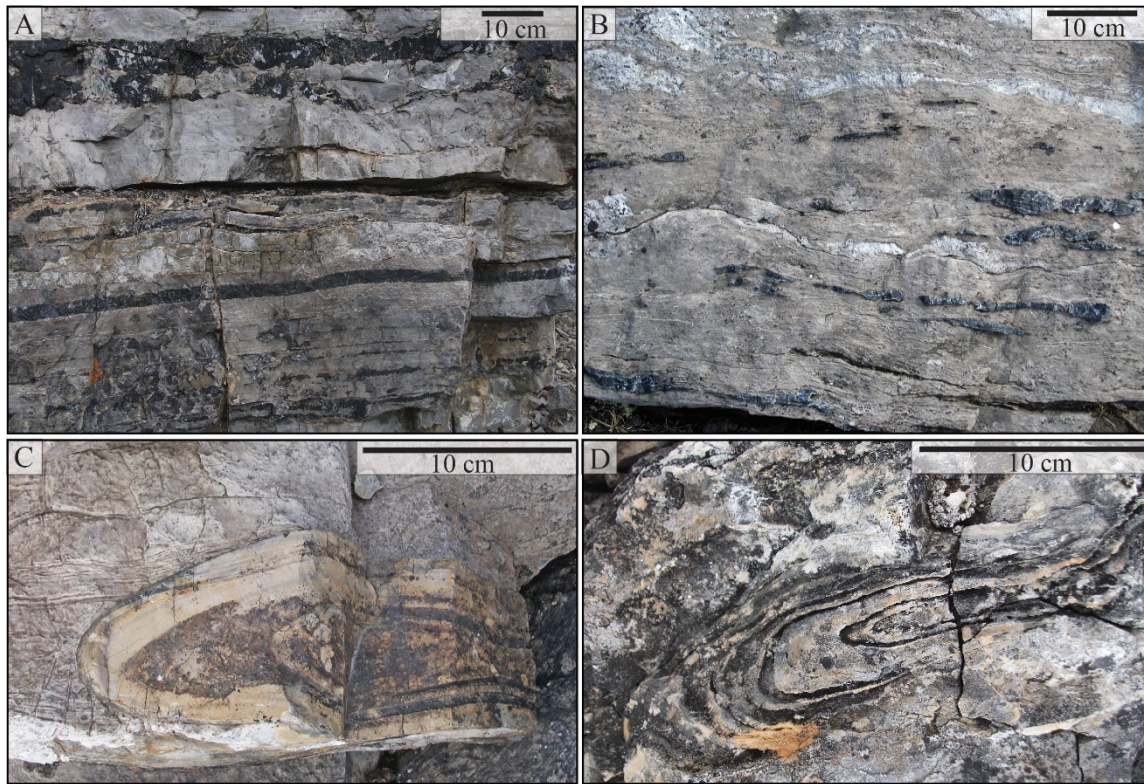


Figure 2.3 Early diagenetic black chert occurs as thin layers (A) to nodules and lenses (B) in the carbonate strata of the Angmaat Formation. Later diagenetic chert is also present in these strata, although they are typically yellow (C) or gray (D) in color.

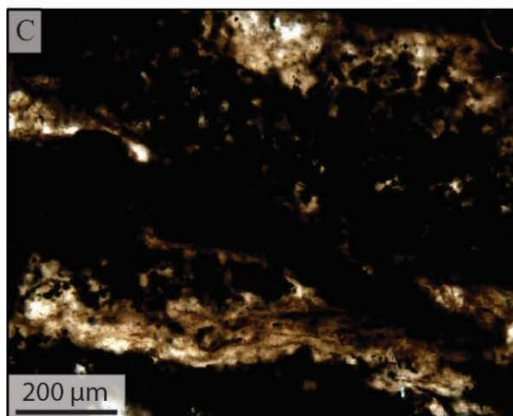
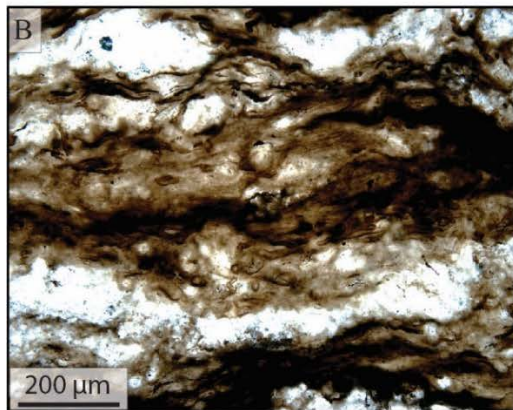
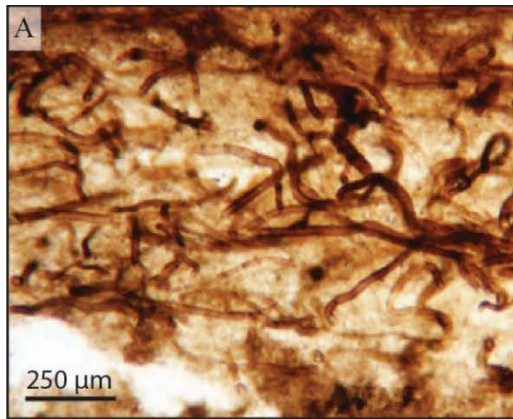


Figure 2.4 Overall mat taphonomy was determined based on quick, petrographic observations. Uncompacted mat fabrics, with abundant microfossils in vertical and horizontal arrangements were given the classification of “good.” “Fair” mat fabrics exhibit more compaction and have obvious, compacted layers that are pigmented light- to dark-brown. Mats labelled as “poor” are often highly compacted, individual microfossils are not easily, or quickly, identified and compacted layers are dark-brown to black in color.


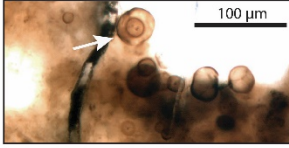



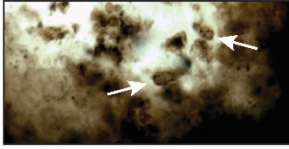
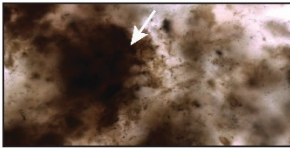
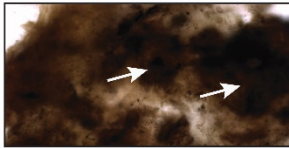
Grade	Description	Filamentous Example	Coccolidal Example
Good	<ul style="list-style-type: none"> • No compaction • Pristine sheath/cell wall • Morphological details of sheath 		
Fair	<ul style="list-style-type: none"> • Little compaction • Initial collapse of sheath/cell wall • Tearing/folding of sheath/cell wall 		
Poor	<ul style="list-style-type: none"> • Compactional distortion • Loss of sheath/cell wall morphology • Homogenization of organic matter 		
Unrecognizable	<ul style="list-style-type: none"> • Homogenized organic matter • Cannot distinguish microfossil morphology 		

Figure 2.5 Taphonomic grades of “good,” “fair,” and “poor” were assigned to individual microfossils. These grades were determined based on the compaction of the microfossil, how pristine the sheath or cell wall appear (i.e. whether it was torn or collapsed). A subcategory of “poor” was used for samples that were too darkly pigmented and the organic matter was too homogenized to determine whether the microfossil had been filamentous or coccolidal. These samples were labelled as “unrecognizable.”

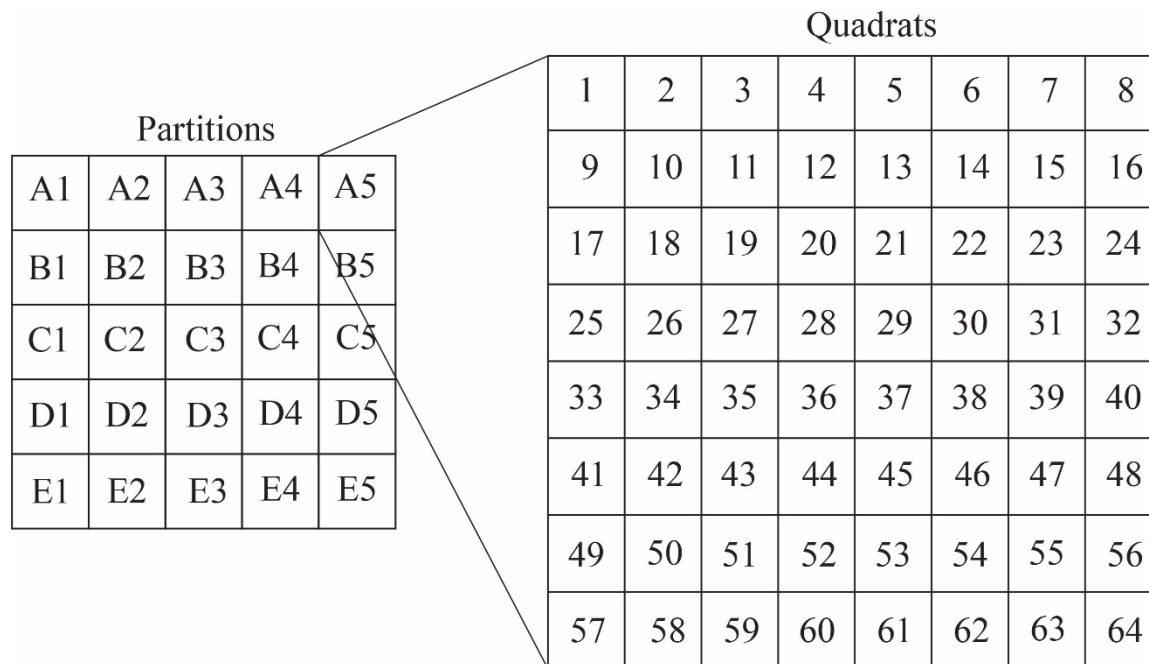


Figure 2.6 A quadrat system was overlain onto each mosaic. The mosaic was first divided into 25 partitions (A1-E5). Each partition was divided into 64 quadrats. For each partition, a random number generator in Microsoft Excel was then used to determine which quadrat would be used in the assessment (1-64).

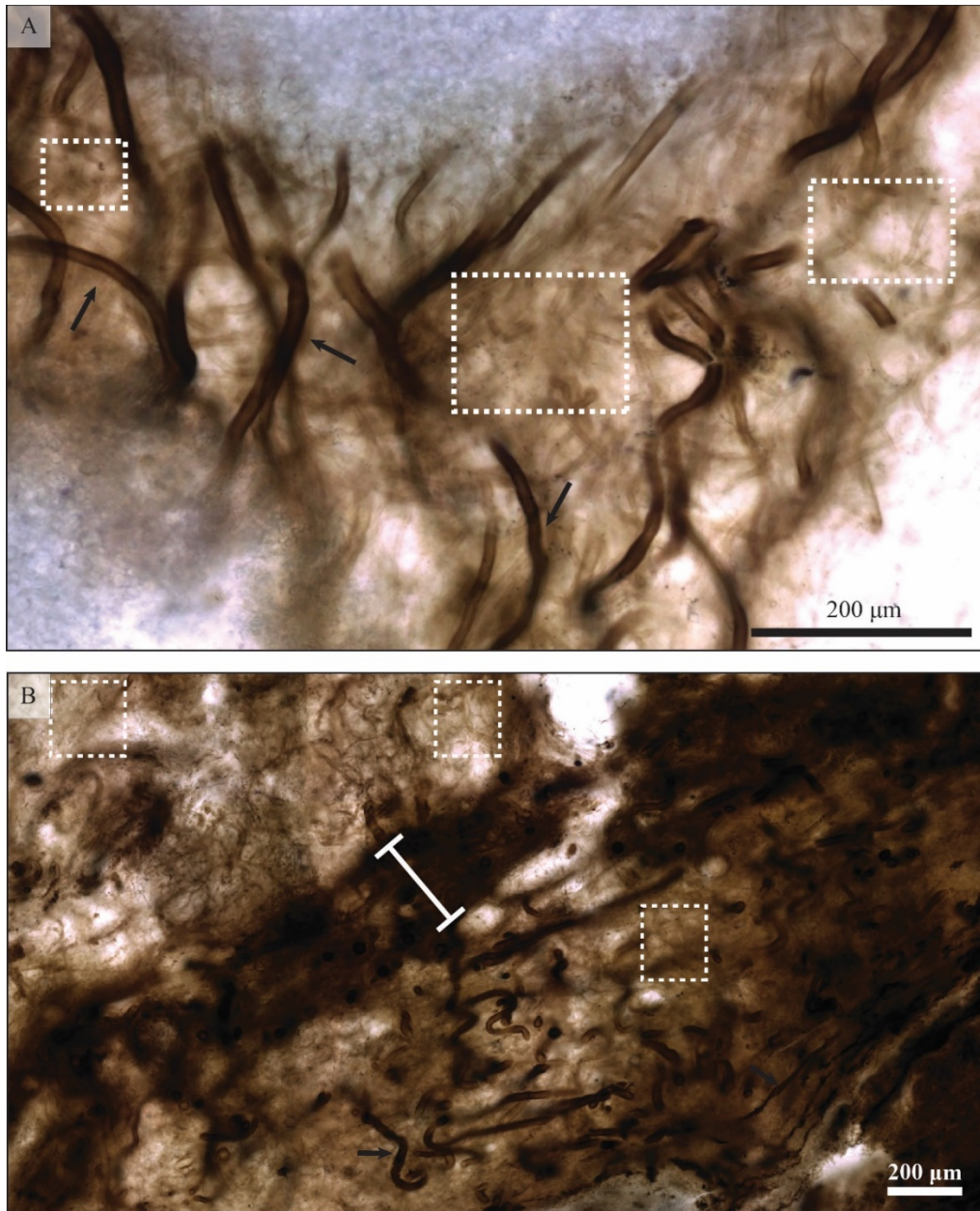


Figure 2.7 Two types of filamentous microfossils are observed in the Angmaat Formation mats. The larger, darker filaments are *Microcoleus* filaments and are highlighted with the black arrow in (A) and (B). The dark, compacted layers (B) observed in these mats, are often the result of bundling of these *Microcoleus* sheaths. The white boxes highlight areas where the second filamentous organisms are easily seen (A and B). These are *Siphonophycus* filaments, which fade during mat decomposition and are not able to be counted for taphonomic analyses.

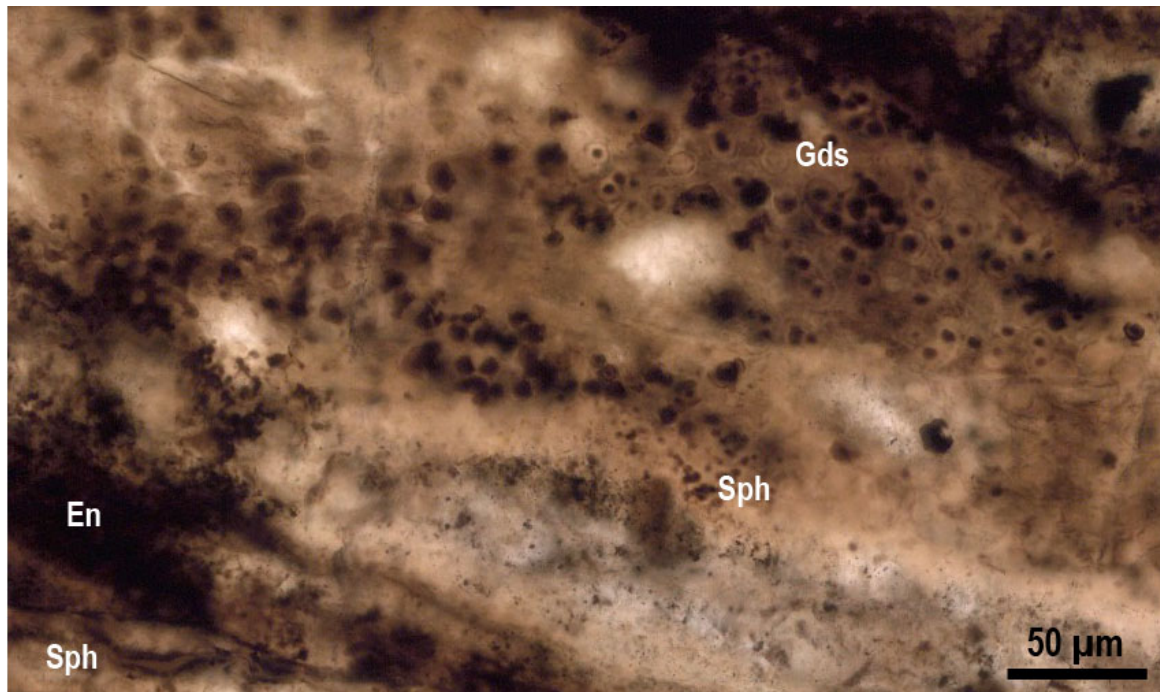


Figure 2.8 Coccoidal organisms preserved in a microbial mat that is visually identified as “fair.” Coccoidal microfossils commonly have a cell wall with a dark center, like the *Gloediniopsis* (Gds) microfossils preserved in the top right corner. This image also contains *Entophysalis* (En), which compose dark patchy areas within a mat and never preserve well. The small (2-3 μm) cells are identified as *Sphaerophycus* (Sph); however, these fossils are too small for an accurate description of their taphonomy.

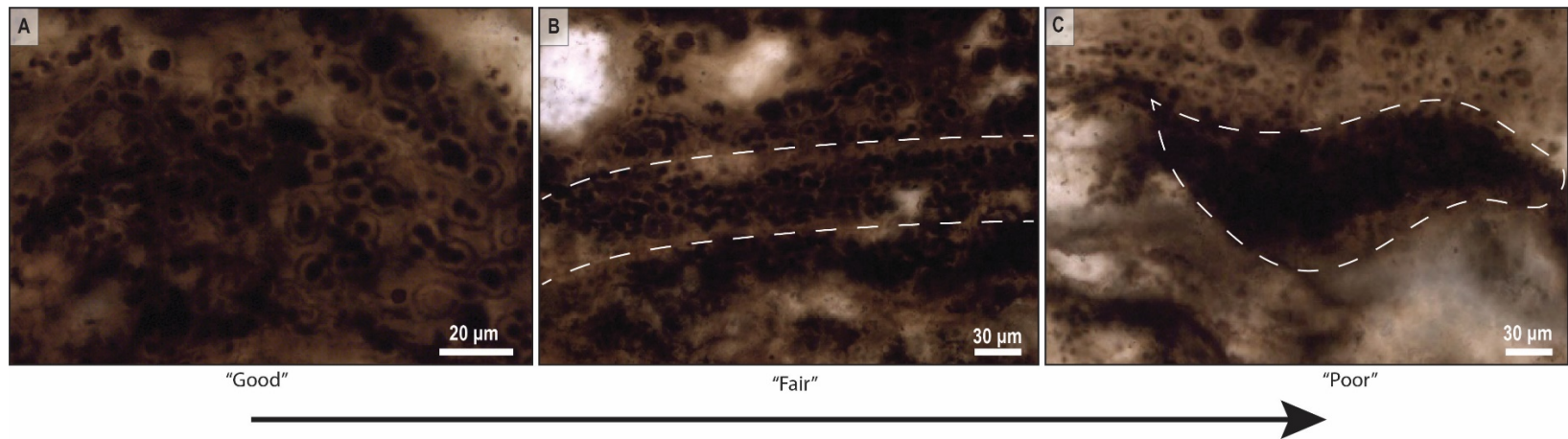


Figure 2.9 Coccoidal microfossils within “good” or “fair” mats tend to accumulate into layers of coccoidal microfossils as they decay. When the coccoidal organisms reach the taphonomic grade of “poor” the organic matter becomes homogenized and forms patches that are almost opaque.

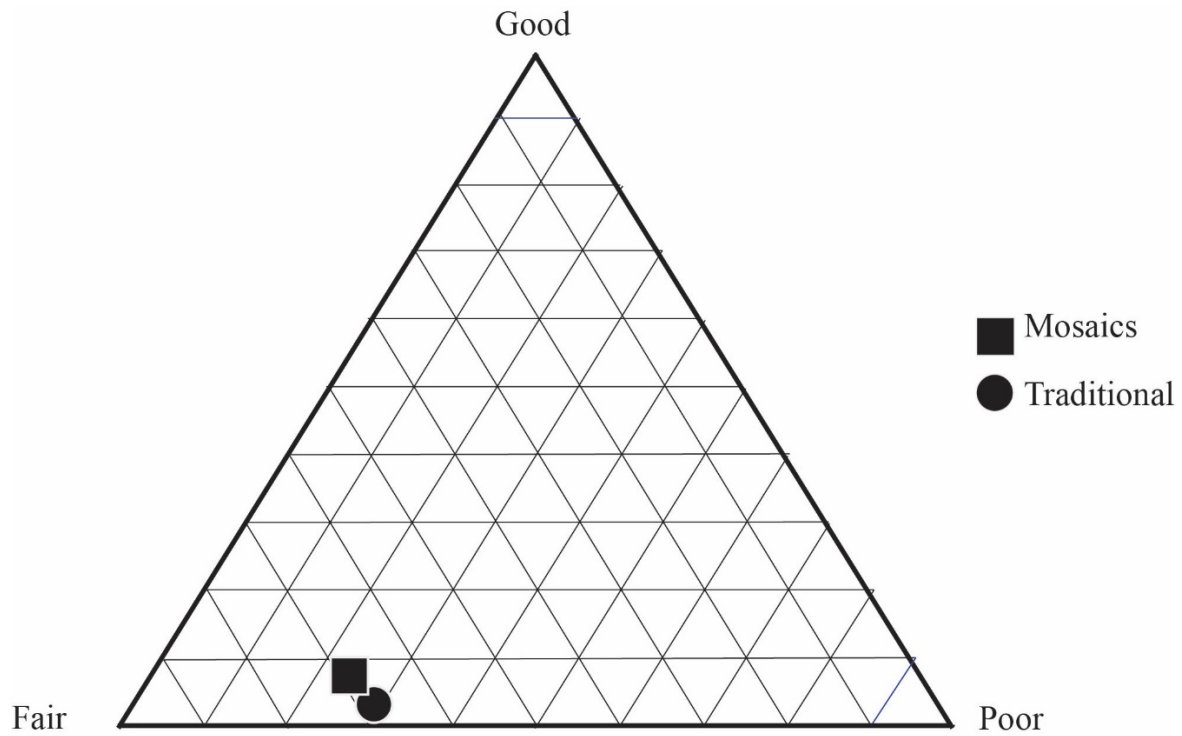


Figure 2.10 A taphonomic assessment was performed on a thin section using traditional point counting techniques on the microscope. The thin section was moved in 2 mm increments from right to left and then down and left to right. Results from this assessment were compared to point counting on an image mosaic with a grid overlay, where microfossils were counted when they were under the intersection point of two gridlines.

Table 2.1. Taphonomic assessment of the microfossils preserved in the Angmaat Formation. Individual microfossils were classified as “good,” “fair,” and “poor.” Over 600 individual microfossils were counted using the quadrat method and the percent area of unrecognizable carbonaceous matter was calculated with ImageJ over the entire thin section.

Sample	Classification	Organisms	Total Counts	Total Filament	Total Coccoid	% G	% F	% P	% area Unrec
DBG-30	Good	Coccolidal	658	75	583	20	49	31	13.1
DBG-42	Fair	Coccolidal	659	283	376	1	28	71	6.1
DBN-4	Poor	Coccolidal	643	133	510	8	34	59	2.0
DAC-15	Good	Filamentous	609	553	56	11	35	53	0.5
DAC-24	Fair	Filamentous	149	148	1	1	41	58	3.6
DAC-16	Fair	Mixed	634	614	20	0	7	93	4.2
DAC-9	Poor	Mixed	175*	162	13	0	9	91	2.6

* Microfossils are rare in this sample, and only 175 microfossils were counted after two passes on the thin section.

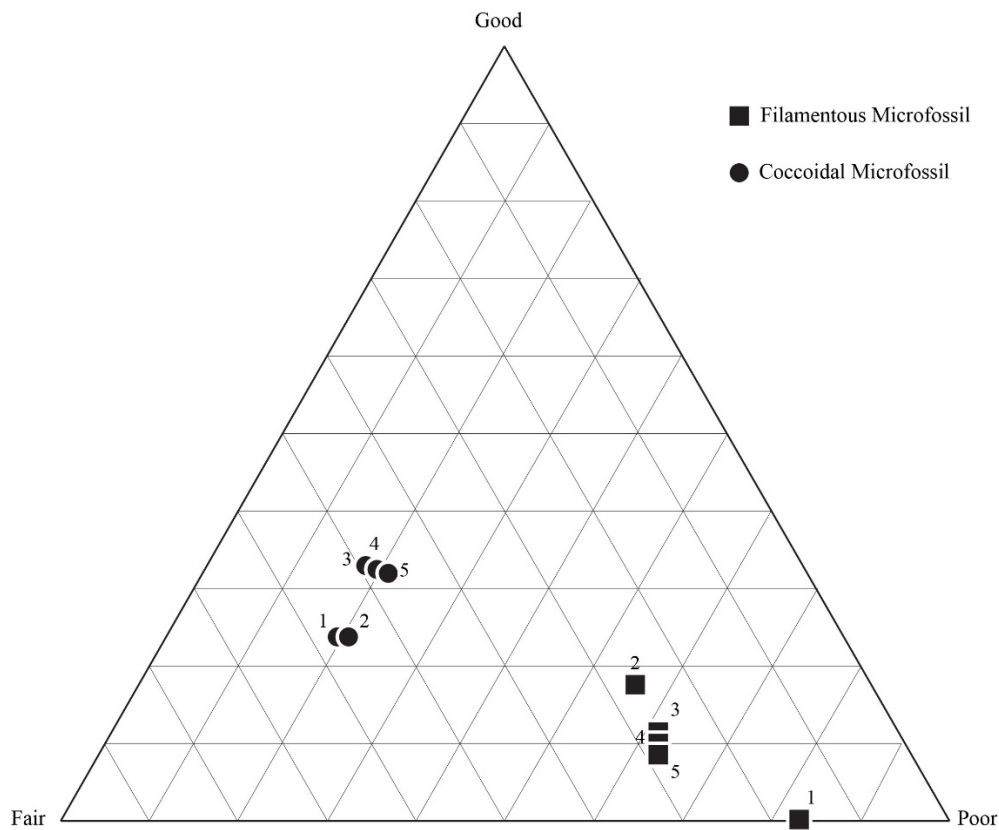


Figure 2.11 A taphonomic assessment was performed on the same sample five times. The assessments were performed on different days to judge the consistency of the observer's taphonomic assessment. Different quadrats were counted in each assessment to determine if using the quadrat sampling technique would provide a more representative assessment of the thin section.

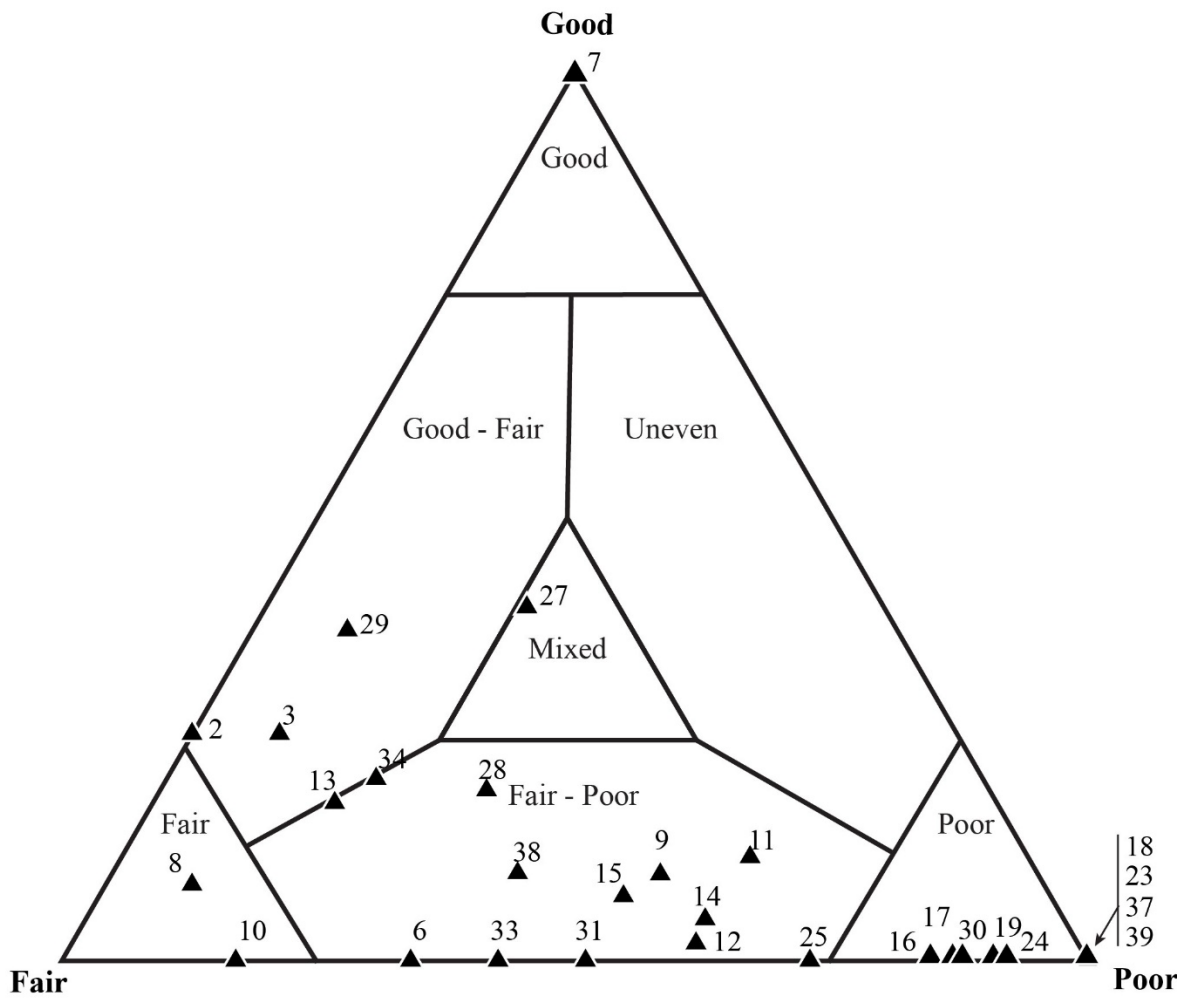


Figure 2.12 Taphonomic variation is observed from one quadrat to another. Each triangle on this ternary plot represents all of the microfossils (filaments and coccoids) that were counted and scored in one quadrat. To obtain the desired 600 microfossil count, 40 quadrats were counted. Each number corresponds to the quadrat number. Data show is for a mat taphonomically identified as "good" (DAC-15). Microfossils in this sample exhibit a wide range of preservation and plot within several of the taphonomic fields of the ternary plot (Kowalewski et al., 1995).

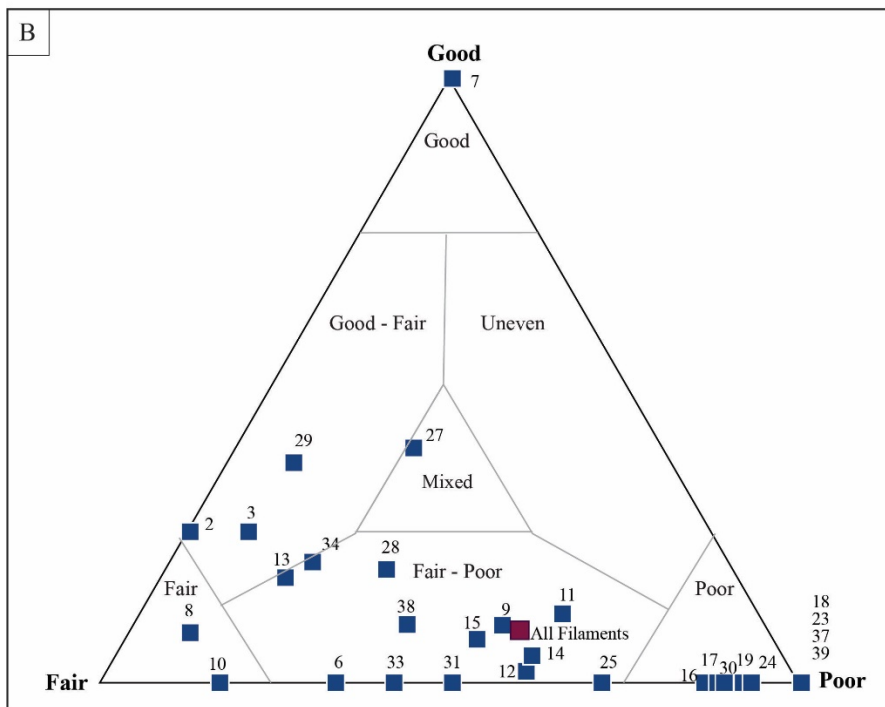
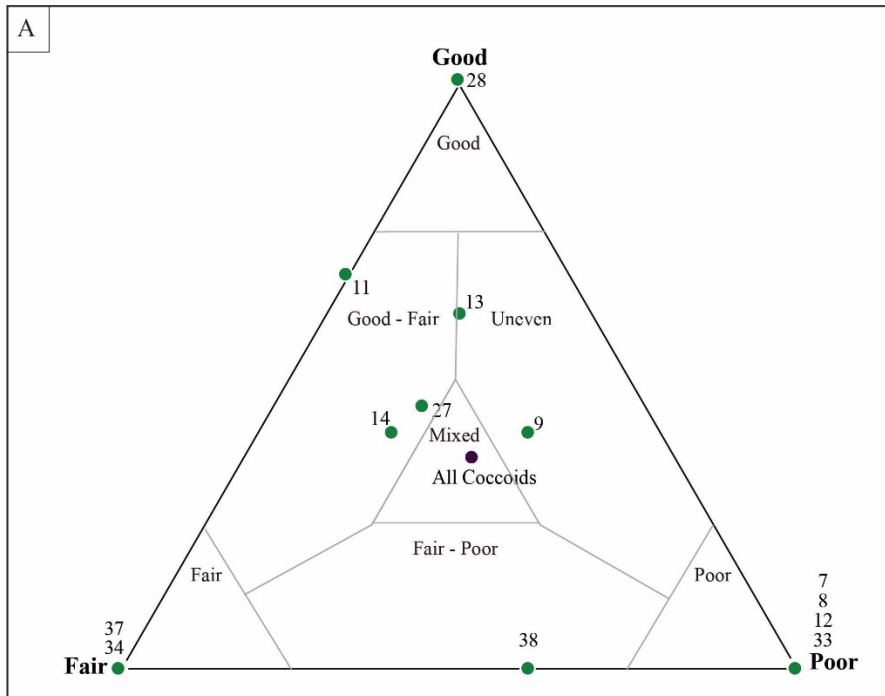


Figure 2.13 Quadrat data for DAC-15, a “good” mat fabric, plotted by the taphonomy of coccoidal microfossils (A) and filamentous microfossils (B) per quadrat. Each of the data labels represents the number of the quadrat.

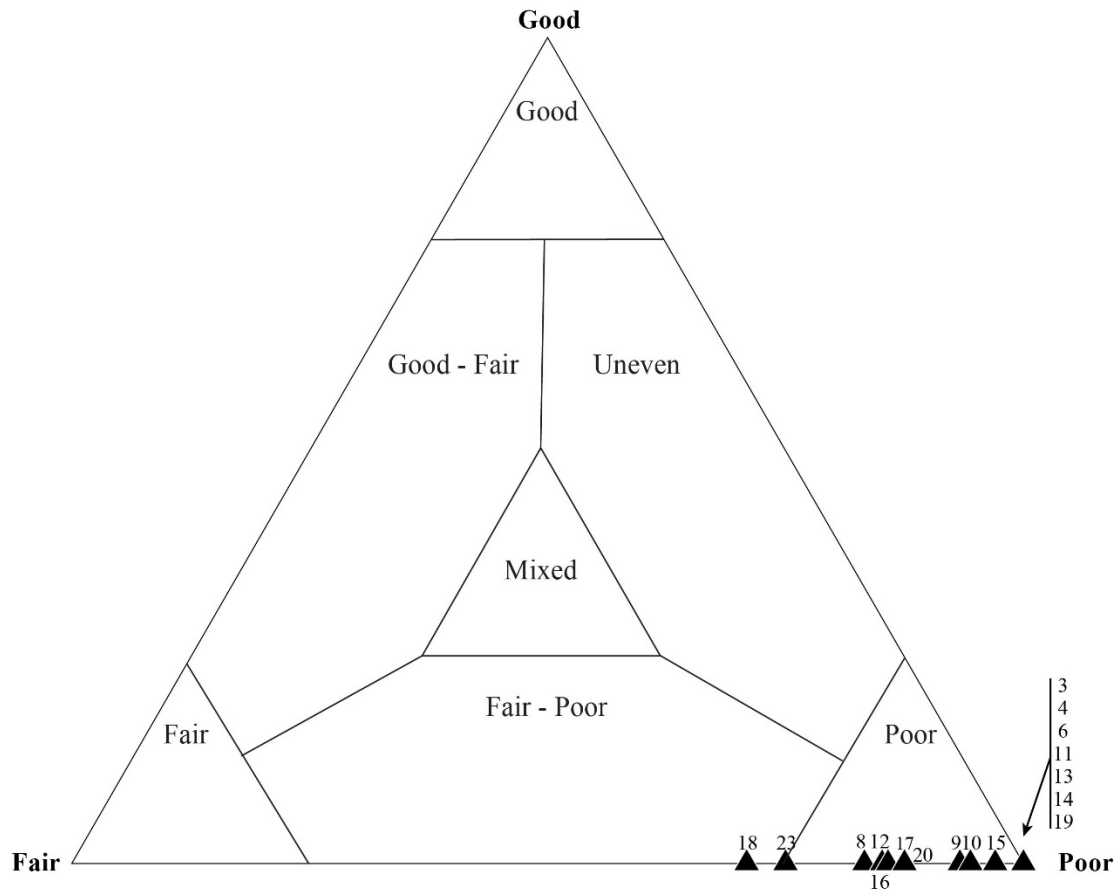


Figure 2.14 Taphonomic assessment of sample DBG-42 by quadrat for a mat fabric that is taphonomically identified as "fair." Most of the microfossils (coccolidal and filamentous) preserve within the taphonomic range of "poor."

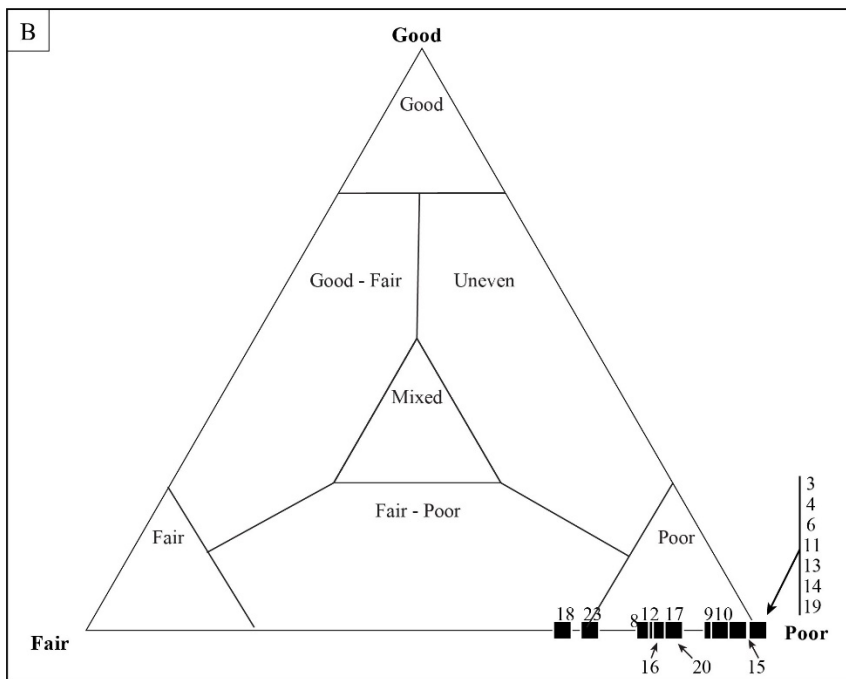
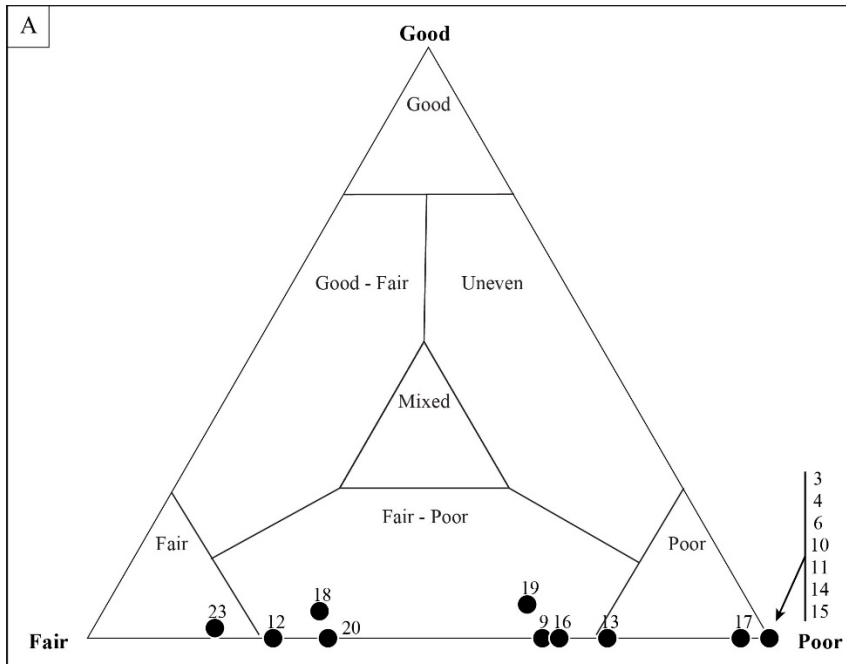


Figure 2.15 Quadrat data for DBG-42 a “fair” mat fabric, plotted by the taphonomy of coccoidal microfossils (A) and filamentous microfossils (B) per quadrat. Each of the data labels represents the number of the quadrat.

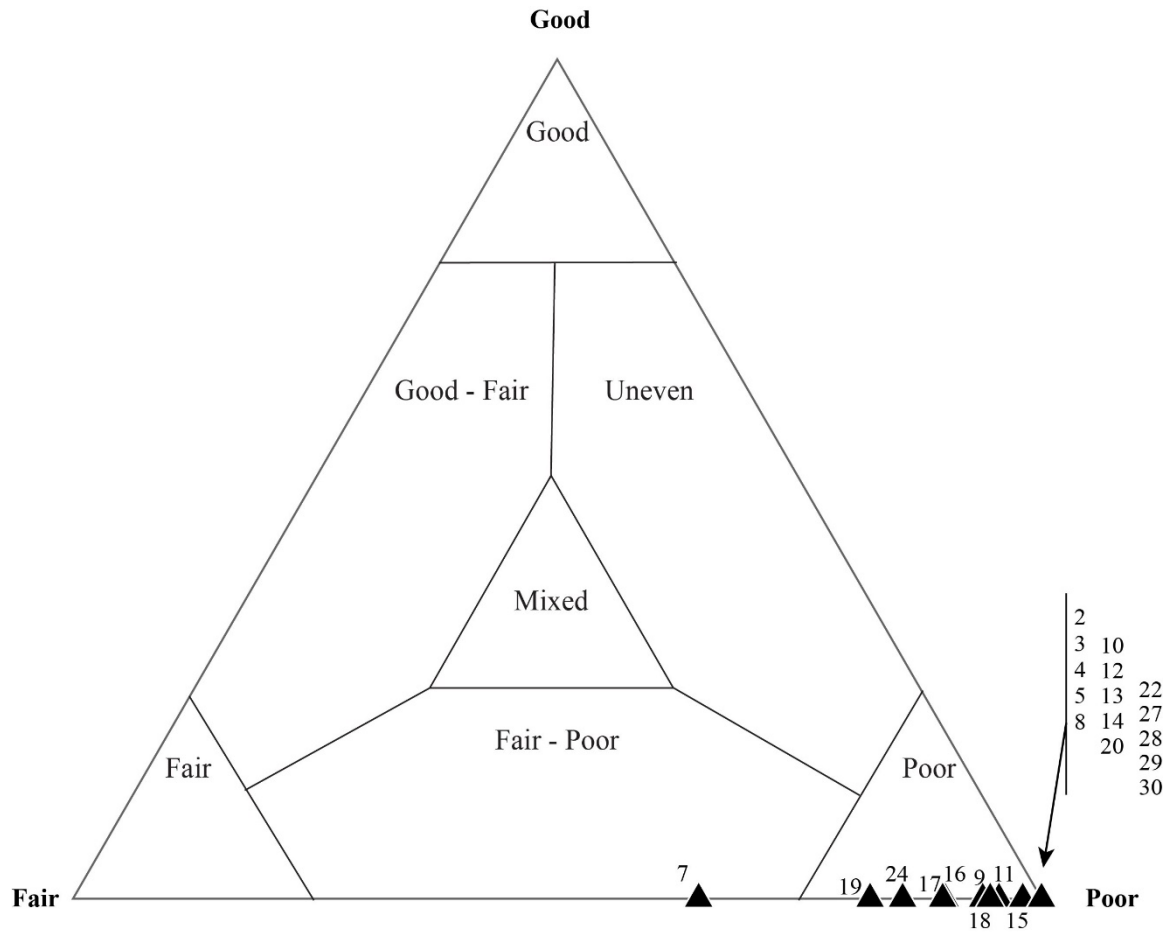


Figure 2.16 Taphonomic assessment of sample DAC-16 by quadrat for a mat fabric that is taphonomically identified as "fair." Most of the microfossils (coccolidal and filamentous) preserve within the taphonomic range of "poor."

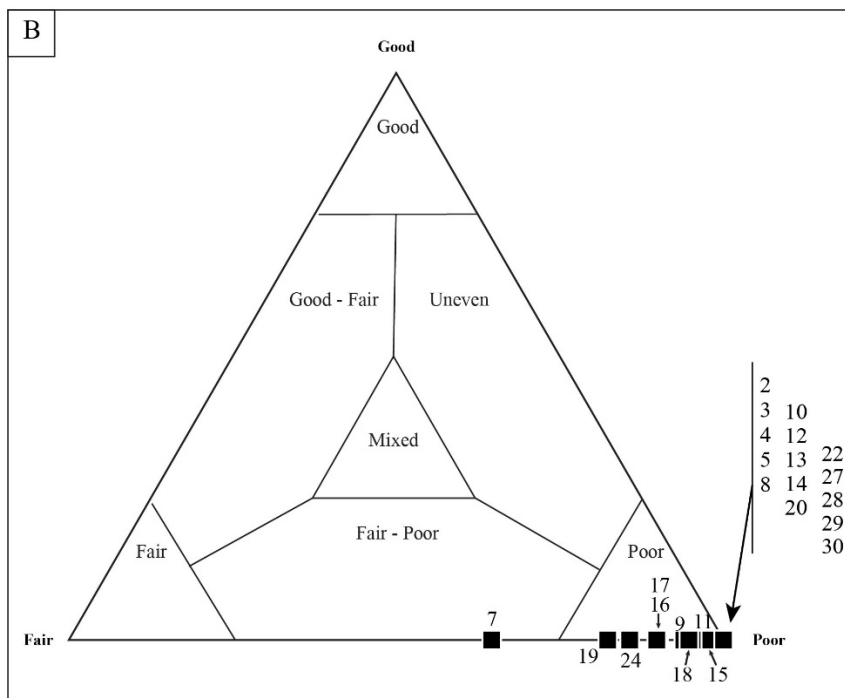
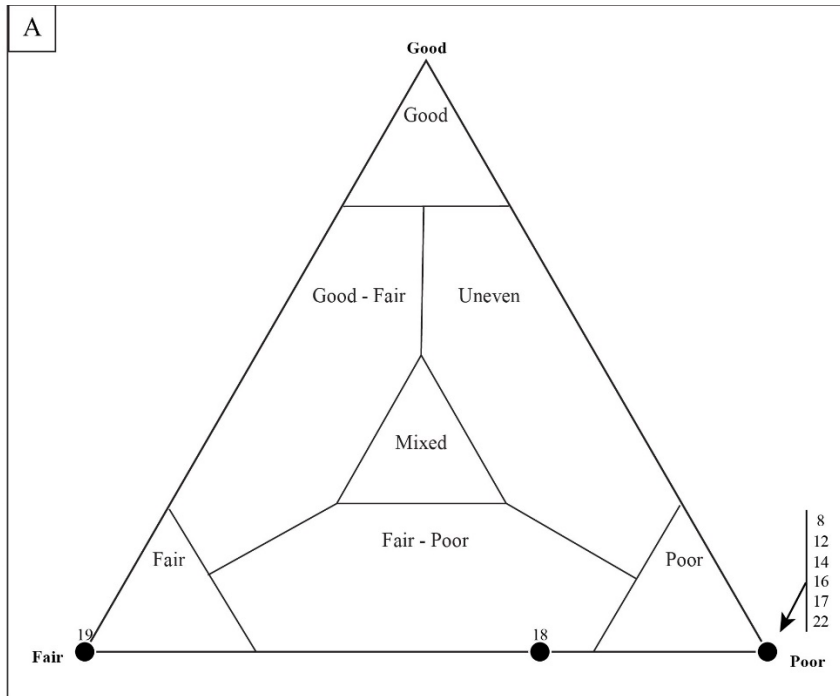


Figure 2.17 Quadrat data for DAC-16, which is identified as a “fair” mat fabric, plotted by the taphonomy of coccoidal microfossils (A) and filamentous microfossils (B) per quadrat. Each of the data labels represents the number of the quadrat.

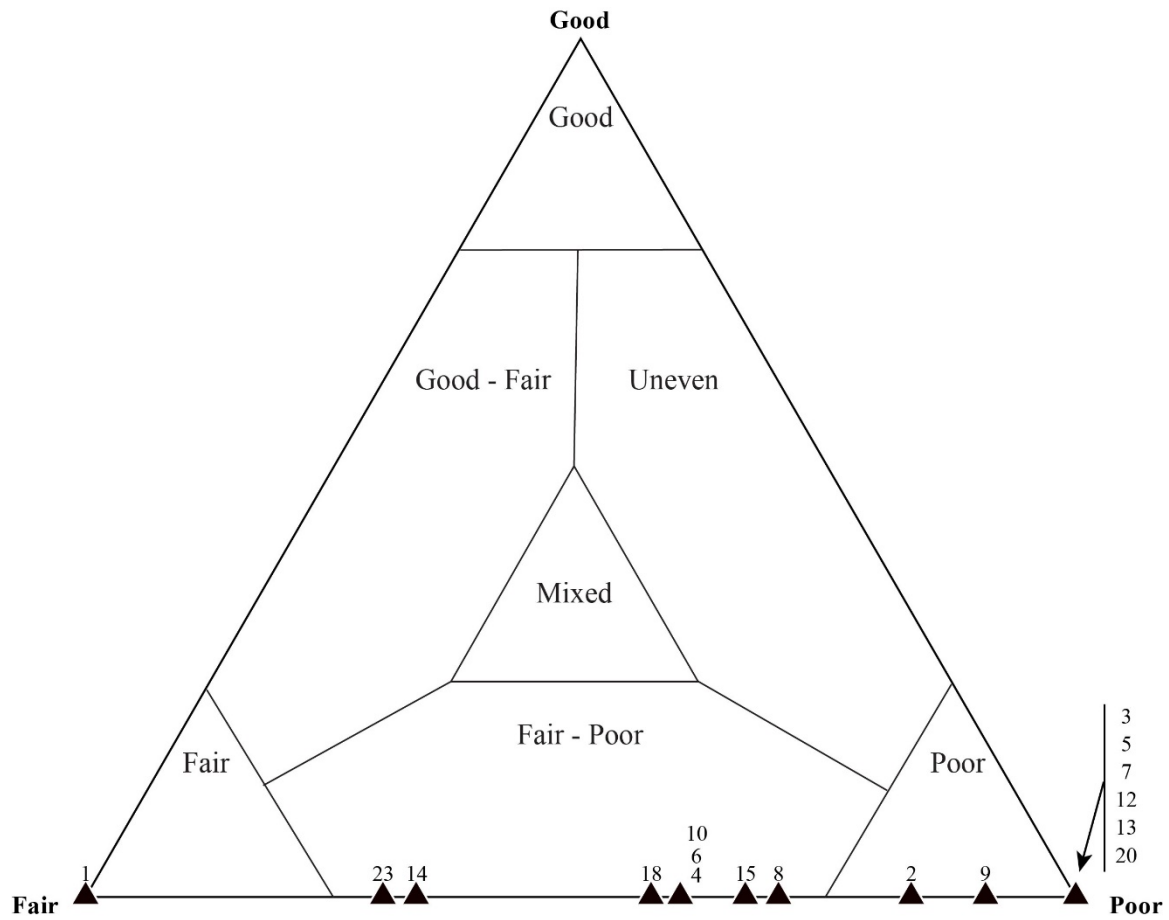


Figure 2.18 Taphonomic assessment of sample DBN-4 by quadrat for a mat fabric that is visually identified as having a “poor” taphonomic grade. Most of the microfossils (coccolidal and filamentous) preserve within the taphonomic range of “fair-poor.”

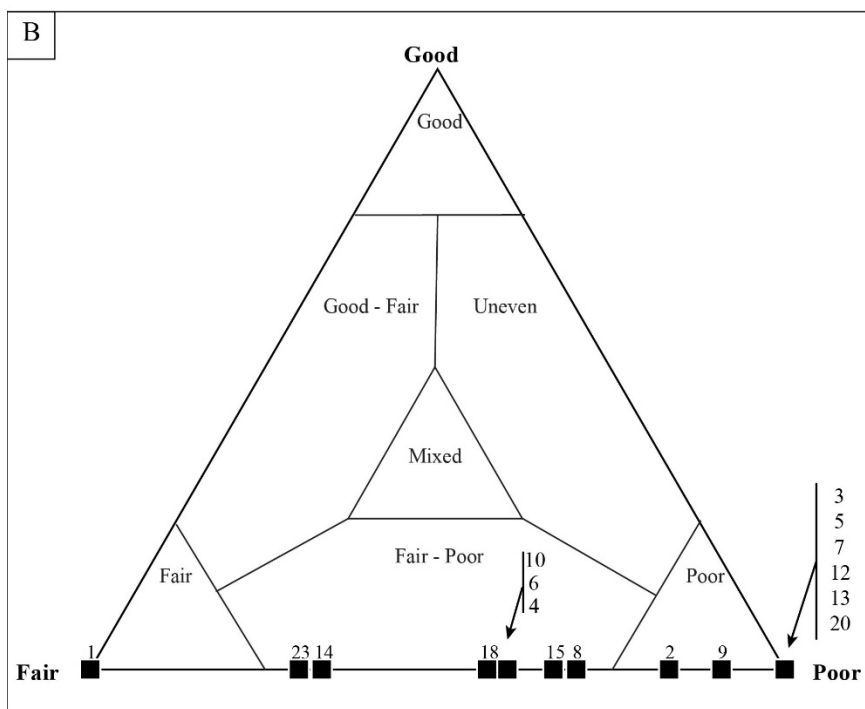
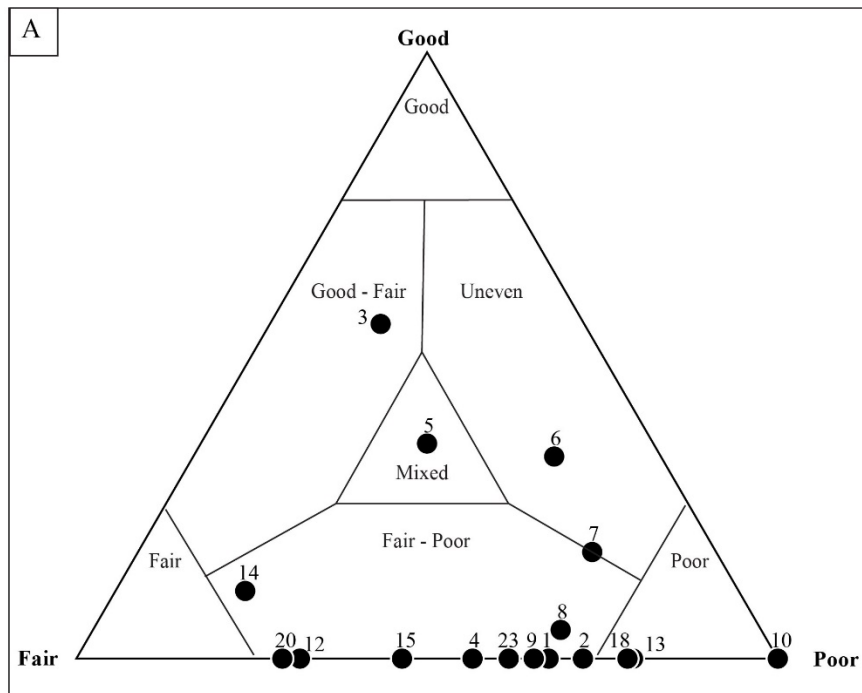
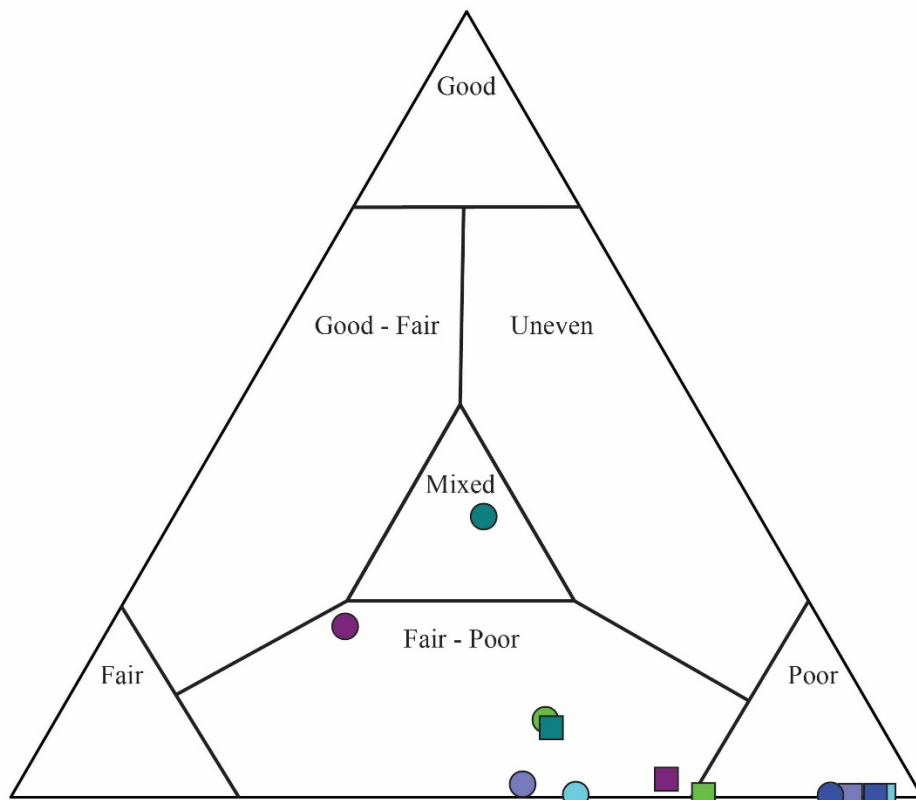


Figure 2.19 Quadrat data for DBN-4 a “fair” mat fabric, plotted by the taphonomy of coccoidal microfossils (A) and filamentous microfossils (B) per quadrat. Each of the data labels represents the number of the quadrat.



Key

- | | |
|---------------------|---------------------|
| ■ DBG-30 Filaments | ■ DAC-16 Filaments |
| ● DBG-30 Coccoliths | ● DAC-16 Coccoliths |
| ■ DAC-15 Filaments | ■ DAC-9 Filaments |
| ● DAC-15 Coccoliths | ● DAC-9 Coccoliths |
| ■ DBG-42 Filaments | ■ DBN-4 Filaments |
| ● DBG-42 Coccoliths | ● DBN-4 Coccoliths |

Figure 2.20 Quadrat data six samples with taphonomic grades ranging from “good” to “poor.” The circles represent the coccolithal microfossil data, which generally have a wider range of taphonomic preservation. Whereas the square represents filamentous microfossil data. The filamentous data plots more consistently in the “poor” taphonomic range.

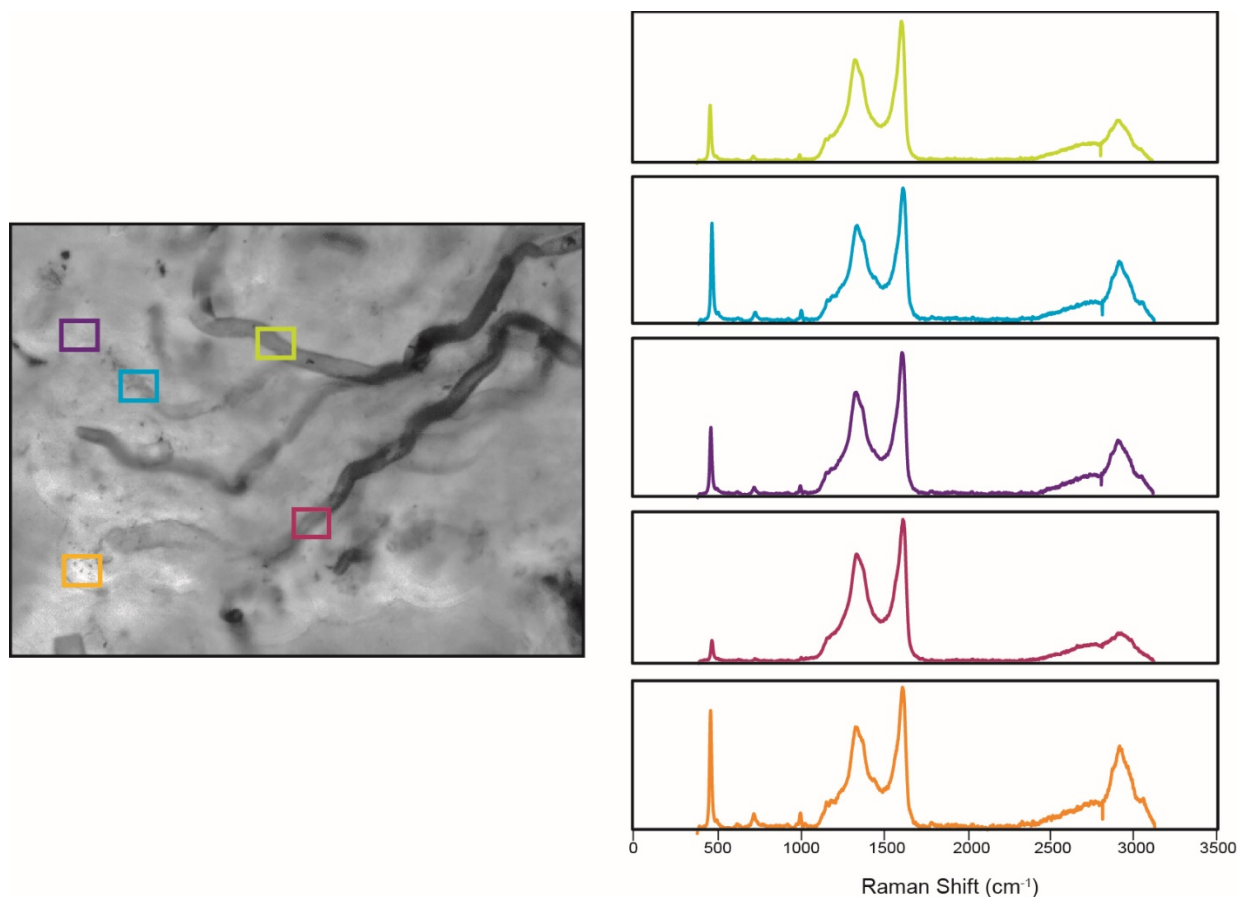


Figure 2.21 Filamentous microfossils are preserved in various taphonomic states within this figure. Each box represents a location where a Raman point spectrum was collected. The color of the Raman spectra correlate to the color box on the figure. Despite the taphonomic grade of the microfossil, the Raman spectra obtained for each box have similar patterns.

Table 2.2 Raman Index Parameters for the Angmaat Formation are around 7. Values closer to 1 are considered more highly altered samples; whereas values closer to 9 indicate less thermal alteration (Schopf et al., 2005).

Sample	Average RIP	Average SD	n
DBG-30	7.42	0.22	10
DAC-15	6.57	0.27	13
DBG-42	7.34	0.25	13
DBN-4	7.08	0.29	13
DAC-18	6.59	0.23	17
Angmaat Average	6.97	0.44	66

CHAPTER 3
GEOCHEMICAL CHARACTERIZATION OF PRESERVED LIPIDS
WITHIN SILICIFIED MICROBIAL MATS OF THE ANGMAAT
FORMATION

Abstract

Early diagenetic chert deposits are common in Precambrian strata and preserve textural evidence of primary mineral and organic components. Morphological preservation within early diagenetic chert has been used to identify both the Earth's earliest ecosystems in the Archean, and the timing of evolution of biological complexity (e.g. evolution of eukaryotes, development of multicellularity) in the Proterozoic. Such morphological preservation has also been used to suggest that silicious deposits may be effective targets for the search for extraterrestrial microbial life. Here we address two fundamental questions: (1) to what extent exceptional morphological preservation is reflected in the preservation of molecular geochemistry of the preserved mats, which can provide information about both the environment of deposition and the microbial physiology and processes active at the time of silicification; (2) whether microbial mats that visually record differences in taphonomic preservation (i.e. are more or less degraded at the time of silicification) show differences in molecular composition that can be attributed to heterotrophic microbial activity; and (3) can molecular data be retrieved from samples sizes consistent with current and developing astrobiological investigation.

Strata of the Mesoproterozoic Angmaat Formation, Bylot Supergroup, record deposition of microbial mats within an intertidal to supratidal microbial flat. Silicification preserves microbial growth and decomposition across a range of peritidal environments. Initial organic characterization showed the presence of a variety of lipids, including *n*-alkanes, hopanes, and steranes. Although data resembles that of thermally immature organic matter formed within hypersaline environments, and is consistent with independent interpretation of depositional environments, the similarity of lipid signatures between samples indicates possible post-collection contamination. To rule out such contamination, freshly collected samples were also

analyzed. Bitumen I and bitumen II extractions from these samples revealed no indication of lipids at concentrations distinguishable from background. Data presented here suggests that early diagenetic chert may be unsuitable for preservation of lipids, although these lithologies may still be suitable for analysis of non-lipid biomarkers.

Introduction

Early diagenetic chert deposits are common in Precambrian peritidal carbonate strata. These deposits preserve evidence of mineral and organic precursors and are therefore important deposits to our understanding of life on early Earth. Exceptional preservation of microbial morphologies in early diagenetic chert (Schopf, 1968; Horodyski and Donaldson, 1983; Nyberg and Schopf, 1984; Knoll, 1985; Knoll and Golubic, 1992; Schopf, 1993; Golubic and Seong-Joo, 1999; Knoll, 2012) has resulted in the suggestion that chert and silicified sediments would be a good target for the search for life on Mars (McMahon et al., 2018).

The study of microbial assemblages can increase our understanding of the chemical composition of early Earth environments (Summons et al., 1999; Brocks et al., 2005; Brocks and Pearson, 2005; Buick, 2008); however, our understanding of the geochemistry is dependent on the interpretation of preserved biosignatures and the extent to which biosignatures are retained during preservation (Wacey, 2009; Oehler and Cady, 2014). Investigation of microfossil-bearing chert has focused primarily on taxonomic identification of preserved organisms (Schopf, 1968; Horodyski and Donaldson, 1980; Schopf, 1993), or on understanding the taphonomic changes to morphology and ultrastructure (Bartley, 1996; Bartley et al., 2000; Javaux et al., 2004). Recently, more attention has been given to chemical fossils, or biosignatures, that may be preserved in chert deposits, these include isotopic data, bulk and in situ (Williford et al., 2013; Peng et al.,

2016; Williford et al., 2016; Flannery et al., 2018), the mapping of preserved elements in situ (Wacey, 2009; Wacey, 2014; Wacey et al., 2016). Molecular biomarkers in chert have been explored by Derenne et al. (2008) and Qu et al. (2015); however, techniques are still being created in attempts to accurately describe the molecular preservation preserved in ancient samples (French et al., 2015). As a way to support biogenicity in ancient samples, many of the geochemical techniques are performed on the best-preserved examples (Peng et al., 2016; Williford et al., 2016; Guo et al., 2018)

Here we present the organic geochemical characterization of silicified microbial mats from the Mesoproterozoic Angmaat Formation, northern Baffin Island. Two sets of samples, one collected in 1994 and another set collected in 2017, were used to address questions regarding the extent to which exceptional morphology. Taphonomic analysis of the 1994 samples were performed prior to any geochemical analyses to determine whether variation of preserved chemistry corresponded with differences in taphonomic preservation. Multiple sample sizes were used in this study to investigate whether molecular data can be obtained from sample sizes consistent with sample sizes expected for astrobiological samples expected to be collected by several upcoming Martian missions.

Geologic Framework

Bylot Supergroup

Approximately 6000 m of unmetamorphosed and nearly undeformed Proterozoic sedimentary rock is exposed within the fault-bounded Borden Basin of northern Baffin and Bylot islands (Jackson and Iannelli, 1981; Kah and Knoll, 1996; Kah et al., 1999; Turner, 2009). Basin development is recorded by the Eqalulik, Uluksan, and Nunatsiaq groups (Fig. 3.1) The Eqalulik Group overlies Archean and Paleoproterozoic basement and contains tholeiitic basalt overlain by

a fining upward succession of fluvial and shallow-marine sandstone and marine shale, which records initial rifting of the basin and development of a northwestward-deepening passive margin (Jackson and Iannelli, 1981; Long and Turner, 2012). In the southeastern portions of the basin, the uppermost Eقالulik Group is recorded by shallow marine carbonate, gypsum, and terrigenous redbeds of the Iqqittuq Formation (Turner, 2009).

The Uluksan Group and records the expansion of marine carbonate deposition across the basin. The Ikpiarjuk Formation consists of unusual deep-water reef deposits that mark the boundary between the Eقالulik and Uluksan groups (Hahn et al., 2015). Sea level rise at the onset of the Uluksan Group is marked by restriction of terrigenous input into the basin, by development of a prominent oolitic shoal and restricted lagoonal deposits of the Angmaat Formation (Kah, 1997; Kah, 1999), and by deep-water carbonate deposition of the Nanisivik Formation (Turner, 2009). Although chert occurs throughout the Uluksan Group, it is most abundant within restricted lagoonal deposits of the Angmaat Formation (Hofmann and Jackson, 1991; Manning-Berg and Kah, 2017). The overlying Victor Bay Formation records an increase in regional subsidence and deposition of carbonate ramp, reef, and basin sediments (Jackson and Iannelli, 1981; Sherman et al., 2001; Turner, 2009). Renewed rifting and a potential change in basin polarity is recorded in deep-water deposits of the upper Victor Bay Formation (Sherman et al., 2002), and continues into the overlying Nunatsiaq Group, which consists of a thick succession of sandstone that ultimately drowns out carbonate deposition (Sherman et al., 2002; Turner, 2009).

The maximum age of Bylot Supergroup deposition is constrained by basalt flows within the Eقالulik Group, which provide a depositional age of 1270 ± 4 Ga (LeCheminant and Heaman, 1989). Re-Os isotopic ages of black shale from the Arctic Bay Formation (upper Eقالulik Group)

and the Victor Bay Formation (upper Uluksan Group), bracket the Angmaat Formation and provides ages of 1.048 ± 0.012 Ga and 1.046 ± 0.016 Ga, respectively (Gibson et al., 2017). A late Mesoproterozoic age for the Angmaat Formation is consistent with estimates based on preserved microfossil assemblages (Hofmann and Jackson, 1991; Hofmann and Jackson, 1994) and chemostratigraphic relationships (Kah et al., 1999; Kah et al., 2012). Although strata of the Nunatsiaq Group lack discrete geochronology, Franklinian-aged dikes crosscut the entire Bylot Supergroup, and provide a minimum age of ~ 723 Ma (Pehrsson and Buchan, 1999).

Angmaat Formation chert

Chert is abundant in restricted, evaporative deposits of the Angmaat Formation. Black chert occurs as irregular nodules and lenses, and beds up between 1-10 cm in thickness (Jackson and Iannelli, 1981; Manning-Berg and Kah, 2017) (Fig 2). The lateral extent of individual lenses is typically < 1 meter, although chert lenses can comprise discontinuous beds that can be traced for > 100 meters along outcrop exposures. Black chert is interpreted to be of early diagenetic origin based on evidence for compaction of laminae around chert nodules, the presence of chert clasts in penecontemporaneous high energy event deposits, and by ubiquitous preservation of microfossils (Hofmann and Jackson, 1991) and microbial mat fabrics (Knoll et al., 2013). Microbial mat fabrics often include preservation of primary voids that are interpreted as gas bubbles within benthic mats (Hofmann and Jackson, 1991; Kah and Knoll, 1996; Knoll et al., 2013); such voids are commonly distinguishable as small, white, chalcedony-lined voids within black chert (Fig 2). In addition to lenses and beds of black chert, a variety of white, yellow, and grey chert nodules also occur within the Angmaat Formation. Multi-colored chert occurs as flattened nodules that cross-cut sedimentary bedding and show distinct layering parallel to the nodule margin (Fig. 3.2).

Within black chert of the Angmaat Formation, microbial mat communities are preserved across a range of peritidal environments, wherein persistently subaqueous and lower intertidal environments are dominated by filamentous microbes, and more frequently exposed intertidal to supratidal environments often record a greater abundance of coccoidal microbes (cf. Kah and Knoll, 1996; Knoll et al., 2013). Nearly all identified microbial constituents can be identified with cyanobacteria (see also Knoll et al., 2013). Mat building communities are represented primarily by hollow sheaths of filamentous microbes. Small-diameter (up to 5 μm), thick-walled, lightly pigmented filamentous sheaths have been interpreted as a *Lyngbya*- or *Phormidium*-type cyanobacteria and classified as *Siphonophycus* sp. (Hofmann and Jackson, 1991; Kah and Knoll, 1996; Kah et al., 1999). Large-diameter (10-70 μm), thin walled, strongly pigmented filamentous sheaths have been assigned to *Eomicrocoleus* sp. (Horodyski and Donaldson (1980), and recently interpreted to be analogous to the extant cyanobacteria *Microcoleus chthonoplastes* (Knoll et al., 2013).

Coccoidal populations preserved in Angmaat chert are variable. Within filamentous mats, coccoidal populations are most commonly represented by individual coccoids with distinct directional EPS production, identified as *Polybessurus bipartitus* (Fairchild ex Green et al., 1987), and by small pockets of thin-walled coccoids attributed to *Myxococcoides* sp. (Schopf, 1968). Mats containing more prominent coccoidal communities are mainly dominated by strongly pigmented groups of individual cells within a single enclosing envelope, identified as *Eogloeocapsa bella* (Golovenok and Belova, 1984). These mats commonly also contain individual unicells, dyads, and tetrads marked by multi-laminated envelopes and identified as *Gloeodiniopsis* sp. (Knoll and Golubic, 1979). Rare eukaryotic algae, such as the red alga *Bangiomorpha pubescens* (Butterfield, 2000), also occur in several samples.

Sample sets

Two distinct sample sets were investigated in this study. The first sample set was collected during field seasons in 1993 and 1994. These samples were collected as part of a larger stratigraphic investigation of the Iqqituq and Angmaat formation (then known as the Society Cliffs Formation) carbonate strata (Kah and Knoll, 1996; Kah, 1997; Kah et al., 1999; Kah, 2000; Kah et al., 2001). Chert samples were used to augment the sedimentological interpretation (Kah et al., 1999; Kah et al., 2001), to explore environmental trends in preserved microbiota (Kah and Knoll, 1996), and later as the basis for a more thorough investigation of the microbial communities (Knoll et al., 2013).

A second set of samples was collected during a 2017 field season with the specific intent to perform organic geochemistry on the chert samples. New samples were wrapped in aluminum foil as they were collected and were stored in cotton sample bags to avoid contamination. Samples were shipped immediately to the Astrobiogeochemical Laboratory (abcLab) at NASA's Jet Propulsion Laboratory (JPL) in Pasadena, CA, to provide the most stringent control over sample handling, storage, and curation, in an attempt to limit potential sources of contamination.

In order to potentially inform planning for *in situ* astrobiological analysis and sample-return missions, we also considered a range of sample sizes. In geologic samples, approximately 5-100 grams of whole rock are typically processed for extraction of molecular biomarkers (Price and Clayton, 1992). On the Curiosity rover, organic geochemical analyses are undertaken by the SAM (Sample Analysis at Mars) instrument (Mahaffy et al., 2012). The SAM instrument includes a gas chromatograph-mass spectrometry (GC-MS) capable of measuring organic compounds that have been thermally or chemically extracted from sample powders. Sample powder delivered to the SAM instrument, however, typically ranges from 20-50 mg for a single-portion experiment, or <150 mg for a triple-portion experiment (Abbey et al., in prep). By

contrast, the Mars 2020 rover will be equipped to retrieve drill core from the Martian surface. Drilled samples will be cached on the rover, until a later sample return mission. Upon sample return, only ~15 g of sample will be allotted for geochemical analyses (Summons et al., 2014). Because of limited sample availability, organic material was extracted from ~5g of sample powder from the 1993-1994 field season materials. Samples collected in 2017 were considerably larger, and permitted extractions using ~50 g of sample powder, and replicate extractions with ~500g of sample powder.

Methods

Figure 3.3 provides an outline of sample methods. Although extraction methods varied slightly, depending on sample size, each sample was processed with an associated procedural granitic blank to ensure identification of any contamination that may have been introduced during sample preparation and analyses.

Initial sample preparation

Twenty-three samples from material collected during a 1993-1994 field season were selected for organic geochemical analysis based on the visual taphonomic appearance of the preserved microbial mat. Mats that were selected as “good,” (3 samples) had billowy textures, silicified voids, and lacked compaction. Mats selected as “fair” (9 samples) were slightly darker in color and had multiple compacted dark, brown layers. “Poor” mats (7 samples) were often dark in color or had larger amounts of carbonate associated with the sample). Mats (3 samples) that were completely black in color and lacked lamination were identified as “unrecognizable.” Material from the 1993-1994 field seasons (23 samples) had been previously cut with a water-lubricated saw and were free of external weathering products. Sample chips were rinsed in Milli-Q water and powdered within a porcelain sleeve using a SPEX SamplePrep 8000M ball-mill at

the University of Tennessee. Porcelain sleeves and balls were cleaned between samples using 5M HNO₃ and ashed sand. A total of 5-7 grams of powder was produced for each sample.

Material from the 2017 field season (12 samples) was prepared at NASA's Jet Propulsion Laboratory. Visible lichen was removed from rock surfaces using dichloromethane and a wire brush. For materials consisting of chert and associated carbonate, as well as a single sample of microbially laminated carbonate not associated with chert, each phase was treated as separate samples to investigate the extent to which organic geochemistry are preserved in distinct mineralogical phases.

Samples were cut into billets on a water-lubricated saw using a saw blade that was ashed at 550 °C prior to use and cleaned with methanol in between each sample. Billets were used to make thin sections, and remaining material was broken into chips using a hammer that had been cleaned with a 9:1 dichloromethane (DCM) and methanol (MeOH) mix. Sample chips were sonicated in Milli-Q water for 15 minutes, rinsed, and sonicated for another 15 minutes.

Chert samples were placed in 3N HCl overnight to remove associated carbonate phases, then rinsed. A 5% HF solution was then used to etch the surface of both chert and carbonate samples to remove potential remaining surface contamination. Samples were rinsed to neutrality and allowed to dry overnight. Dry samples were powdered in a Spex Shatterbox using a zirconium puck mill that was cleaned with methanol and a DCM:MeOH prior to use. Because the puck-mill is capable of introducing contaminants, ashed sand was powdered and collected prior to each use of the puck-mill and analyzed for lipids to ensure that the puck-mill was clean. Approximately 0.25-1 g of each powdered sample was set aside for analysis of bulk $\delta^{13}\text{C}_{\text{org}}$.

Bitumen I extraction

Two extraction methods were used to extract bitumen I from the samples. A microwave extraction technique was used to extract bitumen I from the 1994 samples. This technique works best with small sample sizes (ideally around 5 g of powder) and would be the technique used in the ABC Lab for sample return from Mars 2020. The microwave technique, however, cannot be used for larger sample sizes; larger samples (50-500 g) were extracted using a Soxhlet method.

For microwave extraction, approximately 20 mL of solvent, a 9:1 DCM:MeOH mix, was added to 5-7 g of powdered sample to extract potential lipids. The sample was then placed in a CEM MARS 6 Microwave Digestion System and heated to 100 °C for 15 minutes in pressurized Teflon tubes. Solvent was decanted and poured over a 2 µm glass filter, and another 20 mL of solvent was mixed with the sample powder. This process was repeated a total of 3 times to ensure extraction of all the bitumen. After the final extraction, the solvent and powder were removed from the Teflon tube and filtered through the glass filter to retain the remaining solid sample. The powder remaining on the filter was dried and was stored in an ashed glass vial. Approximately 1 g of the remaining powder was set aside for $\delta^{13}\text{C}_{\text{kerogen}}$ analyses and 3 g was saved from a few of these samples for bitumen II extraction.

Samples larger than 10g were extracted via Soxhlet extraction. Approximately 50 g of powder was placed in a cellulose thimble inside a glass Soxhlet and extracted with 60 mL of a 9:1 DCM:MeOH mix. Copper was placed in the bottom of the flat-bottom flask to remove sulfur compounds from the extract. Soxhlets were filtered for 48 hours before the solvent was collected. Remaining powder and thimble were dried and stored in ashed glass vials. Approximately 1 g of the remaining powder was set aside for $\delta^{13}\text{C}_{\text{kerogen}}$ analyses and 3 g of sample was retained from some samples for bitumen II extraction.

Solvents remaining from microwave and Soxhlet extractions were then evaporated using a Rocket evaporator until ~1 mL remained. Each sample was pipetted into an alumina column to remove fine-grained sediment (<2 μm). The total lipid extract was dried down with nitrogen then brought up in Hexane for analysis on a Thermo Scientific Trace Ultra Gas Chromatograph connected to a Thermo Scientific ISQ Series quadrupole mass spectrometer. Helium was used as the carrier gas and the GC was fitted with a 60m Agilent DB-5ms column. One microliter of sample in hexane was injected in splitless mode onto the column which was held at 40°C for two minutes, ramped to 150°C at 10°C per minute, then to 315°C at 3°C per minute where it remained for 20 minutes. Compounds were identified based on retention time, their fragment spectrum, and identified using the NIST GC library. Three samples were further separated into their organic fractions (i.e. saturate, aromatic, and polar fractions) using the methods described by Bastow et al. (2007) to decrease the background-to-noise ratio in the chromatographs.

Bitumen II extractions

Bitumen II was extracted from a subset of samples that included 6 samples collected during the 1993-1994 season and 6 samples collected in the 2017 season. Samples from the 2017 season include both chert samples (4) and chert-associated carbonate samples (1) and one carbonate sample. The same methodology, adapted from Stueken et al. (2015) and French et al. (2015), was used to extract bitumen II from each of these 12 samples. To make sure contaminants were not introduced during the digestion process, Teflon boiling stones were processed through the HF digestion and bitumen II extraction method to verify that the process did not introduce contamination. Teflon boiling stones were selected because they do not dissolve in HF acid. Approximately 3 g of powder remaining after bitumen 1 extraction was weighed into a Teflon test tube. Addition of 6N HCl assured removal of any of carbonate phases.

Although carbonate had been removed from 2017 season chert samples prior to initial powdering, potential carbonate phases had not been removed from the 1993-1994 season samples in an effort to retain as much sample as possible (as envisioned for samples from a Mars sample return mission). Once the reaction ceased, samples were sonicated for an hour to assure reaction completion. Liquid was decanted, and samples were rinsed three times with Milli-Q water.

Following reaction with 6N HCl, HF (48%) was added to the powder to remove silicate phases. Once visible reaction stopped, samples were agitated on a shaking table to assure reaction completion. After approximately 12 hours, samples were spun down in a centrifuge and the supernatant acid was decanted. A BF_3 solution (Stueken et al., 2015) was added to the sample, which was then sonicated for an hour to ensure that the solution interacted with the entire sample. After centrifuging the sample, the solution was decanted, and the sample was rinsed with hot Milli-Q water, sonicated for 15 minutes, centrifuged, decanted, a total of three times. Following the final rinse, solution was decanted, and the sample was freeze dried for two days. Once dry, bitumen was extracted via using a 9:1 DCM:MeOH mix. The extraction step was repeated three times to ensure that all bitumen was removed.

The extracted bitumen and solvents were evaporated using a Rocket evaporator until ~1 mL remained. Each sample was pipetted over glass filter above an alumina column to remove fine-grained sediment (<2 μm). The total lipid extract was dried down with nitrogen then brought up in Hexane for analysis on the GCMS. Helium was used as the carrier gas and the GC was fitted with a 60m Agilent DB-5ms column. One microliter of sample in hexane was injected in splitless mode onto the column which was held at 40°C for two minutes, ramped to 150°C at 10°C per minute, then to 315°C at 3°C per minute where it remained for 20 minutes. Compounds

were identified based on retention time, their fragment spectrum, and identified using the NIST GC library.

Carbon isotope ratios

Total organic carbon (TOC) was measured for each sample, and carbon isotopes were measured of both bulk organic matter ($\delta^{13}\text{C}_{\text{org}}$) and kerogen ($\delta^{13}\text{C}_{\text{kerogen}}$). For analysis of bulk organic matter, approximately 0.25 g to 1 g of bulk sample powder was set aside prior to the extraction of bitumen. These aliquots included mixed carbonate-chert phases (from 1993-1994 season samples), chert phases with carbonate removed (from 2017 season samples) and carbonate phases (from 2017 season samples). Once bitumen I is extracted, only the mineral matrix and insoluble kerogen remains in the sample powder. For analysis of kerogen, a 0.5 to 1 g aliquot of powder was set aside before extraction of bitumen II.

Sample preparation was identical for all samples. Samples were acidified for 24 hours in a 30% HCl solution to remove carbonate phases, washed to neutrality, and dried at 50°C. Carbonate-free residues were weighed into tin capsules and organic carbon converted to CO₂ for isotopic analysis using a Costech 4010 elemental analyzer coupled to a Thermo Fisher Delta V Plus stable isotope ratio mass spectrometer via a Thermo Fisher ConFlo IV interface. The mean range of values between duplicate samples for TOC (% C_{org}) was less than 2% of the measured abundance. Raw $\delta^{13}\text{C}_{\text{org}}$ isotope values were corrected using a dual point calibration (Coplen et al., 2006) with NBS19 (limestone, 1.95‰) and LSVEC (lithium carbonate, -46.6‰), and expressed in delta notation.

Blanks

Contamination was a concern throughout sample preparation and analysis. At various points during the sample preparation methods, including crushing the samples into powders, and

digesting the powders for bitumen II extraction, contaminants could be introduced to the samples. To ensure that contamination was not introduced to the samples, a granite, collected just outside of JPL was used as a procedural blank. The granite was treated like every other sample and went through each step that the Angmaat Formation samples. During the crushing of the samples, ashed sand was powdered in the ball-mill and puck-mill and analyzed as part of the sample set to ensure that the mill was clean. For the HF digestion process, Teflon boiling stones were used as a blank and analyzed the same way all of the bitumen II examples. Teflon boiling stones were used instead of sand because they do not dissolve in HF acid.

Results and Interpretation

Bitumen I extracts

Despite restricted sample amounts, materials collected during the 1993-1994 season show evidence a wide variety of lipids, including n-alkanes, hopanes, and steranes. Lipids fragment in specific patterns in the mass spectrometer; therefore, primary evidence for such lipids is identified by ion chromatograms that focus on specific mass fragments – *n*-alkanes typically fragment at a mass charge (m/z) of 85, hopanes fragment at a m/z of 191, and steranes fragment at a m/z 217. Within the m/z 85 ion chromatogram, an even-over-odd carbon preference is observed for all of the 1994 samples. A representative subset is shown in figure 3.4. The m/z 191 ion chromatograms also show evidence of preserved hopanes in these samples, with peaks in the $t = 45$ and 70 minutes range. The m/z 217 ion chromatograms for each of the 1994 samples also contain evidence for steranes, with visible peaks between 50 and 70 minutes (Fig. 3.4).

The even-over-odd predominance in the *n*-alkanes (Fig. 3.5) is indicative of a hypersaline, carbonate environment (ten Haven et al., 1988). Carbon predominance is typically lost with increased degradation and thermal alteration (Peters et al., 2007); therefore, the

presence of an even-over-odd predominance suggests that extracted organic matter is thermally immature. Thermal maturity can also be determined based on the relative stability of C₂₇ hopanes (Peters et al., 2007). During catagenesis, the C₂₇ 17 α -trishnorhopane (Tm) is less stable than the C₂₇ 18 α -trishnorhopane II (Ts) (Seifert and Michael Moldowan, 1978). The Ts/(Ts+Tm) ratio is dependent on source and maturity of the organics and is commonly used as a thermal maturity indicator (Seifert and Michael Moldowan, 1978; Moldowan et al., 1986; Peters et al., 2007) The Ts and Tm peaks (Fig. 3.5) are observed in the m/z 191 ion chromatograms at t= 51.5 and t=52.5 minutes, respectively. Higher peaks of Tm in each of the samples indicate that the organic matter has experienced little thermal alteration. The Ts/ (Ts+Tm) ratio is 0 for immature organic matter and 1 for mature organics (Peters et al., 2007). The ratio for the Angmaat Formation samples is 0.30. Hopanes seen at the end of the m/z 191 ion chromatogram are the C₃₁-C₃₅ hopanes, which are commonly preserved in bitumen from a carbonate-rich environment (Subroto et al., 1991). Peaks between 50 and 70 minutes in the m/z 217 ion chromatogram are interpreted to represent sterane peaks, however, the identification of the steranes cannot be performed on the single quad GC-MS used in these analyses.

In sharp contrast to the wide variety of lipids obtained from samples from the 1993-1994 season, chromatograms from chert samples and chert-associated carbonate samples collected in 2017 lack evidence of preserved lipids, despite much larger sample sizes (Fig. 3.6). Peaks observed in the total ion chromatograms of these samples are identified as siloxane compounds (Fig. 3.7). Siloxane is a compound within the column used in the gas chromatograph and represents contamination from the GC itself. In some of the samples, peaks observed in the m/z 85 ion chromatogram between 60 and 70 minutes are identified as phthalates (Fig. 3.7). No evidence of hopanes are observed in the m/z 191 ion chromatograms, although peaks are seen

around 21 and 25 minutes each of the samples. Peaks within the m/z 191 ion chromatogram are observed around $t=21$ minutes and $t=23$ minutes. The first peak is identified as phenol (formula: $C_{14}H_{22}O$) with a molecular weight of 206. The peak seen around $t=23$ minutes is identified as diethyltoluamide, a mosquito repellent known as DEET (Fig. 3.8). There is some variation (± 5 minutes) in the timing at which the phenol and DEET compounds elude from sample to sample. In most cases, the m/z 217 ion chromatograms also lack peaks that are readily distinguished from background.

The chert-associated carbonate samples show the same peaks as those identified in the ion chromatograms of the chert samples. The carbonate sample also contains the peaks for phenol and DEET. Pristane (formula: $C_{19}H_{40}$; molecular weight of 268 g/mol) is also identified in the m/z 85 ion chromatogram (Fig. 3.9) of the carbonate sample; however, phytane (C_{20}), which should be present as a doublet with the C_{18} peak, was not observed in the chromatogram.

Bitumen II extracts

The bitumen II chromatograms for the 1994 samples, the 2017 chert samples and the 2017 chert-associated carbonate samples do not contain evidence for the presence of *n*-alkanes, hopanes, or steranes. There are two prominent peaks in most of the chromatograms, which elude around $t= 39.8$ minutes and $t= 46$ minutes (Fig 3.10). These peaks are identified as fatty acid methyl esters, specifically palmitic acid and stearic acid. Fatty acid peaks are not observed in the chromatograms of the Teflon boiling stones. To determine if the fatty acids observed in the chromatograms were indigenous to the bitumen II extracts hexane was run over a glass filter and an alumina column. The fatty acid methyl esters were present in the hopane when it was analyzed with the GC-MS; therefore, it is likely that the glass filter was the source of contamination.

Carbon isotope ratios

Total organic carbon (TOC) for samples range from 0.03-15.86 % carbon (Average = $0.889\% \pm 2.6$, n=37). Mixed carbonate-chert samples from the 1993-1994 season averaged 0.412% (n=23); chert-only samples from the 2017 season averaged $0.08\% \pm 0.00$ (n=10); and chert-associated carbonate samples from the 2017 season averaged $2.25\% \pm 0.01$ (n=3). The carbonate-only sample had a TOC value of $15.86\% \pm 0.18$ (n=1). This data indicates that, despite the exquisite morphological detail of organic constituents preserved within chert phases, the actual concentration of organic material is quite low. This is noted particularly in comparison of season 2017 chert and chert-associated carbonate samples, which record a difference of nearly 2.18% TOC between the two phases.

Carbon isotopes composition of bulk organic matter in samples from the 1994 season range from -30.83‰ to -27.54‰ (averaging $-27.70\text{‰} \pm 0.01$, n=23). Carbon isotope composition of the kerogen for these samples are slightly heavier, ranging from -30.83‰ to -27.54‰ (averaging $-28.89\text{‰} \pm 0.18$, n=12). Similarly, carbon isotope composition of bulk organic matter from samples collected in 2017 range from -30.71‰ to -5.40‰ , where the isotopic composition of chert averaged $-21.75\text{‰} \pm 0.60$ (n=10), the isotopic composition of chert-associated carbonate averaged $-24.57\text{‰} \pm 0.09$ (n=3), and the isotopic composition of the single carbonate sample was -27.90‰ . Chert samples from 2017 season have substantially higher errors associated with isotopic measurements ($\pm 0.6 \text{‰}$ rather than $\pm 0.01 \text{‰}$), likely resulting from low TOC in the samples. To produce reliable isotopic data, each sample needed to contain 24 μg of carbon. However, to meet this requirement, several of samples required up to 2 g of powder be placed used for EA-IRMS analyses, which prevented the samples from fully

combusting in the elemental analyzer. These higher errors, however, do not affect the average compositions of samples.

In general, isotopic compositions fall within the range expected for $\delta^{13}\text{C}_{\text{org}}$ of photosynthetic bacteria, which is expected to have an isotopic value around $-25 \pm 5\%$ (Hayes et al., 1999; House et al., 2000; Schidlowski, 2000). Although values between -12 and -17% are commonly reported for cyanobacteria (Oehler, 1976; Schidlowski et al., 1984), Moers et al. (1993) report isotopically enriched organic carbon ranging from -1.7 to -7.7% from hypersaline, intertidal, carbonate environments. Cyanobacteria in hypersaline mats do not exhibit large isotopic fractionations because the availability of CO_2 for photosynthesis is reduced (Schidlowski et al., 1984; Moers et al., 1993). The heavier isotope values observed in the Angmaat Formation chert and chert-associated carbonate samples (heavier than -10% ; Schidlowski et al., 1994) may be a reflection of the depositional environment and represent preservation of organic productivity under evaporative conditions.

Discussion

Preservation of organic compounds in chert

The GC-MS spectra collected from mixed chert-carbonate samples from the 1993-1994 season exhibit a wide range of lipids, including n-alkanes, hopanes, and a variety of steranes. At its face, these results are exciting. An even-over-odd carbon preference within n-alkanes is a common characteristic of marine organic matter within hypersaline, evaporative carbonate environments (ten Haven et al., 1988; Peters et al., 2007). This is consistent with previous environmental interpretations of the Angmaat Formation (Kah and Knoll, 1996; Kah, 1997; Kah et al., 1999; Kah et al., 2001; Turner, 2009, 2011), as well as with the occurrence of silicified gypsum and halite crystals within Angmaat cherts (Kah et al., 2001; Manning-Berg and Kah,

2017). Additionally, because carbon preference is reduced during thermal alteration (Peters et al., 2007), the strong even-over-odd preference recorded in the data is consistent with independent interpretation of thermal immaturity of preserved organic matter from Raman spectroscopy data collected on 12 of the 1994 samples (RIP values around 7; Schopf et al., 2005; Manning-Berg et al., *in prep*), and supports the hypothesis that early diagenetic silicification may aid in the geochemical preservation of organic compounds (Derenne et al., 2008; Oehler and Cady, 2014; Qu et al., 2015).

The presence of hopanes and steranes are also consistent with petrographic observations of Angmaat chert (Hofmann and Jackson, 1991; Kah and Knoll, 1996; Knoll et al., 2013). Hopanes are the chemical break down products of hopanoids, which are compounds found in the cell walls of prokaryotic organisms (Peters and Moldowan, 1993; Summons et al., 1999; Brocks and Summons, 2003; Newman et al., 2016; Schwarzbauer and Jovančićević, 2016b). The primary microbial constituents preserved within Angmaat chert include filamentous sheaths analogous to those produced by modern *Lyngbia*, *Phormidium*, and *Microcoleous* cyanobacteria (Knoll and Golubic, 1992; Knoll et al., 2013). Although many Proterozoic coccoids are not uniquely identifiable to specific species (e.g. myxococcoides), Angmaat chert also contains abundant forms analogous to modern *Gloeocapsa*, and an unnamed polybessurus-like cyanobacteria (Knoll and Golubic, 1992).

The presence of steranes is particularly interesting. Steranes are the chemical break down products of steroids, which are compounds found in the cell walls of eukaryotic organisms (Peters and Moldowan, 1993; Brocks and Summons, 2003; Volkman, 2003; Newman et al., 2016; Schwarzbauer and Jovančićević, 2016b). Eukaryotic organisms are not uncommon by the late Mesoproterozoic. Abundant unicellular eukaryotes have been identified in Mesoproterozoic

shale (Javaux et al., 2001, 2004; Javaux and Knoll, 2016), and the multicellular red alga, *Bangiomorpha pubescens* (Butterfield, 2000) has been identified in Angmaat chert (Knoll et al., 2013). The preservation of steranes in these samples, however, would indicate that eukaryotic organisms were predominant enough in the environment to be preserved (Blumenberg et al., 2012). The oldest evidence of preserved steranes occur in the 1.64 Ga Barney Creek Formation (Brocks et al., 2005; French et al., 2015; Gold et al., 2017). Steranes in the ~1.1 Ga Angmaat Formation would therefore be some of the earliest preserved steranes.

Alternatively, the presence of a wide variety of lipids recorded in the 1993-1994 sample set may indicate contamination of the samples, either within the geologic environment, or after collection. The data from each of the 23 samples from the 1993-1994 season are remarkably similar (cf. Fig 3.4), regardless of the visual taphonomic grade of the sample or the predominant microbial constituents. These similarities suggest that observed lipids are not syngeneic to the Angmaat samples. Furthermore, bitumen I extracts from chert and chert-associated carbonate samples collected in 2017 do not show similar patterns to the those of the lipids preserved in the 1994 samples. Instead, all of the 2017 samples lack preserved lipids, except for the contaminants discussed earlier.

Another mechanism of determining whether preserved lipids are indigenous to the rock is via bitumen II extraction. Bitumen I extraction recovers soluble (non-kerogen) organic matter that occurs on the surfaces of the powdered sample, a substantial fraction of which may be represented by organic matter along grain boundaries. By contrast, the bitumen II extraction process involves dissolution of original mineral matrix, and therefore recovers soluble (non-kerogen) organic matter that was preserved *in situ* within mineral grains (Fig. 3.11, Wilhelms et al., 1991; Sherman et al., 2007). Chromatograms from bitumen II extractions (including mixed

chert-carbonate samples from the 1993-1993 season, chert from the 2017 season, and chert-associated carbonate from the 2017 season) lacked evidence for *n*-alkanes, hopanes, and steranes (Fig. 3.12). The lack of preserved lipids in these samples suggests that the lipids preserved in bitumen I extracts are, in fact, contamination.

Sources of contamination

A significant amount of effort went into establishing sample preparation methods that did not introduce organic contaminants to the Angmaat Formation chert samples. This is a critical step for the analysis of any organic matter (cf. French et al., 2015; Fox et al., 2017). In terms of ancient samples, which are commonly used to constrain early life on Earth, the syngeneity of hydrocarbons in Archean rocks have been called into question and deemed to be the result of contamination by younger organic molecules (French et al., 2015). Producing a method that has the lowest blank possible will also be crucial for any extraterrestrial samples return mission.

Spectra of each of the procedural blanks used during sample preparation indicate that, with the exception of the bitumen II methodology, the methods used to prepare the Angmaat Formation chert samples for bitumen I analyses did not introduce organic contamination (Fig. 3.13). However, several contaminants were found in the spectra of the 2017 samples, both chert and chert-associated carbonate (Table 3.1). The most prevalent contaminant in the 2017 samples was DEET, which was used by the field party that collected the samples, in addition to mosquito netting, as a mosquito repellent. It is likely, therefore, that this compound was introduced to the samples during field collection. The absence of such contaminants in samples from the 1993-1994 season likely reflects colder climates and the absence of mosquitos during those field seasons.

Peaks indicative of phthalates were identified in a few of the samples from the 2017 field season. Both chert and chert-associated carbonates were contaminated with phthalates; however, the source of the phthalates is not known. Fyrol fr 2, a fire retardant, was also identified in two spectra of chert samples from the 2017 field season. The source of this compound is not known. Phenol compounds, common to most plants (Vermerris and Nicholson, 2006), were also identified in all of the spectra from the 2017 samples. Phenol compounds are common, so a specific source of the contamination was identified. Other potential contaminants, including ergosterol, squalene, diploptene, and bute hydrocarbon (likely pristane, based on the molecular weight of the compound and the elution time on the chromatogram) are present in the carbonate sample but do not show up consistently in the 2017 samples. However, each of these is common in modern fungi, bacteria, and mosses (Pancost and Sinninghe Damsté, 2003; Killops and Killops, 2005; Schwarzbauer and Jovančićević, 2016a). For the 2017 samples, the contamination was likely introduced during sample collection. Contamination present in the chert samples could be the result of younger bitumen migrating through the samples during later stages of diagenesis (Nagy, 1970). For the 1994 samples, contaminants may have been introduced during storage (Leider et al., 2016) in the collections at Harvard University for 20 years prior to any geochemical analyses being performed. The older samples were stored in an uncontrolled environment, which likely included storage in cardboard boxes and plastic sample bags.

Carbon isotopes

Organic carbon isotope values range from -5 to -30 ‰ (Table 2). These values are consistent with those of organic matter formed in a hypersaline environment (Schidlowski et al., 1984; Moers et al., 1993; Schidlowski et al., 1994), which is consistent independent interpretation of the depositional environment (Kah et al., 2001; Turner, 2009). Isotopically

enriched organic carbon has been reported from organic matter from hypersaline, intertidal, carbonate environments (Schidlowski et al., 1984; Moers et al., 1993). While only a couple of the samples are enriched in ^{13}C , these values may represent a preservation of organic productivity under evaporative conditions. Stratigraphic evidence (Kah, 1997) and facies-dependent modelling of silicification environments (Manning-Berg and Kah, 2017) suggest that restricted environments of the Angmaat Formation likely experienced cyclic variation in environment, including flooding by open marine waters, evaporation (sometimes to gypsum and halite saturation), and influx of non-marine waters.

Carbon isotope values of the kerogen also show enrichment of ^{13}C with increased degradation of the mat fabric. Samples with an overall well-preserved mat fabric have an average $\delta^{13}\text{C}_{\text{kerogen}}$ value of -28.4 ‰, mat fabrics that are considered to have fair-preservation have an average $\delta^{13}\text{C}_{\text{kerogen}}$ value of -28.0 ‰, poorly-preserved mat fabrics have an average $\delta^{13}\text{C}_{\text{kerogen}}$ value of -27.4 ‰, and mat fabrics that are unrecognizable have an average $\delta^{13}\text{C}_{\text{kerogen}}$ value of -26.8 ‰ (Fig. 3.14). Organic carbon of both bulk (Macko et al., 1993; Schidlowski, 2000) and kerogen (Lewan, 1986) is expected to have an isotope value around -25 ± 5 ‰ (Macko et al., 1993; House et al., 2000; Schidlowski, 2000). Values that are isotopically lighter than average are interpreted to reflect evidence of heterotrophic decomposition (Guo et al., 2013).

Heterotrophic bacteria utilize ^{13}C -depleted organic matter produced by autotrophic organisms as their primary source of carbon and thus have more depleted $\delta^{13}\text{C}$ values (Hollander and Smith, 2001; Guo et al., 2013). Bulk $\delta^{13}\text{C}$ values of organic matter is also decreases during heterotrophic degradation (Macko and Estep, 1984; Macko et al., 1993; Lehmann et al., 2002) as an organic matter fraction enriched in ^{13}C , like carbohydrates and proteins (Degens, 1969), is preferentially removed from the system, or an increase in organic components that are more

depleted in ^{13}C , like lipids (Degens, 1969). Carbohydrates and proteins are more susceptible to microbial degradation than lipids (Lewan, 1986; Harvey et al., 1995; Lehmann et al., 2002); therefore, as heterotrophic organisms preferentially degrade the carbohydrates and proteins, the residual organic matter (lipids) would lead to a decreased $\delta^{13}\text{C}$ value (Harvey et al., 1995; Lehmann et al., 2002). An increase in carbon composition is expected with a decrease in preservation if we assume that the well-preserved mat fabrics represent the top of a microbial mat and the poorly-preserved or unrecognizable fabrics represent the lower, more degraded portions of a mat.

Silicification process

Although the lack of evidence for lipids within the bitumen II chromatograms may indicate that the organic compounds observed in the bitumen I extracts are contamination, the lack of evidence for lipids in the bitumen II, which provides direct evidence of organic lipids preserved within the mineral matrix, may instead provide insight into the silicification process. Exceptional preservation of microbial morphologies requires that silicification occurs during earliest diagenesis (Knoll, 1985; Knauth, 1994; Toporski et al., 2002; Peng et al., 2016; Manning-Berg and Kah, 2017), and actualistic experiments demonstrate that this silicification likely occurs on the order of days to weeks (Francis et al., 1978; Westall et al., 1995; Bartley, 1996; Toporski et al., 2002).

Silicified microbial mats within the Angmaat Formation record exceptional preservation of microbial mat fabrics and individual microbial morphologies across a range of taphonomic preservation (Knoll et al., 2013; Manning-Berg et al., *in prep*). Mats have been classified as “good,” “fair,” or “poor,” based on the amount of compaction and discoloration observed and have been related to the individual sheath morphologies preserved. Mats of “good” preservation

have been interpreted to represent the top of a microbial mat, where cyanobacteria are thriving and actively building the mat. The middle of a microbial mat, below the cyanobacteria, where compaction has occurred, and heterotrophic organisms are recycling the organic carbon is represented by “fair” preservation. “Poor” preservation is interpreted to represent the lowest portion of the mat that has experienced the most bacterial decomposition. Mat fabrics are dominated by filamentous or coccoidal sheath morphologies, which are dependent on the environment in which the mat formed (Knoll et al., 2013).

For the majority of the preserved Angmaat Formation microbial mats, filamentous sheaths are the dominant mat builders. The preservation state of the sheaths varies, some exhibit a reddish-brown color, tearing, folding, and swelling or shrinking. Other sheaths are clear and seem to fade until discrete individual sheaths are not identifiable. In each sample, however, all of the observed sheaths were empty; in other words, the actual cellular trichomes, often observed in their modern counterparts and in the artificial fossilization experiments (Oehler and Schopf, 1971; Oehler, 1976; Bartley, 1996), were absent. The absence of trichomes within microbial sheaths are common in Proterozoic silicified microbial communities (Knoll, 1985; Lee and Golubic, 1998). The predominance of empty suggests that either mats may have been silicified only *after* accretion of new mat layers (mat growth occurs by trichomes evacuating their sheaths and migrating to the new mat interface, where they create new sheaths (Ortega-Calvo et al., 1991; Hoiczky and Baumeister, 1995; Lee and Golubic, 1998).

In an alternative scenario, the lack of preserved biomarkers in the chert samples may be the result of the silicification process. Silica precipitates as a gel and entombs the active microbial mat, at which point the trichomes leave the sheath to escape the silica. This would leave only the sheaths to be permineralized, which happens readily (Oehler and Schopf, 1971;

Oehler, 1976; Westall et al., 1995; Bartley, 1996; Bartley et al., 2000; Toporski et al., 2002). However, because sheaths are composed primarily of polysaccharides (Drews and Weckesser, 1982; Bartley, 1996), they do not contain lipids, like hopanes. Instead, it is the membranes in trichomes and cell walls that would contain hopanes (Brocks and Summons, 2003; Schwarzbauer and Jovančićević, 2016b). This preservation model is different than that of shale and carbonate samples that preserve biomarkers. In these situations, the trichomes may be preserved as a result of burial of the mat. The overlying sediment would then trap the organisms and the trichomes would still be present in the sheaths or at least in the microbial mat layers.

Filamentous cyanobacteria are motile and are therefore able to abandon their sheaths if the environment changes rapidly. However, coccoidal organisms are non-motile and depend on EPS to protect them from rapid changes in their environment (Decho, 1990; Decho, 1994; Sergeev et al., 2002). Therefore, the silicification process would affect coccoidal mats differently. However, the filamentous cyanobacteria are the mat-builders of the silicified microbial mats in the Angmaat Formation.

Biomarkers have been pulled from ancient samples (Brocks et al., 2005; Brocks and Grice, 2011; Grice and Brocks, 2011; French et al., 2015); however, the data are typically from carbonate and shale (Summons et al., 1999; Dutkiewicz et al., 2003; Blumenberg et al., 2012). It is unclear from the literature as to whether clear, indigenous biomarkers have been obtained from silica, although n-alkanes have been reported from Devonian-aged chert (Preston and Genge, 2010). Young hydrothermal silica deposits have also yielded lipid biomarker data (Gibson et al., 2008; Kaur et al., 2008; Jaeschke et al., 2014; Lei et al., 2017); however, older sinter deposits, like those from the Archean, have not produced definitive biomarker data (French et al., 2015; Flannery et al., 2018; McMahon et al., 2018). Hydrothermal silica deposits, however,

fundamentally differ from the silicification process identified here. Precipitation from silica-enriched hydrothermal fluids effectively entomb organic material (Phoenix et al., 2000; Yee et al., 2003; Benning et al., 2004; Konhauser et al., 2004). During cooling of silica-rich fluids, silica polymers aggrade and condense on cyanobacterial sheaths (Benning et al., 2004); however, the sheaths and organisms remain viable until vital physiological processes become inhibited by silicification (Phoenix et al., 2000). Conversely, early diagenetic chert, although rapid, likely initiated as a hydrous silica gel that permeates organic structures. This results in a period of time during the formation of the silica gel that microbial organisms can react to the changing environment and potentially abandon their sheaths and escape silicification. Data presented in this study suggest that lipids are not readily preserved in early diagenetic chert. Therefore, amorphous silica-rich sedimentary deposits proposed as potential localities where ancient Martian life may be found (cf. McMahon et al., 2018) may not be a valuable source of molecular biomarkers.

Conclusions

Early diagenetic chert commonly preserves exceptional microbial morphologies and are thus valuable resources for understanding Precambrian ecosystems. Therefore, sedimentary deposits, especially those with high concentrations of amorphous silica, have been suggested as potential targets for the search for extraterrestrial life on Mars. However, the extent of preservation of the microbial life may only be morphologic preservation. Molecular biomarkers, such as lipids, are commonly extracted from shale and carbonate. These lipids provide information regarding the microbial processes that were active at the time of preservation. Despite exceptional preservation of microbial mat fabrics, and individual microfossils within the

Angmaat Formation, data presented here indicate that lipids are not preserved in these early diagenetic chert samples.

Initial data from samples collected during the 1994 field season provided evidence for *n*-alkanes, hopanes, and steranes, and resembled that of thermally immature organic matter deposited within a hypersaline carbonate environment. However, the similarity of the data between each of the 23 samples suggests that the detected lipids may be contamination. Samples collected during a 2017 field season were also analyzed. The 2017 samples included samples that were chert and chert-associated carbonate. Chromatograms for all of the 2017 samples do not provide evidence of preserved hopanes, and steranes. Bitumen II was extracted for a subset of the 1994 samples and the 2017 samples. Resulting chromatograms also lack evidence of lipid preservation.

The silicification process may hinder the preservation of lipids. In peritidal, hypersaline, carbonate environments the rapid precipitation of silica gel halts bacterial decomposition (Bartley, 1996; Bartley et al., 2000) and ultimately permeates through the filamentous sheaths that build the preserved microbial mats. However, in each sample all observed sheaths were empty and lacked cellular trichomes, which abandon sheaths to move to new mat layers, where they grow new sheaths. The absence of trichomes within microbial sheaths are common in Proterozoic silicified microbial communities (Knoll, 1985; Lee and Golubic, 1998) and suggests that either mats may have been silicified only after accretion of new mat layers or motile filamentous microorganisms abandon their sheaths as the silica gel forms to escape from the change in their environment.

References

- Abbey, W., Anderson, R., Beegle, L., Horowitz, J., Williford, K. H., Peters, G., Morookian, J. M., Collins, C., Feldman, J., Kinnett, R., Jandura, L., Limonadi, D., Logan, C., McCloskey, S., Melko, J., Okon, A., Robinson, M., Roumeliotis, C., Syeybold, C., Singer, J., and Warner, N., *in prep*, A Look Back: Drilling on Mars: The First 669 Sols: The Drilling Campaign of the Curiosity Rover during the Mars Science Laboratory's Prime Mission: Icarus.
- Bartley, J., Knoll, A., P Grotzinger, J., and Sergeev, V., 2000, Lithification and fabric genesis in precipitated stromatolites and associated peritidal carbonates, Mesoproterozoic Billyakh Group, Siberia.
- Bartley, J. K., 1996, Actualistic Taphonomy of Cyanobacteria: Implications for the Precambrian Fossil Record: *PALAIOS*, v. 11, no. 6, p. 571-586.
- Bastow, T. P., van Aarssen, B. G. K., and Lang, D., 2007, Rapid small-scale separation of saturate, aromatic and polar components in petroleum: *Organic Geochemistry*, v. 38, no. 8, p. 1235-1250.
- Benning, L. G., Phoenix, V., Yee, N., and Konhauser, K., 2004, The dynamics of cyanobacterial silicification: an infrared micro-spectroscopic investigation: *Geochimica et Cosmochimica Acta*, v. 68, no. 4, p. 743-757.
- Blumenberg, M., Thiel, V., Riegel, W., Kah, L. C., and Reitner, J., 2012, Biomarkers of black shales formed by microbial mats, Late Mesoproterozoic (1.1 Ga) Taoudeni Basin, Mauritania: *Precambrian Research*, v. 196-197, p. 113-127.
- Brocks, J. J., and Grice, K., 2011, Biomarkers (Molecular Fossils), *in* Reitner, J., and Thiel, V., eds., *Encyclopedia of Geobiology*: Dordrecht, Springer Netherlands, p. 147-167.
- Brocks, J. J., Love, G. D., Summons, R. E., Knoll, A. H., Logan, G. A., and Bowden, S. A., 2005, Biomarker evidence for green and purple sulphur bacteria in a stratified Palaeoproterozoic sea: *Nature*, v. 437, no. 7060, p. 866-870.
- Brocks, J. J., and Summons, R. E., 2003, 8.03 - Sedimentary Hydrocarbons, Biomarkers for Early Life, *in* Turekian, H. D. H. K., ed., *Treatise on Geochemistry*: Oxford, Pergamon, p. 63-115.
- Butterfield, N. J., 2000, *Bangiomorpha pubescens* n. gen., n. sp.: implications for the evolution of sex, multicellularity, and the Mesoproterozoic/Neoproterozoic radiation of eukaryotes: *Paleobiology*, v. 26, no. 03, p. 386-404.
- Decho, A. W., 1990, Microbial Exopolymer Secretions in Ocean Environments: Their Role (s) in Food Webs and Marine Processes: *Oceanogr. Mar. Biol. Annu. Rev.*, v. 28, p. 73-153.
- Decho, A. W., *Exopolymers in microbial mats: Assessing their adaptive roles*, Berlin, Heidelberg, 1994, Springer Berlin Heidelberg, p. 215-219.
- Degens, E. T., 1969, Biogeochemistry of Stable Carbon Isotopes, *in* Eglinton, G., and Murphy, M. T. J., eds., *Organic Geochemistry: Methods and Results*: Berlin, Heidelberg, Springer Berlin Heidelberg, p. 304-329.
- Derenne, S., Robert, F., Skrzypczak-Bonduelle, A., Gourier, D., Binet, L., and Rouzaud, J.-N., 2008, Molecular evidence for life in the 3.5 billion year old Warrawoona chert: *Earth and Planetary Science Letters*, v. 272, no. 1, p. 476-480.
- Drews, G., and Weckesser, J., 1982, Function, Structure and Composition of Cell Walls and External Layers, *in* Carr, N. G., and Whitton, B. A., eds., *The Biology of Cyanobacteria*: Boston, Blackwell Scientific Publications, p. 333-357.

- Dutkiewicz, A., Volk, H., Ridley, J., and George, S., 2003, Biomarkers, brines, and oil in the Mesoproterozoic, Roper Superbasin, Australia: *Geology*, v. 31, no. 11, p. 981-984.
- Flannery, D. T., Allwood, A. C., Summons, R. E., Williford, K. H., Abbey, W., Matys, E. D., and Ferralis, N., 2018, Spatially-resolved isotopic study of carbon trapped in ~3.43 Ga Strelley Pool Formation stromatolites: *Geochimica et Cosmochimica Acta*, v. 223, p. 21-35.
- Fox, P. M., Nico, P. S., Tfaily, M. M., Heckman, K., and Davis, J. A., 2017, Characterization of natural organic matter in low-carbon sediments: Extraction and analytical approaches: *Organic Geochemistry*, v. 114, p. 12-22.
- Francis, S., Barghoorn, E. S., and Margulis, L., 1978, On the experimental silicification of microorganisms. III. Implications of the preservation of the green prokaryotic alga prochloron and other coccoids for interpretation of the microbial fossil record: *Precambrian Research*, v. 7, no. 4, p. 377-383.
- French, K. L., Hallmann, C., Hope, J. M., Schoon, P. L., Zumberge, J. A., Hoshino, Y., Peters, C. A., George, S. C., Love, G. D., Brocks, J. J., Buick, R., and Summons, R. E., 2015, Reappraisal of hydrocarbon biomarkers in Archean rocks: *Proceedings of the National Academy of Sciences*, v. 112, no. 19, p. 5915-5920.
- Gibson, R. A., Talbot, H. M., Kaur, G., Pancost, R. D., and Mountain, B., 2008, Bacteriohopanepolyol signatures of cyanobacterial and methanotrophic bacterial populations recorded in a geothermal vent sinter: *Organic Geochemistry*, v. 39, no. 8, p. 1020-1023.
- Gibson, T. M., Shih, P. M., Cumming, V. M., Fischer, W. W., Crockford, P. W., Hodgskiss, M. S. W., Wörndle, S., Creaser, R. A., Rainbird, R. H., Skulski, T. M., and Halverson, G. P., 2017, Precise age of *Bangiomorpha pubescens* dates the origin of eukaryotic photosynthesis: *Geology*, v. 46, no. 2, p. 135-138.
- Gold, D. A., Caron, A., Fournier, G. P., and Summons, R. E., 2017, Paleoproterozoic sterol biosynthesis and the rise of oxygen: *Nature*, v. 543, no. 7645, p. 420-423.
- Golovenok, V., and Belova, M. Y., 1984, Rifeyskiye mikrobioty v kremnyakh iz billyakhskoy serii Anabarskogo podniatiya [Riphean microbiotas in cherts of the Billyakh Group on the Anabar Uplift] *Paleontol. Zh.*, v. 4, p. 23-32.
- Green, J. W., Knoll, A. H., Golubi, x, S., and Swett, K., 1987, Paleobiology of Distinctive Benthic Microfossils from the Upper Proterozoic Limestone-Dolomite "Series," Central East Greenland: *American Journal of Botany*, v. 74, no. 6, p. 928-940.
- Grice, K., and Brocks, J. J., 2011, Biomarkers (Organic, Compound-Specific Isotopes), *in* Reitner, J., and Thiel, V., eds., *Encyclopedia of Geobiology*: Dordrecht, Springer Netherlands, p. 167-182.
- Guo, H., Du, Y., Kah, L. C., Huang, J., Hu, C., Huang, H., and Yu, W., 2013, Isotopic composition of organic and inorganic carbon from the Mesoproterozoic Jixian Group, North China: Implications for biological and oceanic evolution: *Precambrian Research*, v. 224, p. 169-183.
- Guo, Z., Peng, X., Czaja, A. D., Chen, S., and Ta, K., 2018, Cellular taphonomy of well-preserved Gaoyuzhuang microfossils: A window into the preservation of ancient cyanobacteria: *Precambrian Research*, v. 304, no. Supplement C, p. 88-98.
- Hahn, K. E., Turner, E. C., Babechuk, M. G., and Kamber, B. S., 2015, Deep-water seep-related carbonate mounds in a Mesoproterozoic alkaline lake, Borden Basin (Nunavut, Canada): *Precambrian Research*, v. 271, p. 173-197.

- Harvey, R. H., Tuttle, J. H., and Bell, T. J., 1995, Kinetics of phytoplankton decay during simulated sedimentation: Changes in biochemical composition and microbial activity under oxic and anoxic conditions: *Geochimica et Cosmochimica Acta*, v. 59, no. 16, p. 3367-3377.
- Hayes, J. M., Strauss, H., and Kaufman, A. J., 1999, The abundance of ^{13}C in marine organic matter and isotopic fractionation in the global biogeochemical cycle of carbon during the past 800 Ma: *Chemical Geology*, v. 161, no. 1-3, p. 103-125.
- Hofmann, H. J., and Jackson, G., 1994, Shale-facies microfossils from the Proterozoic Bylot Supergroup, Baffin Island, Canada: *Memoir (The Paleontological Society)*, p. 1-39.
- Hofmann, H. J., and Jackson, G. D., 1991, Shelf-Facies Microfossils from the Uluksan Group (Proterozoic Bylot Supergroup), Baffin Island, Canada: *Journal of Paleontology*, v. 65, no. 3, p. 361-382.
- Hoiczyk, E., and Baumeister, W., 1995, Envelope structure of four gliding filamentous cyanobacteria: *Journal of Bacteriology*, v. 177, no. 9, p. 2387-2395.
- Hollander, D. J., and Smith, M. A., 2001, Microbially mediated carbon cycling as a control on the $\delta^{13}\text{C}$ of sedimentary carbon in eutrophic Lake Mendota (USA): new models for interpreting isotopic excursions in the sedimentary record: *Geochimica et Cosmochimica Acta*, v. 65, no. 23, p. 4321-4337.
- Horodyski, R. J., and Donaldson, J. A., 1980, Microfossils from the Middle Proterozoic Dismal Lakes Groups, Arctic Canada: *Precambrian Research*, v. 11, no. 2, p. 125-159.
- House, C. H., Schopf, J. W., McKeegan, K. D., Coath, C. D., Harrison, T. M., and Stetter, K. O., 2000, Carbon isotopic composition of individual Precambrian microfossils: *Geology*, v. 28, no. 8, p. 707-710.
- Jackson, G., and Iannelli, T., 1981, Rift-related cyclic sedimentation in the Neohelikian Borden Basin, northern Baffin Island: *Geological Survey of Canada, Paper 81-10*, p. 269-302.
- Jaeschke, A., Eickmann, B., Lang, S. Q., Bernasconi, S. M., Strauss, H., and Früh-Green, G. L., 2014, Biosignatures in chimney structures and sediment from the Loki's Castle low-temperature hydrothermal vent field at the Arctic Mid-Ocean Ridge: *Extremophiles*, v. 18, no. 3, p. 545-560.
- Javaux, E. J., and Knoll, A. H., 2016, Micropaleontology of the lower Mesoproterozoic Roper Group, Australia, and implications for early eukaryotic evolution: *Journal of Paleontology*, v. 91, no. 2, p. 199-229.
- Javaux, E. J., Knoll, A. H., and Walter, M. R., 2001, Morphological and ecological complexity in early eukaryotic ecosystems: *Nature*, v. 412, no. 6842, p. 66-69.
- , 2004, TEM evidence for eukaryotic diversity in mid-Proterozoic oceans: *Geobiology*, v. 2, no. 3, p. 121-132.
- Kah, L. C., 1997, Sedimentological, geochemical, and paleobiological interactions on a Mesoproterozoic carbonate platform: Society Cliffs Formation, northern Baffin Island, Arctic Canada.
- Kah, L. C., 2000, Depositional $\delta^{18}\text{O}$ signatures in Proterozoic dolostones: constraints on seawater chemistry and early diagenesis.
- Kah, L. C., Bartley, J. K., and Teal, D. A., 2012, Chemostratigraphy of the Late Mesoproterozoic Atar Group, Taoudeni Basin, Mauritania: Muted isotopic variability, facies correlation, and global isotopic trends: *Precambrian Research*, v. 200-203, p. 82-103.
- Kah, L. C., and Knoll, A. H., 1996, Microbenthic distribution of Proterozoic tidal flats: Environmental and taphonomic considerations: *Geology*, v. 24, no. 1, p. 79-82.

- Kah, L. C., Lyons, T. W., and Chesley, J. T., 2001, Geochemistry of a 1.2 Ga carbonate-evaporite succession, northern Baffin and Bylot Islands: implications for Mesoproterozoic marine evolution: *Precambrian Research*, v. 111, no. 1–4, p. 203-234.
- Kah, L. C., Sherman, A. G., Narbonne, G. M., Knoll, A. H., and Kaufman, A. J., 1999, $\delta^{13}\text{C}$ stratigraphy of the Proterozoic Bylot Supergroup, Baffin Island, Canada: implications for regional lithostratigraphic correlations: *Canadian Journal of Earth Sciences*, v. 36, no. 3, p. 313-332.
- Kaur, G., Mountain, B. W., and Pancost, R. D., 2008, Microbial membrane lipids in active and inactive sinters from Champagne Pool, New Zealand: Elucidating past geothermal chemistry and microbiology: *Organic Geochemistry*, v. 39, no. 8, p. 1024-1028.
- Killops, S., and Killops, V., 2005, *Introduction to Organic Geochemistry*, 2nd edn (paperback): *Geofluids*, v. 5, no. 3, p. 236-237.
- Knauth, L. P., 1994, Petrogenesis of chert: *Reviews in Mineralogy and Geochemistry*, v. 29, no. 1, p. 233-258.
- Knoll, A. H., 1985, Exceptional Preservation of Photosynthetic Organisms in Silicified Carbonates and Silicified Peats: *Philosophical Transactions of the Royal Society B: Biological Sciences*, v. 311, no. 1148, p. 111-122.
- Knoll, A. H., and Golubic, S., 1979, Anatomy and taphonomy of a precambrian algal stromatolite: *Precambrian Research*, v. 10, no. 1–2, p. 115-151.
- Knoll, A. H., and Golubic, S., 1992, Proterozoic and living cyanobacteria, *Early Organic Evolution*, Springer, p. 450-462.
- Knoll, A. H., Wörndle, S., and Kah, L. C., 2013, Covariance of microfossil assemblages and microbialite textures across an upper Mesoproterozoic carbonate platform: *Palaios*, v. 28, no. 7, p. 453-470.
- Konhauser, K. O., Jones, B., Phoenix, V. R., Ferris, G., and Renaut, R. W., 2004, The Microbial Role in Hot Spring Silicification: *AMBIO: A Journal of the Human Environment*, v. 33, no. 8, p. 552-558.
- LeCheminant, A. N., and Heaman, L. M., 1989, Mackenzie igneous events, Canada: Middle Proterozoic hotspot magmatism associated with ocean opening: *Earth and Planetary Science Letters*, v. 96, no. 1–2, p. 38-48.
- Lee, S. J., and Golubic, S., 1998, Multi-trichomous cyanobacterial microfossils from the Mesoproterozoic Gaoyuzhuang Formation, China: Paleocological and taxonomic implications: *Lethaia*, v. 31, no. 3, p. 169-184.
- Lehmann, M. F., Bernasconi, S. M., Barbieri, A., and McKenzie, J. A., 2002, Preservation of organic matter and alteration of its carbon and nitrogen isotope composition during simulated and in situ early sedimentary diagenesis: *Geochimica et Cosmochimica Acta*, v. 66, no. 20, p. 3573-3584.
- Lei, J., Chu, F., Yu, X., Li, X., and Tao, C., 2017, Lipid Biomarkers Reveal Microbial Communities in Hydrothermal Chimney Structures from the 49.6°E Hydrothermal Vent Field at the Southwest Indian Ocean Ridge: *Geomicrobiology Journal*, v. 34, no. 6, p. 557-566.
- Leider, A., Schumacher, T. C., and Hallmann, C., 2016, Enhanced procedural blank control for organic geochemical studies of critical sample material: *Geobiology*, v. 14, no. 5, p. 469-482.
- Lewan, M. D., 1986, Stable carbon isotopes of amorphous kerogens from Phanerozoic sedimentary rocks: *Geochimica et Cosmochimica Acta*, v. 50, no. 8, p. 1583-1591.

- Macko, S., Engel, M., and Parker, P., 1993, Early Diagenesis of Organic Matter in Sediments, *in* Engel, M., and Macko, S., eds., *Organic Geochemistry*, Volume 11, Springer US, p. 211-224.
- Macko, S. A., and Estep, M. L. F., 1984, Microbial alteration of stable nitrogen and carbon isotopic compositions of organic matter: *Organic Geochemistry*, v. 6, p. 787-790.
- Mahaffy, P. R., Webster, C. R., Cabane, M., Conrad, P. G., Coll, P., Atreya, S. K., Arvey, R., Barciniak, M., Benna, M., Bleacher, L., Brinckerhoff, W. B., Eigenbrode, J. L., Carignan, D., Cascia, M., Chalmers, R. A., Dworkin, J. P., Errigo, T., Everson, P., Franz, H., Farley, R., Feng, S., Frazier, G., Freissinet, C., Glavin, D. P., Harpold, D. N., Hawk, D., Holmes, V., Johnson, C. S., Jones, A., Jordan, P., Kellogg, J., Lewis, J., Lyness, E., Malespin, C. A., Martin, D. K., Maurer, J., McAdam, A. C., McLennan, D., Nolan, T. J., Noriega, M., Pavlov, A. A., Prats, B., Raaen, E., Sheinman, O., Sheppard, D., Smith, J., Stern, J. C., Tan, F., Trainer, M., Ming, D. W., Morris, R. V., Jones, J., Gundersen, C., Steele, A., Wray, J., Botta, O., Leshin, L. A., Owen, T., Battel, S., Jakosky, B. M., Manning, H., Squyres, S., Navarro-González, R., McKay, C. P., Raulin, F., Sternberg, R., Buch, A., Sorensen, P., Kline-Schoder, R., Coscia, D., Szopa, C., Teinturier, S., Baffes, C., Feldman, J., Flesch, G., Forouhar, S., Garcia, R., Keymeulen, D., Woodward, S., Block, B. P., Arnett, K., Miller, R., Edmonson, C., Gorevan, S., and Mumm, E., 2012, The Sample Analysis at Mars Investigation and Instrument Suite: *Space Science Reviews*, v. 170, no. 1, p. 401-478.
- Manning-Berg, A. R., and Kah, L. C., 2017, Proterozoic microbial mats and their constraints on environments of silicification: *Geobiology*, v. 15, no. 4, p. 469-483.
- McMahon, S., Bosak, T., Grotzinger, J. P., Milliken, R. E., Summons, R. E., Daye, M., Newman, S. A., Fraeman, A., Williford, K. H., and Briggs, D. E. G., 2018, A Field Guide to Finding Fossils on Mars: *Journal of Geophysical Research: Planets*, v. 0, no. 0.
- Moers, M. E. C., Jones, D. M., Eakin, P. A., Fallick, A. E., Griffiths, H., and Larter, S. R., 1993, Carbohydrate diagenesis in hypersaline environments: application of GC-IRMS to the stable isotope analysis of derivatized saccharides from surficial and buried sediments: *Organic Geochemistry*, v. 20, no. 7, p. 927-933.
- Moldowan, J. M., Sundararaman, P., and Schoell, M., 1986, Sensitivity of biomarker properties to depositional environment and/or source input in the Lower Toarcian of SW-Germany: *Organic Geochemistry*, v. 10, no. 4, p. 915-926.
- Nagy, B., 1970, Porosity and permeability of the early precambrian onverwacht chert: Origin of the hydrocarbon content: *Geochimica et Cosmochimica Acta*, v. 34, no. 4, p. 525-527.
- Newman, D. K., Neubauer, C., Ricci, J. N., Wu, C.-H., and Pearson, A., 2016, Cellular and Molecular Biological Approaches to Interpreting Ancient Biomarkers: *Annual Review of Earth and Planetary Sciences*, v. 44, no. 1, p. 493-522.
- Oehler, D., and Cady, S., 2014, Biogenicity and Syngeneity of Organic Matter in Ancient Sedimentary Rocks: Recent Advances in the Search for Evidence of Past Life: *Challenges*, v. 5, no. 2, p. 260.
- Oehler, J. H., 1976, Experimental studies in Precambrian paleontology: Structural and chemical changes in blue-green algae during simulated fossilization in synthetic chert: *Geological Society of America Bulletin*, v. 87, no. 1, p. 117-129.
- Oehler, J. H., and Schopf, J. W., 1971, Artificial Microfossils: Experimental Studies of Permineralization of Blue-Green Algae in Silica: *Science*, v. 174, no. 4015, p. 1229-1231.

- Ortega-Calvo, J. J., Hernandez-Marine, M., and Saiz-Jimenez, C., 1991, Biodeterioration of building materials by cyanobacteria and algae: *International Biodeterioration*, v. 28, no. 1, p. 165-185.
- Pancost, R. D., and Sinninghe Damsté, J. S., 2003, Carbon isotopic compositions of prokaryotic lipids as tracers of carbon cycling in diverse settings: *Chemical Geology*, v. 195, no. 1, p. 29-58.
- Pehrsson, S. J., and Buchan, K. L., 1999, Borden dykes of Baffin Island, Northwest Territories: a Franklin U-Pb baddeleyite age and a paleomagnetic reinterpretation: *Canadian Journal of Earth Sciences*, v. 36, no. 1, p. 65-73.
- Peng, X. T., Guo, Z. X., House, C. H., Chen, S., and Ta, K. W., 2016, SIMS and NanoSIMS analyses of well-preserved microfossils imply oxygen-producing photosynthesis in the Mesoproterozoic anoxic ocean: *Chemical Geology*, v. 441, p. 24-34.
- Peters, K., Walters, C., and Moldowan, J., 2007, *The biomarker guide: Volume 2, Biomarkers and isotopes in petroleum systems and earth history*, Cambridge University Press.
- Peters, K. E., and Moldowan, J. M., 1993, *The biomarker guide: interpreting molecular fossils in petroleum and ancient sediments*.
- Phoenix, V. R., Adams, D. G., and Konhauser, K. O., 2000, Cyanobacterial viability during hydrothermal biomineralisation: *Chemical Geology*, v. 169, no. 3-4, p. 329-338.
- Price, L. C., and Clayton, J. L., 1992, Extraction of whole versus ground source rocks: Fundamental petroleum geochemical implications including oil-source rock correlation: *Geochimica et Cosmochimica Acta*, v. 56, no. 3, p. 1213-1222.
- Qu, Y., Engdahl, A., Zhu, S., Vajda, V., and McLoughlin, N., 2015, Ultrastructural Heterogeneity of Carbonaceous Material in Ancient Cherts: Investigating Biosignature Origin and Preservation: *Astrobiology*, v. 15, no. 10, p. 825-842.
- Schidlowski, M., 2000, Carbon Isotopes and Microbial Sediments, *in* Riding, R. E., and Awramik, S. M., eds., *Microbial Sediments*: Berlin, Heidelberg, Springer Berlin Heidelberg, p. 84-95.
- Schidlowski, M., Gorzawski, H., and Dor, I., 1994, Carbon isotope variations in a solar pond microbial mat: Role of environmental gradients as steering variables: *Geochimica et Cosmochimica Acta*, v. 58, no. 10, p. 2289-2298.
- Schidlowski, M., Matzigkeit, U., and Krumbein, W. E., 1984, Superheavy organic carbon from hypersaline microbial mats: *Naturwissenschaften*, v. 71, no. 6, p. 303-308.
- Schopf, J. W., 1968, Microflora of the Bitter Springs Formation, Late Precambrian, Central Australia: *Journal of Paleontology*, v. 42, no. 3, p. 651-688.
- Schwarzbauer, J., and Jovančičević, B., 2016a, *From Biomolecules to Chemofossils*, Springer.
- , 2016b, *Isoprenoids, From Biomolecules to Chemofossils*: Cham, Springer International Publishing, p. 27-76.
- Seifert, W. K., and Michael Moldowan, J., 1978, Applications of steranes, terpanes and monoaromatics to the maturation, migration and source of crude oils: *Geochimica et Cosmochimica Acta*, v. 42, no. 1, p. 77-95.
- Sergeev, V. N., Gerasimenko, L. M., and Zavarzin, G. A., 2002, The Proterozoic History and Present State of Cyanobacteria: *Microbiology*, v. 71, no. 6, p. 623-637.
- Sherman, A. G., James, N. P., and Narbonne, G. M., 2002, Evidence for reversal of basin polarity during carbonate ramp development in the Mesoproterozoic Borden Basin, Baffin Island: *Canadian Journal of Earth Sciences*, v. 39, no. 4, p. 519-538.

- Sherman, A. G., Narbonne, G. M., and James, N. P., 2001, Anatomy of a cyclically packaged Mesoproterozoic carbonate ramp in northern Canada: *Sedimentary Geology*, v. 139, no. 3–4, p. 171-203.
- Sherman, L. S., Waldbauer, J. R., and Summons, R. E., 2007, Improved methods for isolating and validating indigenous biomarkers in Precambrian rocks: *Organic Geochemistry*, v. 38, no. 12, p. 1987-2000.
- Stueken, E. E., Buick, R., Guy, B. M., and Koehler, M. C., 2015, Isotopic evidence for biological nitrogen fixation by molybdenum-nitrogenase from 3.2 Gyr: *Nature*, v. advance online publication.
- Subroto, E. A., Alexander, R., and Kagi, R. I., 1991, 30-Norhopanes: their occurrence in sediments and crude oils: *Chemical Geology*, v. 93, no. 1, p. 179-192.
- Summons, R. E., Jahnke, L. L., Hope, J. M., and Logan, G. A., 1999, 2-Methylhopanoids as biomarkers for cyanobacterial oxygenic photosynthesis: *Nature*, v. 400, no. 6744, p. 554-557.
- Summons, R. E., Sessions, A. L., Allwood, A. C., Barton, H. A., Beaty, D. W., Blakkolb, B., Canham, J., Clark, B. C., Dworkin, J. P., Lin, Y., Mathies, R., Milkovich, S. M., and Steele, A., 2014, Planning Considerations Related to the Organic Contamination of Martian Samples and Implications for the Mars 2020 Rover: *Astrobiology*, v. 14, no. 12, p. 969-1027.
- ten Haven, H. L., de Leeuw, J. W., Sinninghe Damsté, J. S., Schenck, P. A., Palmer, S. E., and Zumberge, J. E., 1988, Application of biological markers in the recognition of palaeohypersaline environments: Geological Society, London, Special Publications, v. 40, no. 1, p. 123-130.
- Toporski, J. K., Steele, A., Westall, F., Thomas-Keprta, K. L., and McKay, D. S., 2002, The simulated silicification of bacteria-New clues to the modes and timing of bacterial preservation and implications for the search for extraterrestrial microfossils: *Astrobiology*, v. 2, no. 1, p. 1-26.
- Turner, E. C., 2009, Mesoproterozoic carbonate systems in the Borden Basin, Nunavut: *Canadian Journal of Earth Sciences*, v. 46, no. 12, p. 915-938.
- , 2011, Structural and Stratigraphic Controls on Carbonate-Hosted Base Metal Mineralization in the Mesoproterozoic Borden Basin (Nanisivik District), Nunavut: *Economic Geology*, v. 106, no. 7, p. 1197-1223.
- Vermerris, W., and Nicholson, R., 2006, Families of Phenolic Compounds and Means of Classification, *Phenolic Compound Biochemistry*: Dordrecht, Springer Netherlands, p. 1-34.
- Volkman, J., 2003, Sterols in microorganisms: *Applied Microbiology and Biotechnology*, v. 60, no. 5, p. 495-506.
- Westall, F., Boni, L., and Guerzoni, E., 1995, The experimental silicification of microorganisms: *Palaeontology*, v. 38, no. 3, p. 495-528.
- Wilhelms, A., Larter, S. R., and Leythaeuser, D., 1991, Influence of bitumen-2 on Rock-Eval pyrolysis: *Organic Geochemistry*, v. 17, no. 3, p. 351-354.
- Williford, K. H., Ushikubo, T., Lepot, K., Kitajima, K., Hallmann, C., Spicuzza, M. J., Kozdon, R., Eigenbrode, J. L., Summons, R. E., and Valley, J. W., 2016, Carbon and sulfur isotopic signatures of ancient life and environment at the microbial scale: Neoproterozoic shales and carbonates: *Geobiology*, v. 14, no. 2, p. 105-128.

Yee, N., Phoenix, V. R., Konhauser, K. O., Benning, L. G., and Ferris, F. G., 2003, The effect of cyanobacteria on silica precipitation at neutral pH: implications for bacterial silicification in geothermal hot springs: *Chemical Geology*, v. 199, no. 1–2, p. 83-90.

Appendix

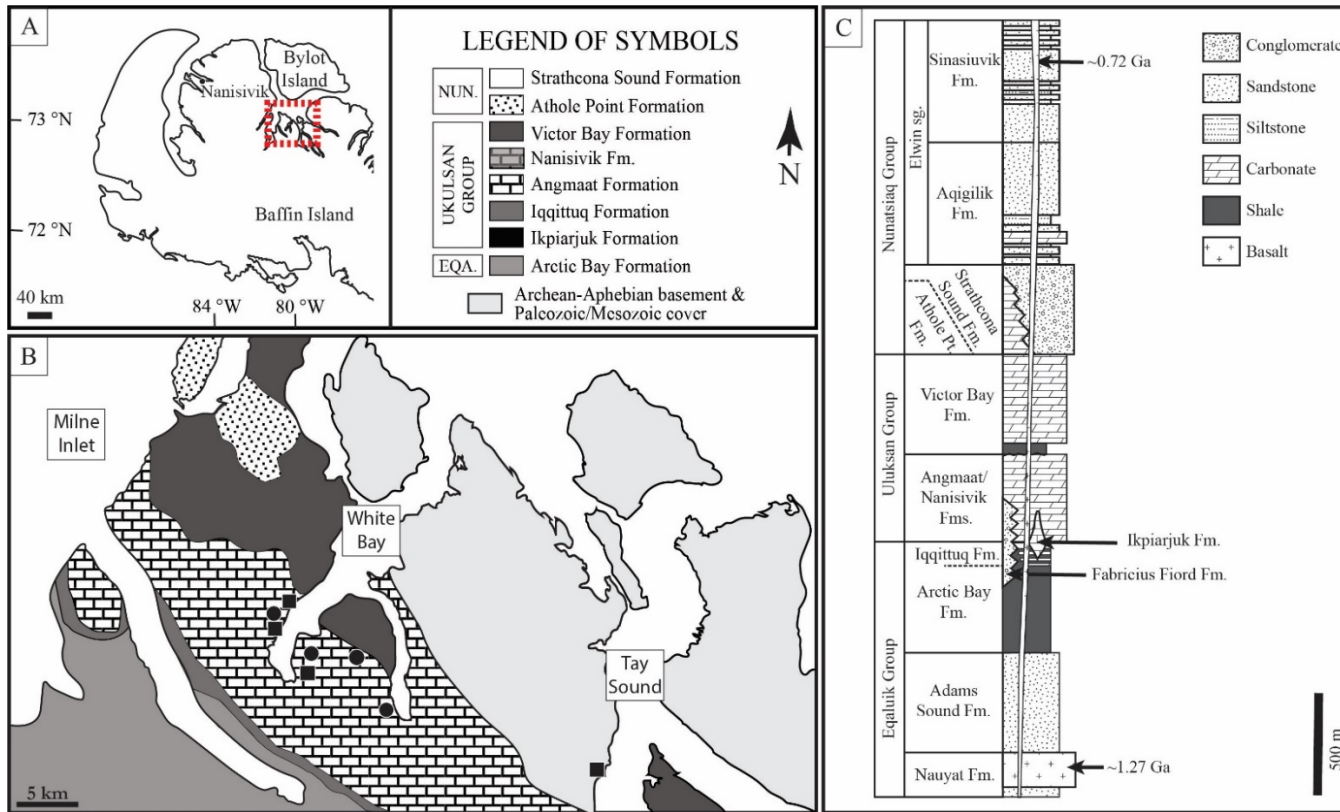


Figure 3.1 Map of Baffin Island (A). Samples were collected near White Bay (B) within the carbonate strata of the Angmaat Formation of the Bylot Supergroup (C). The squares represent sample localities for the 1994 samples used in this study, and the circles represent samples that were collected during the 2017 field season (B).

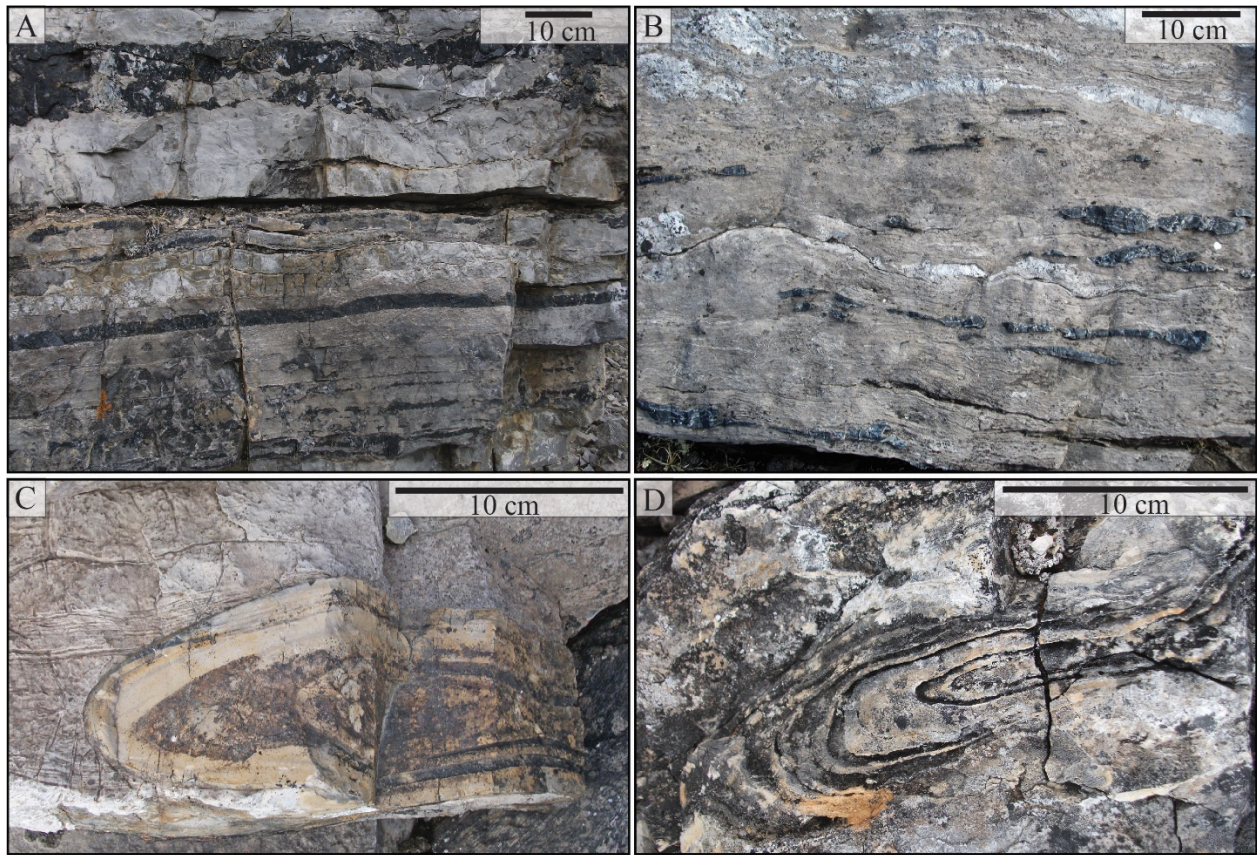


Figure 3.2 Early diagenetic chert within the Angmaat Formation occurs as beds up to ~10 cm thick (A) or as nodules and lenses (B). Examples of late diagenetic chert nodules are also observed in the field area. Late diagenetic chert nodules were yellow in color (C) or gray (D) and the concentric rings were always within the nodules.

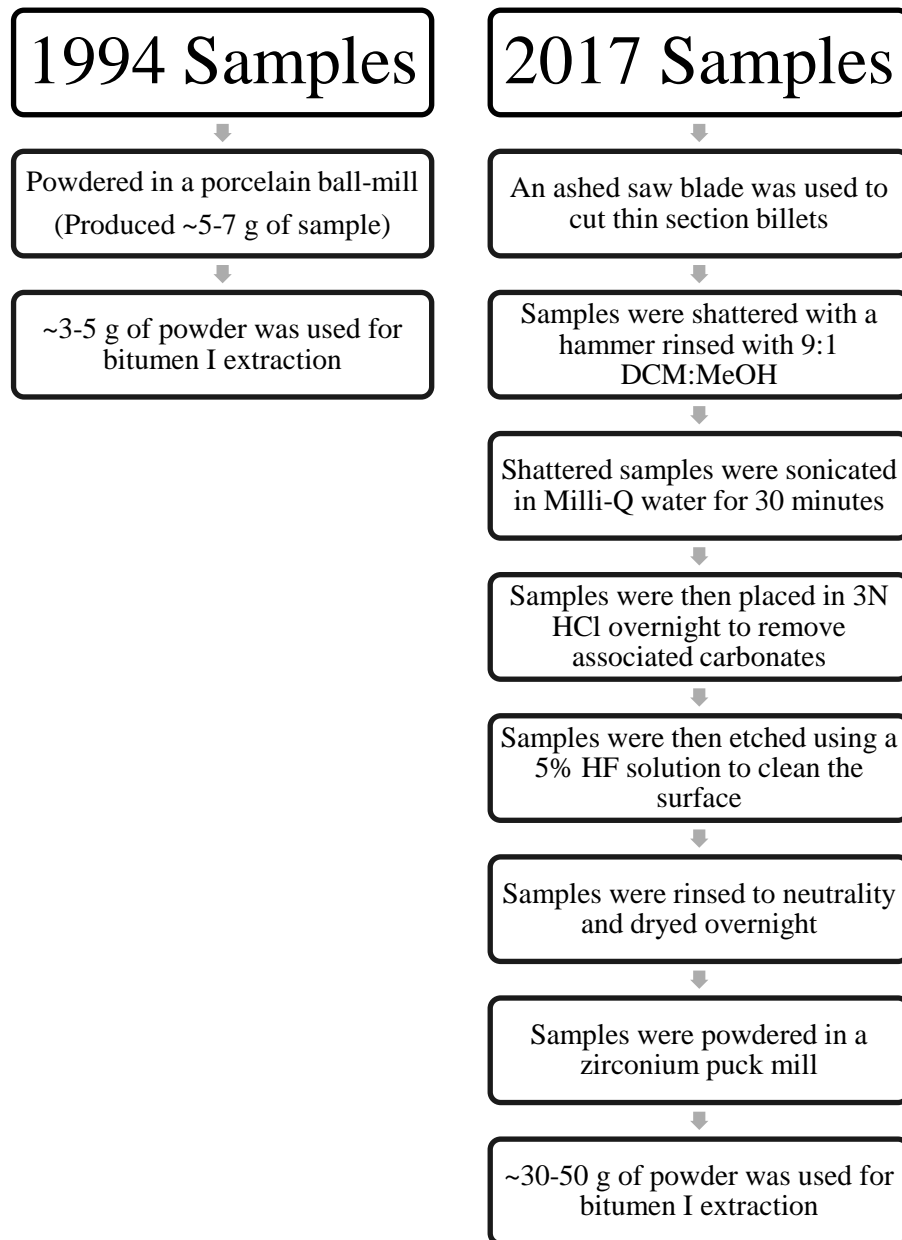


Figure 3.3 Two sample sets were used in this study. The first set was collected during a 1993-1994 field season and had been stored in the collections at Harvard University. The sample billets were used for geochemical analyses, which limited the amount of sample available. A second set of samples was collected in 2017. To minimize potential contamination, these samples were sent immediately to JPL. The methods used for bitumen I and II, and isotopic analyses, were used on both sets of samples. The largest difference in sample prep were the steps taken to ensure that contaminants were not introduced to the 2017 samples.

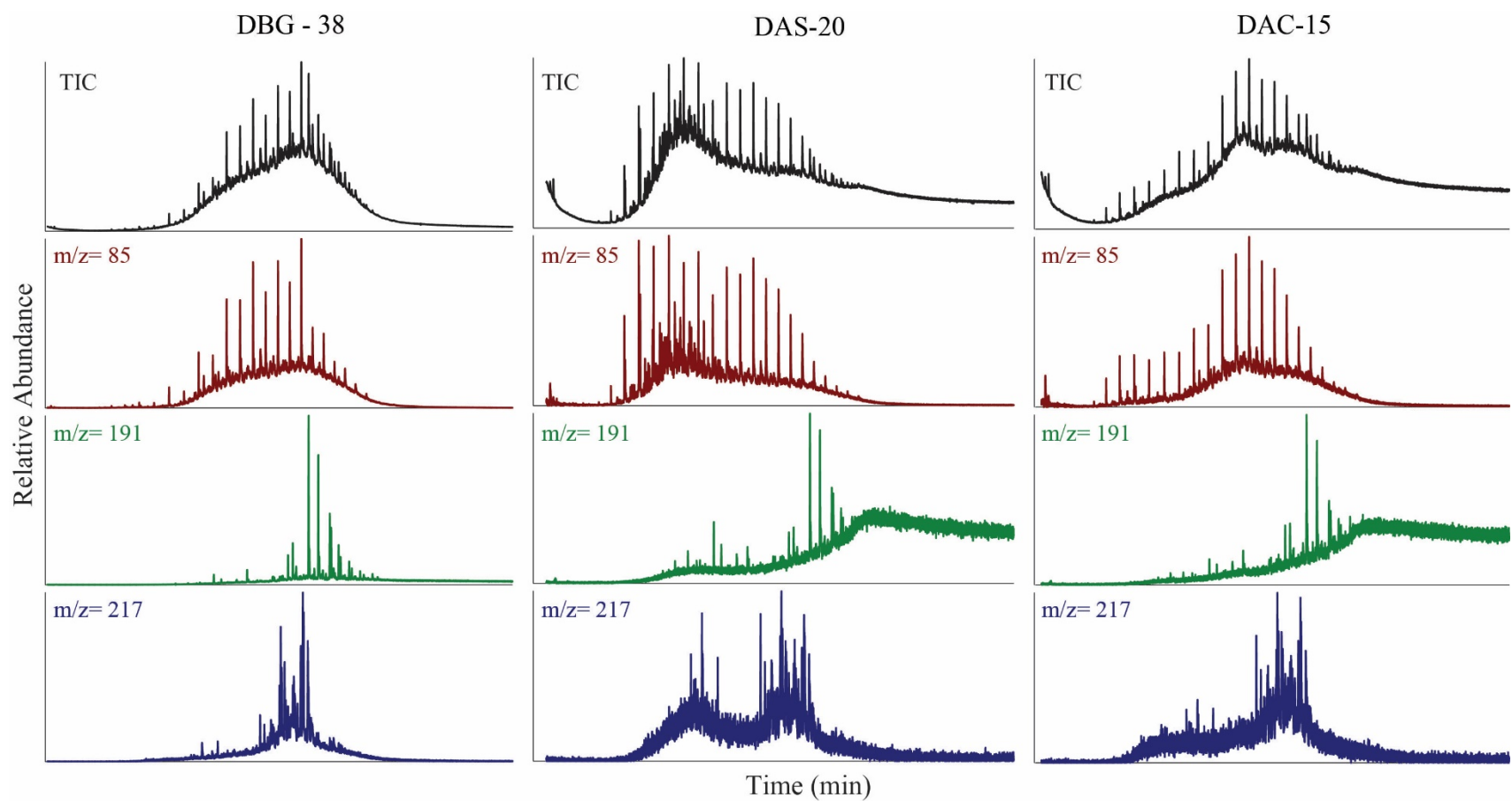


Figure 3.4 Total Ion Chromatograms (TIC) are shown for several of the 1994 samples. Mass ion chromatograms provide evidence for the preservation of *n*-alkanes ($m/z=85$), hopanes ($m/z=191$), and steranes ($m/z=217$).

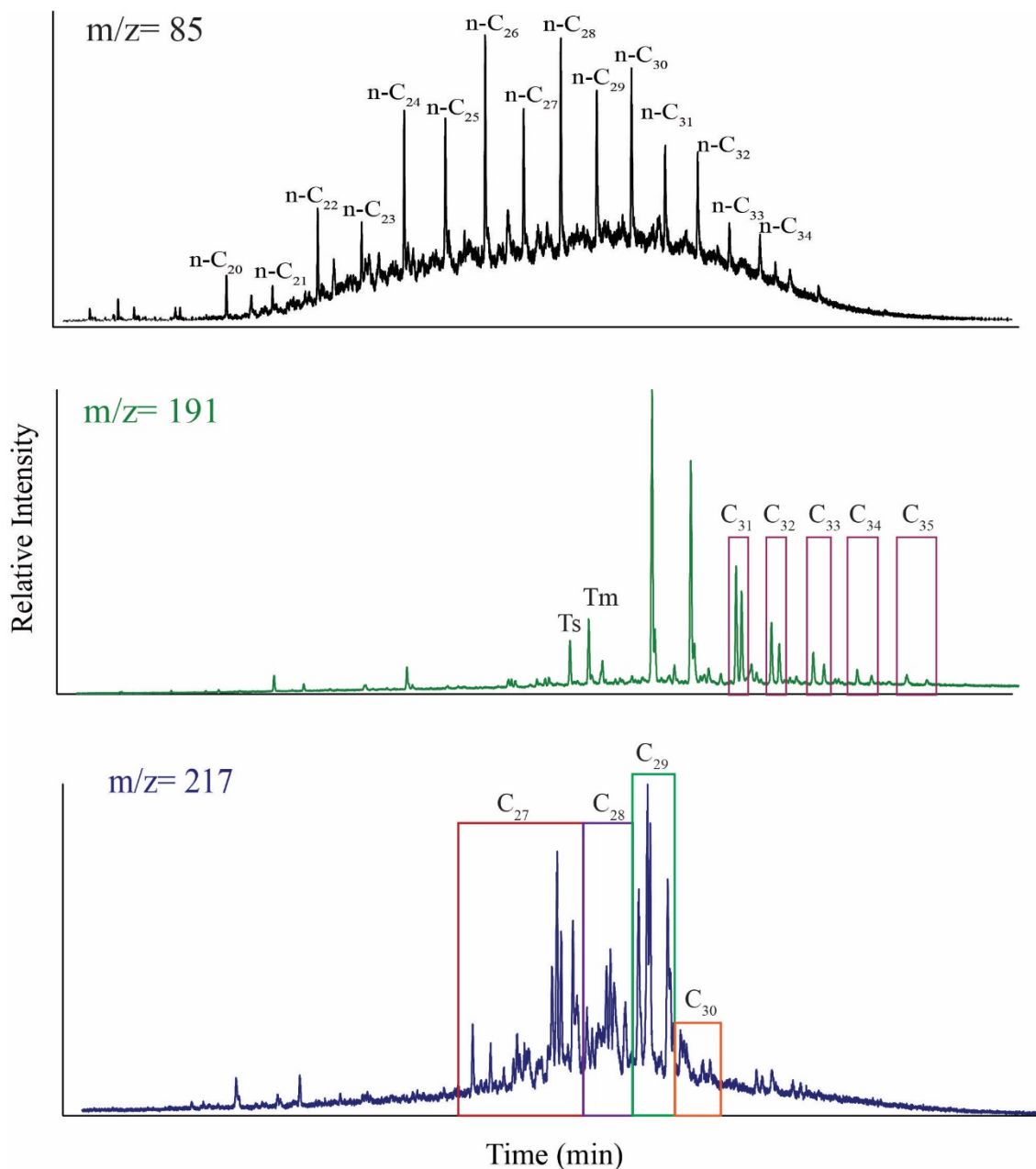


Figure 3.5 Detailed data for one of the 23 samples from the 1994 sample suite. In the m/z 85 ion chromatogram, *n*-alkanes are identified and exhibit an even-over-odd carbon preference. The Ts and Tm peaks are labeled on the m/z 191 ion chromatogram. Long-chain carbon hopanes are also identified on this ion chromatogram. Within the m/z 217 chromatogram, C₂₇ – C₃₀ steranes are highlighted.

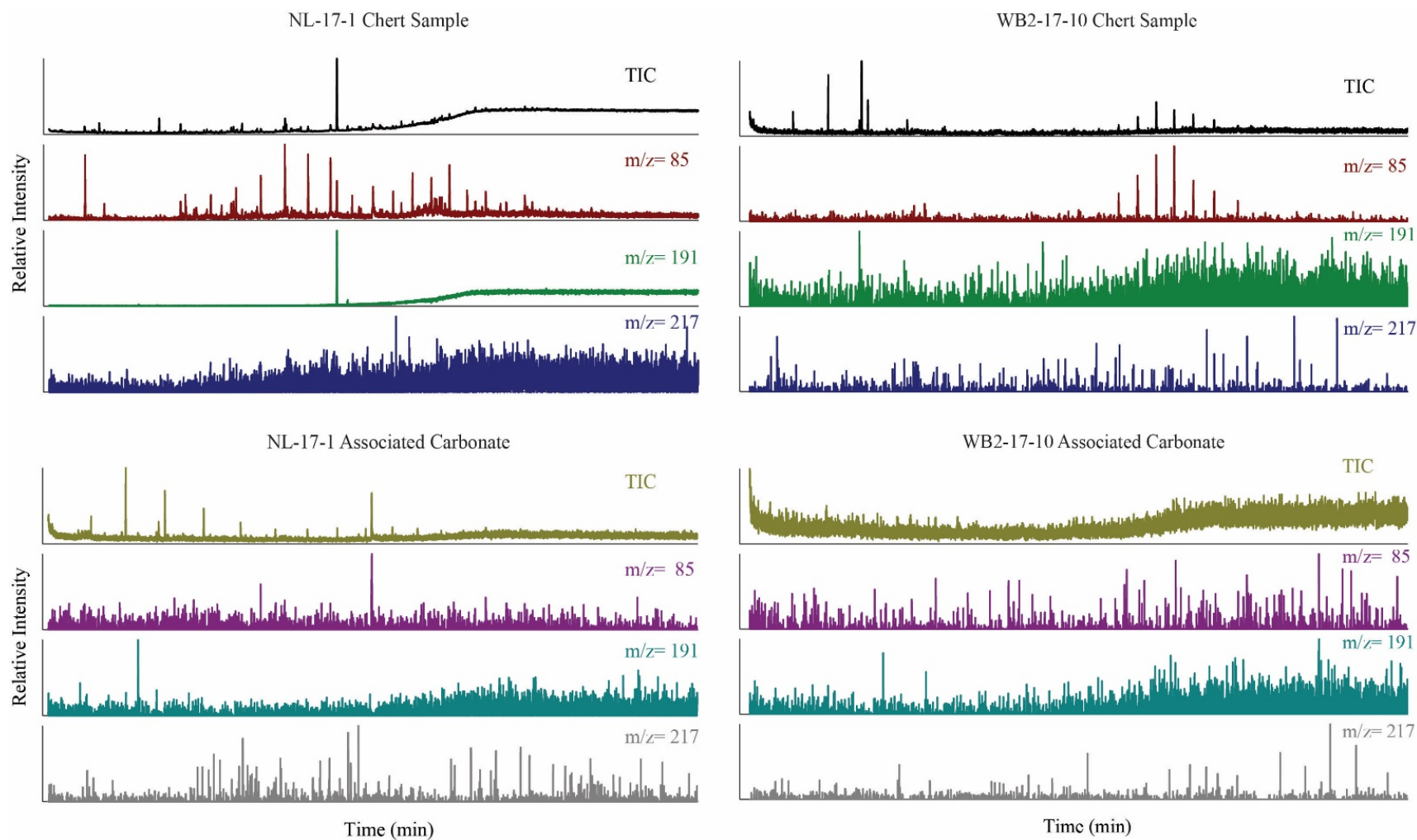


Figure 3.6 Chromatograms for chert samples (on top) and the chromatograms of the chert-associated carbonate samples below them. The chromatograms of the chert samples and their corresponding carbonate samples do not show the same peaks. A similar distribution of peaks would be expected for the chert and carbonate because the two phases were from the same samples and should therefore have the same lipids preserved.

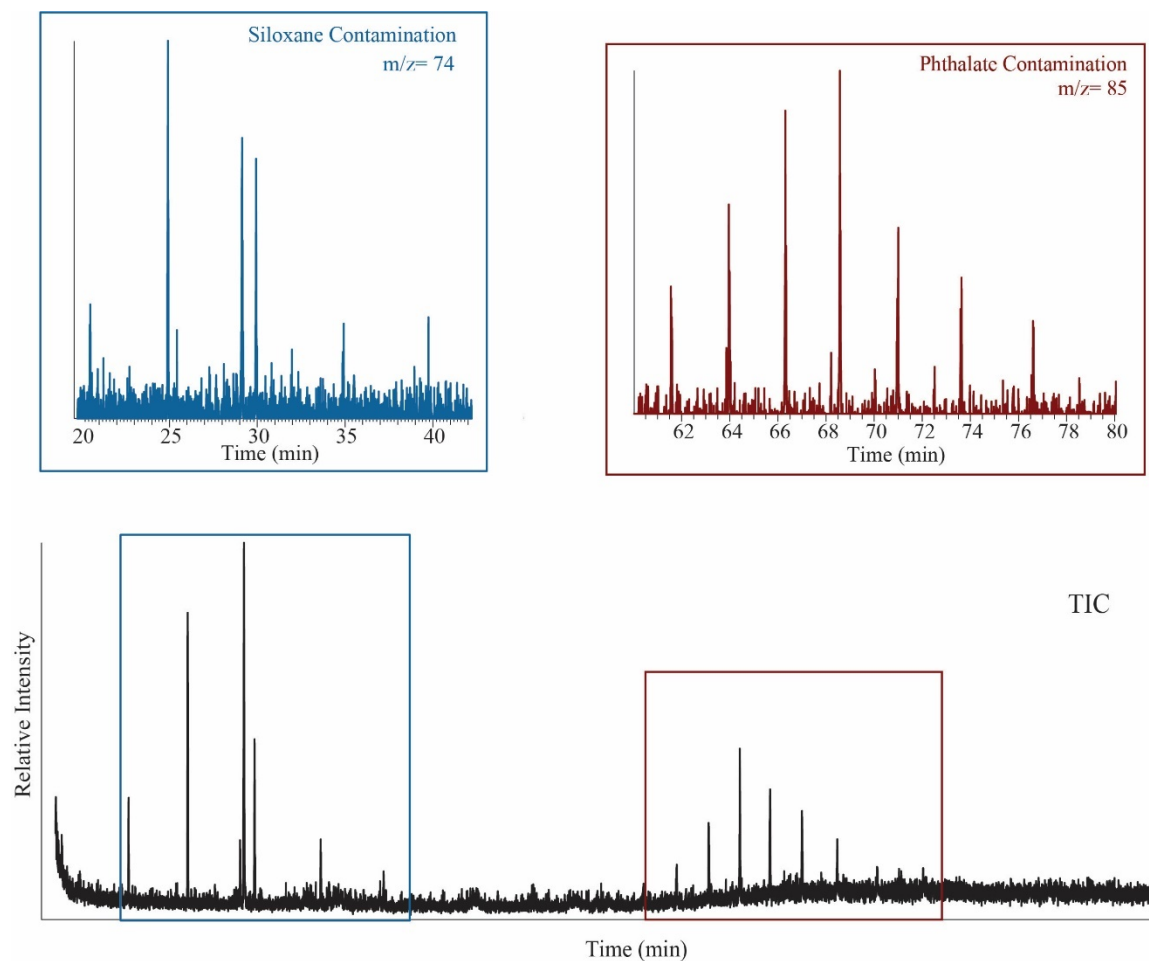


Figure 3.7 Two major contaminants are identified from the TIC of a 2017 sample. Siloxane contamination is seen in the early in the measurement. These compounds typically have a mass fragment of 74 and are therefore identified in the m/z 74 ion chromatogram. Siloxanes are seen in all of the TIC for the 2017 samples and are the result of contamination by the GC column. Other common contaminants in the 2017 samples are a group of phthalates that elude between 60 and 80 minutes in the chromatogram. These compounds are identified in the mass 85 ion chromatogram.

Diethyltoluamide (DEET) Contamination

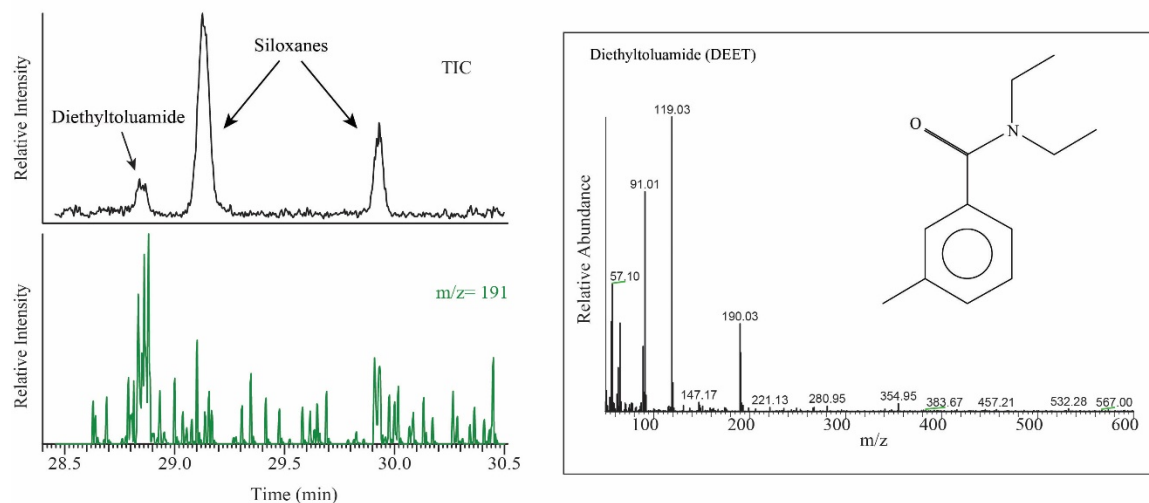


Figure 3.8 The most common contaminant in the 2017 samples was DEET. On the left, the TIC peak is highlighted and seen in the m/z 191 ion chromatogram directly below the TIC. The spectra associated with the DEET compound is shown on the right of this figure with the chemical structure. This was identified using the NIST standard library.

WB2-17-13 Total Lipid Extract

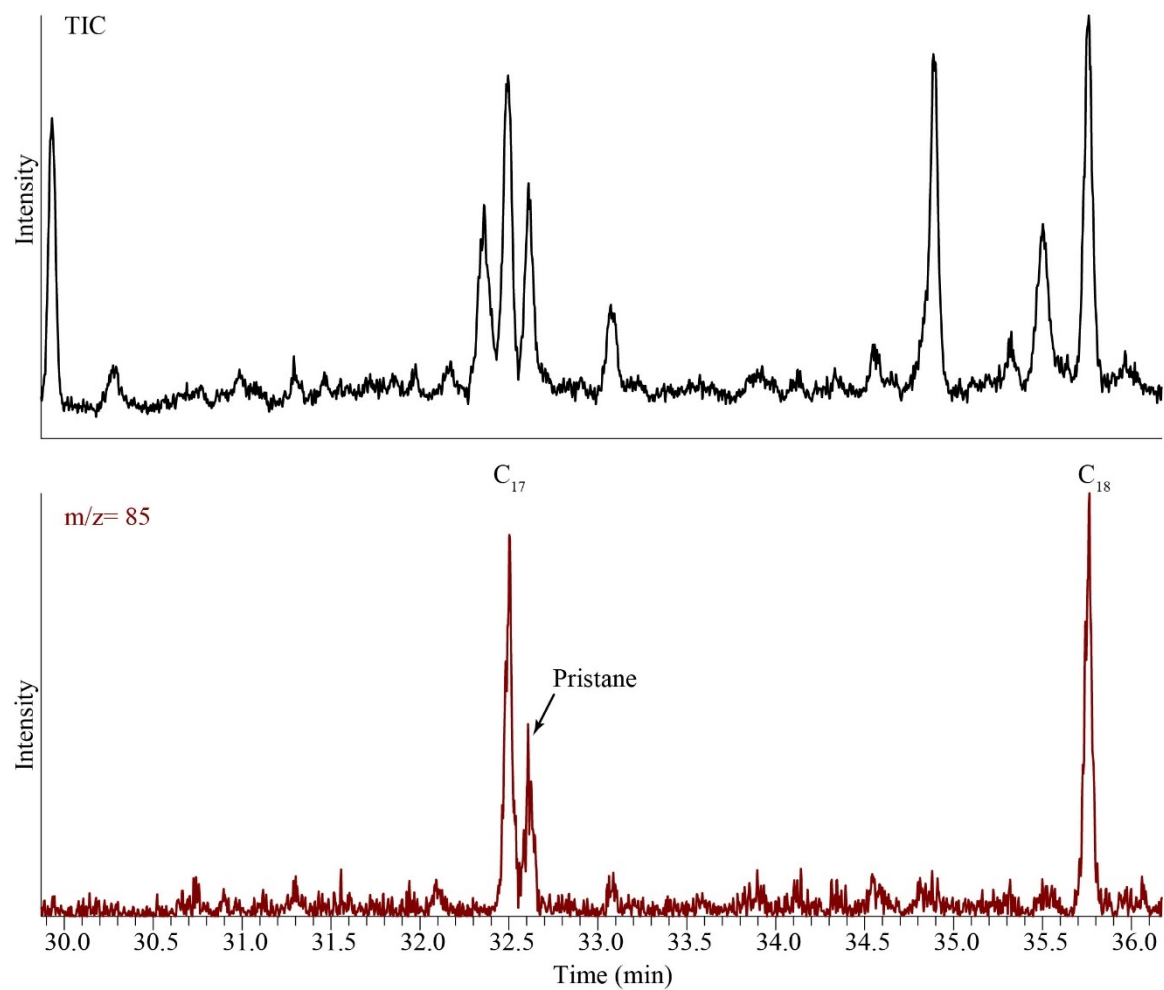


Figure 3.9 Pristane was observed in one of the carbonate samples collected in 2017. The peak eludes immediately after the n - C_{17} alkane.

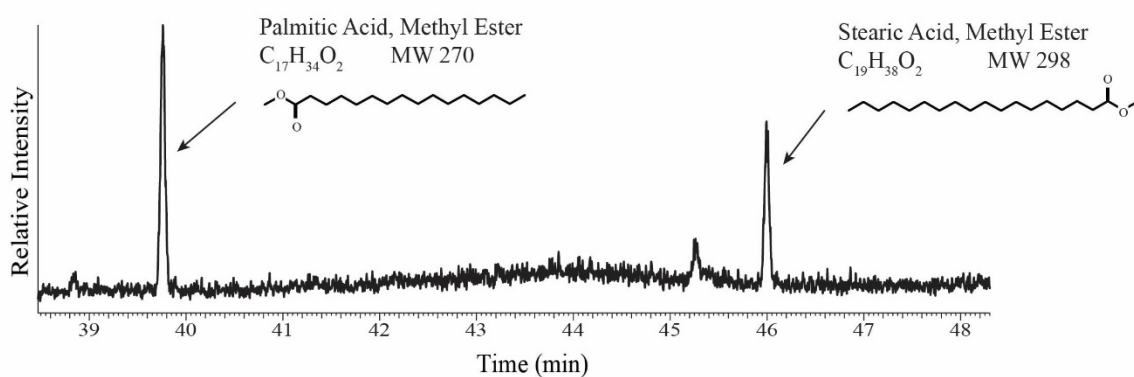
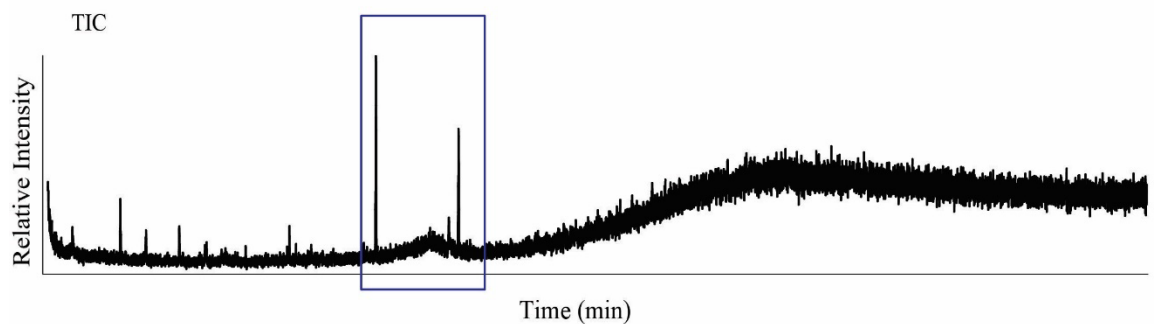


Figure 3.10 Fatty acid methyl esters were found in all of the bitumen II samples. These were the two most prominent peaks in the TICs. The top TIC is the entire TIC and the bottom graph is a zoomed-in view of the same TIC.

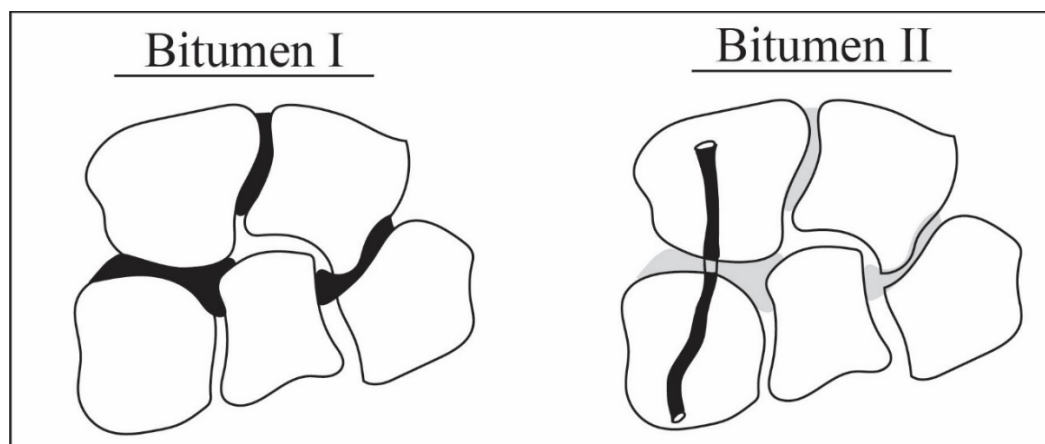


Figure 3.11 Cartoon showing the difference between bitumen I and bitumen II. Bitumen I is the solvent-soluble organic matter that is preserved between the crystals of the mineral phase and bitumen II is the soluble organic matter that is incorporated into the crystal of the mineral phase.

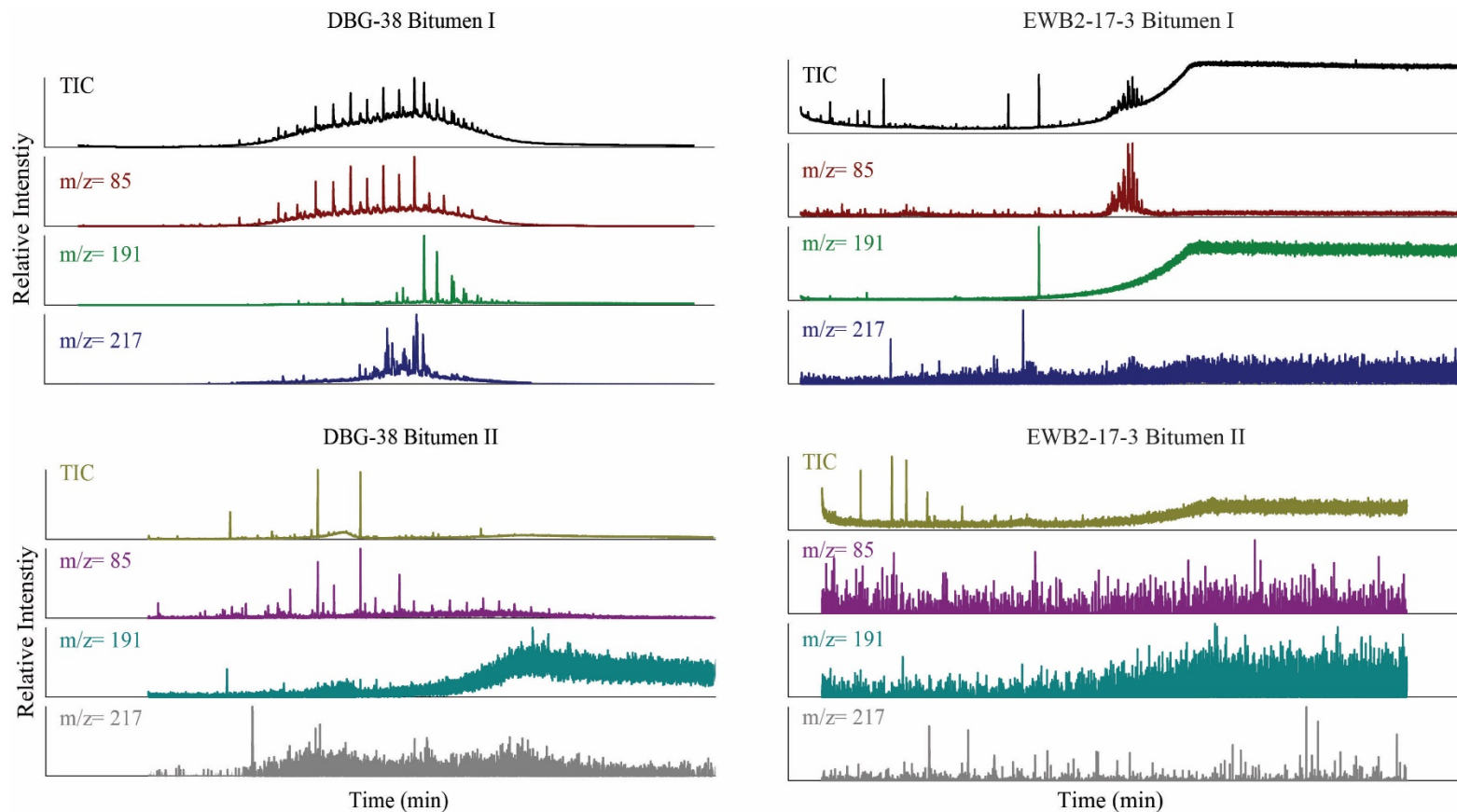


Figure 3.12 Bitumen I and II chromatograms were different for the 1994 and 2017 samples. A TIC is provided for each sample, as are the mass ion chromatograms 85 (*n*-alkanes), 191 (hopanes), and 217 (steranes). On the left is the comparison of a 1994 sample to the bitumen II data. No evidence for the presence of hopanes or steranes is observed in the bitumen II data. On the right, a sample from the 2017 sample collection. The bitumen II data look different from the bitumen I data for these samples as well. Bitumen II data do not preserve the same geolipids at the bitumen I data, which suggests that the bitumen I data are contaminants.

Table 3.1 Major sources of contamination identified throughout the 2017 samples. Phthalates, siloxanes, DEET, Pheols, and Fryol fr 2 are observed in chert samples. Whereas the Ergosterol, squalenes, dioloptene, and bute hydrocarbon occur in the carbonate sample.

Chemical Compound	m/z	Molecular Weight	Formula	Source
Phthalates	85	418	C ₂₆ H ₄₂ O ₄	Man-made; Plastics
Siloxanes	74	Variable	Variable	GC column
Diethyltoluamide	191	191	C ₁₂ H ₁₇ NO	Mosquito repellent (DEET) - contamination in during field collection
Phenol 2,4-di-tert-butyl	191	206	C ₁₄ H ₂₂ O	Plastics, plants, or microorganisms
7,9 – di-tert-butyl-oxaspiro	191	276		Associated with fungi that like starchy substrates
Fyrol fr 2	191	428	C ₉ H ₁₅ Cl ₆ O ₄ P	Fire retardant – unknown source
Ergosterol	217	396	C ₂₈ H ₄₄ O	Component of fungal cell membranes
Squalene	217	410	C ₃₀ H ₅₀	Precursor for all plant and animal sterols
Dipolente	191	410	C ₃₀ H ₅₀	Common in bacteria, mosses, and ferns
Bute hydrocarbon	85	268	C ₁₉ H ₄₀	An isomer of an isoprenoid- based on the molecular weight and the location of the peak on the chromatogram, this is probably pristane

Table 3.2 Carbon isotopes data for the 1994 sample suite and the 2017 suite. The data are sorted according to the lithology of the mat fabric.

Sample	Lithology	TOC	$\delta^{13}\text{C}_{\text{org}}$	Error	$\delta^{13}\text{C}_{\text{kerogen}}$	Error
DBG-30	mixed	0.603	-27.89	0.09	-27.89	0.46
DBN-2	mixed	0.101	-28.58	0.04	-28.86	0.18
DAC-16	mixed	0.233	-29.29	0.09	-30.83	0.16
DAC-15	mixed	1.183	-28.28	0.07	-28.77	0.04
DBG-44	mixed	0.224	-29.02	0.18	-28.86	0.34
DBG-32	mixed	0.525	-28.53	0.01	-28.85	—
DAS-20	mixed	0.356	-29.77	0.02	-30.03	0.00
DBG-42	mixed	0.290	-27.97	0.04	-28.48	0.02
DAC-31	mixed	0.649	-27.86	0.03	-28.50	0.06
DAC-5	mixed	0.473	-27.73	0.03	-28.24	0.08
DBN-20	mixed	0.354	-26.49	0.01	-27.54	0.18
DBG-38	mixed	0.331	-29.80	0.00	-29.81	0.46
DBN-6	mixed	0.154	-24.87	0.10	—	—
DBG-26	mixed	0.763	-28.17	0.06	—	—
DAC-18	mixed	0.342	-28.84	0.12	—	—
DAC-24	mixed	0.853	-28.56	0.03	—	—
DAC-1	mixed	0.282	-26.23	0.19	—	—
DAC-9	mixed	0.220	-23.10	0.14	—	—
DAC-14	mixed	0.251	-27.61	0.21	—	—
DAC-20	mixed	0.208	-27.05	0.28	—	—
DBG-40	mixed	0.509	-28.45	0.02	—	—
DBN-4	mixed	0.183	-27.23	0.37	—	—
DBN-7	mixed	0.391	-25.84	0.12	—	—
EWB2-17-3	chert	0.08	-5.4	0.1	—	—
NL-17-5	chert	0.08	-11.8	0.8	—	—
NL-17-1A	chert	0.06	-18.6	3.3	—	—
NL-17-6	chert	0.04	-19.7	1.0	—	—
NL-17-3	chert	0.08	—	—	-21.4	0.2
NL-17-3A	chert	0.12	—	—	-23.1	0.1
WB2-17-10A	chert	0.03	-27.9	0.0	—	—
NL-17-14	chert	0.17	-29.2	0.1	—	—
NL-17-4	chert	0.09	-30.1	0.2	—	—
WWB-17-9A	chert	0.05	-30.2	0.1	—	—
WB2-17-13	carbonate	15.86	-27.9	0.0	—	—
WB2-17-10B	carbonate	0.16	-12.5	0.1	—	—
WWB-17-9B	carbonate	1.57	-30.5	0.0	—	—
NL-17-1B	carbonate	5.03	-30.7	0.1	—	—
Ashed sand	sand	0.038	—	—	—	—

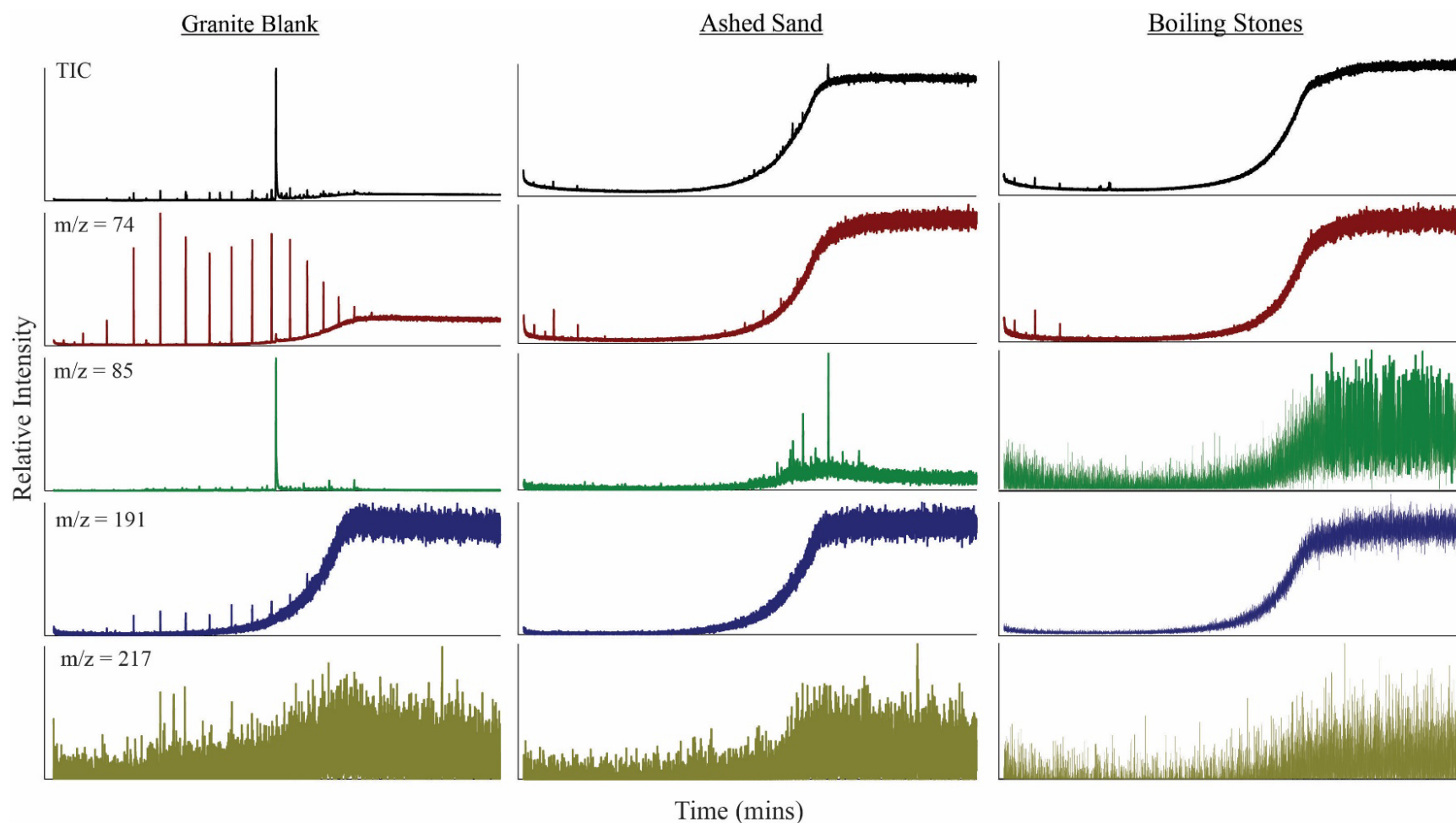


Figure 3.13 Several blanks were used throughout the method development. The granite acted as a procedural blank for the 2017 sample set. At various stages in the preparation method, blanks were analyzed if there was potential for contamination. Ashed sand was used to ensure that the puck-mill and ball-mill were clean while powdering the 1994 and 2017 samples. Teflon boiling stones were used as blanks during the bitumen II extractions. The chromatogram in each of these blanks indicate that contamination was not introduced by the methods. Siloxanes, where are present in the m/z 74 ion chromatograms, are likely the result of compounds from the column of the GC.

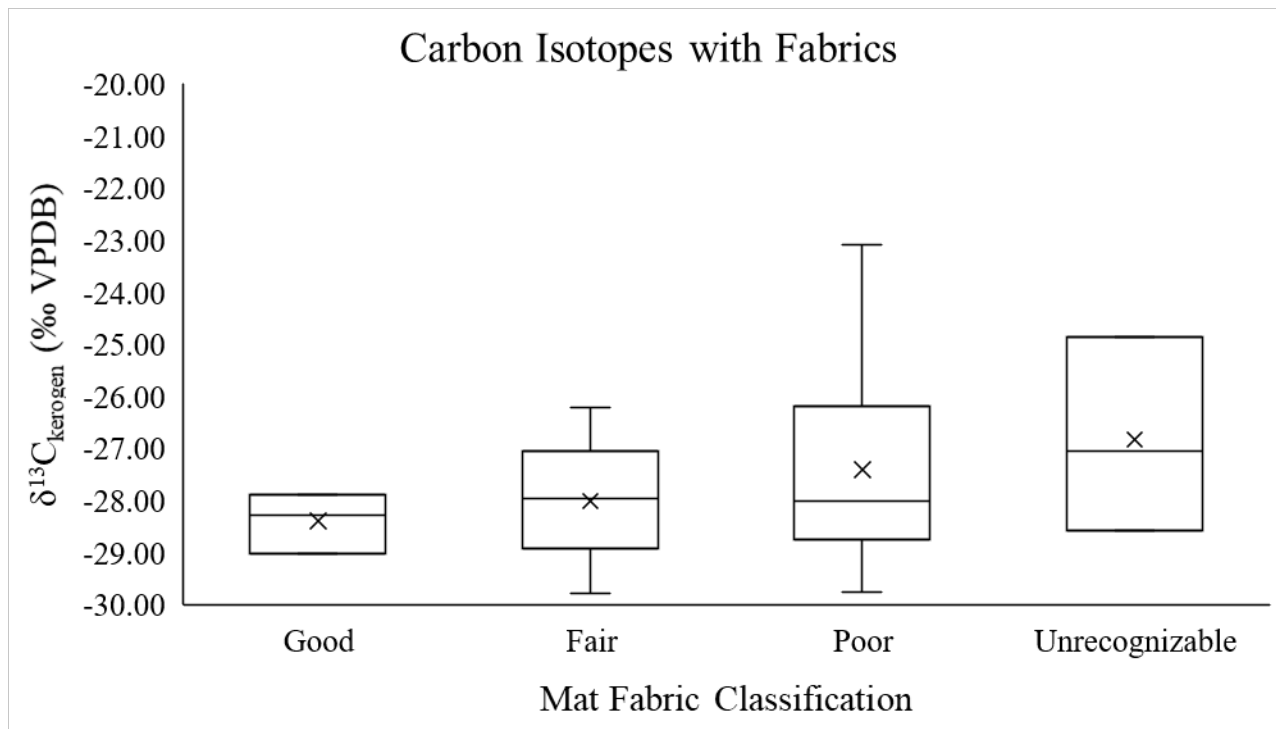


Figure 3.14 Carbon isotope samples of the mats are grouped by their assigned taphonomic grade. As samples become less well-preserved, and more unrecognizable, the samples become with more enriched ^{13}C . More data are required to support this trend.

CONCLUSIONS

The work outlined in the three chapters of this dissertation provide insight on the potential environments of silica deposition and the extent to which organisms are able to be preserved in early diagenetic chert deposits. Silicification, occurring as beds and nodules, is common in Meso- to Neoproterozoic carbonate strata and commonly contain exquisitely preserved microfossils (Schopf, 1968; Awramik and Barghoorn, 1977; Knoll, 1985). Increased silica concentrations in the Precambrian, combined with the absence of silica-secreting organisms, resulted in rapid precipitation of a silica gel that ultimately formed chert (Maliva and Siever, 1988; Maliva et al., 1989; Maliva et al., 2005). Rapid preservation of the microfossils suggests that environmental conditions and microbial processes that were active at the time of preservation can be inferred from the morphology and preserved biochemistry within chert samples.

Early diagenetic chert deposits provide a critical window through which we can understand environmental conditions and interactions of microbial ecosystems present on the early Earth. Recognition of the well-preserved microfossils in early diagenetic chert, and the contribution of taxonomic, taphonomic, and geochemical studies of these chert deposits has prompted the astrobiological community to consider the possibility of silica-rich deposits, especially those with increased amorphous silica content, as potential locations to find evidence of extraterrestrial life on Mars (Milliken et al., 2008; McMahon et al., 2018). As part of the Mars 2020 mission, the rover will drill and cache samples of interest. These samples will be collected by a subsequent mission to Mars and brought back to Earth for analyses. The conclusions of this work can be used to understand the types of data that we might be able to obtain from silica-rich Mars samples.

Early diagenetic chert deposits occur in peritidal environments, where frequent changes to water chemistry are caused by evaporation or the introduction of freshwater. In chapter one, major ion concentrations of Proterozoic seawater (Spear et al., 2014) were used to model possible Proterozoic seawater chemistries and the chemistry of their evaporated brines in the geochemical modeling program PHREEQ-C. The seawater chemistries, and the brine chemistries were mixed with a modeled freshwater solution. Changes in water chemistry effected the minerals that were able to precipitate, and the mineral phases present were compared to the mineral phases observed in the Angmaat Formation chert deposits.

To consider whether one model was able to depict a viable water chemistry for the formation of early diagenetic chert, water chemistries had to be able to replicate mineral phases and associated textures observed in petrographic observations of the Angmaat Formation chert. Primary silica and carbonate phases are present in these chert deposits. Primary silica occurs within the microbial mats, which lack crystalline material between the filaments. Primary chalcedony occurs as a void-filling phase, generally silicifying areas of the microbial mat interpreted to represent gas bubbles (Knoll et al., 2013). Primary carbonate phases are associated with the silica phases. The two mineral phases often exist together in the same sample, where a large portion of the sample is silicified, and the rest of the sample is dolomite. When the two phases occur next to each other, they record the same microbial fabrics or individual microfossils, however, preservation is always better in the silica phase. Secondary silica and carbonate phases are also observed in these samples. Silicified carbonate is common in voids, silicified gypsum and halite crystals are documented in the Angmaat Formation (Kah et al., 2001), and many of the fabrics preserved in the microbial mats resemble chicken-wire textures common in evaporite phases. Fabric destructive dolomite rhombs occur throughout several of the

samples. The thermodynamic models indicate that a variety of Proterozoic water chemistries were able to precipitate the mineral phases preserved in the Angmaat Formation chert. However, each of the starting solutions had to be a brine in order to precipitate evaporite phases. Mixtures of the brine chemistries with freshwater were able to produce amorphous silica phases, opal-A and silica gel, until the solution was composed of 50% or 70% freshwater, respectively. Opal-A only formed in solutions that started from a brine. These amorphous silica phases are crucial to the preservation of microfossils in early diagenetic chert.

The exquisite preservation of microfossils in early diagenetic chert requires that silicification occurs early during diagenesis (Schopf, 1968; Schopf, 1975; Hofmann, 1976; Knoll, 1985; Knoll et al., 1988; Golubic and Seong-Joo, 1999; Knoll, 2012), to halt active bacterial degradation (Bartley, 1996; Bartley et al., 2000). Silicification occurs in several steps, starting with the formation of a gel phases that permeates through the sheaths and cell envelopes and converts to microcrystalline quartz over time (Oehler and Schopf, 1971; Hesse, 1989). Coccoidal organisms within the Angmaat Formation consistently demonstrated a wider range of preservation than the empty filamentous sheaths. Most of the sheaths exhibited “poor” preservation, while the coccoids commonly plotted in the “fair” to “fair-poor” range.

The notably better preservation of the coccoids may be the result of a taphonomic bias, wherein the filaments and coccoids experience different decomposition pathways, determined by their motility. Filamentous organisms are motile. They can abandon their sheaths when necessary, leaving behind bundles of empty sheaths that ultimately get buried in the mat (Ortega-Calvo et al., 1991; Golubic and Lee, 1999). Conversely, the coccoidal organisms are generally insulated by the presence of extracellular polymeric substances (EPS), which protect the cell from drastic changes in the surrounding environment, including the introduction of toxins and

metals, or desiccation (Decho, 1990; Decho, 1994). The EPS allows the cell to continue to survive and maintain its cellular components (Krylov et al., 1989; Sergeev et al., 2002).

A new technique was also presented in chapter 2 for performing a taphonomic assessment. Image mosaics were created at the abcLab at JPL from thousands of photomicrographs. An advantage of the image mosaics is that they provide a holistic view of the thin section because the user can rapidly change the scales, i.e. mesoscale (thin-section) to microscale (individual fossil), at which the user is making observations. With the mosaics, it is easy to look at individual microfossils and then zoom-out to see how the individuals fit into the larger picture, the mat fabric. The quadrat system used to count and score microfossils for the taphonomic assessment allowed for a more representative assessment of the entire thin section than using traditional point counting techniques. The method is also faster than traditional point counting on a microscopy, and the methodology is modular, which allows the observer to stop and come back at a later point in time to add more counts to their assessment.

Finally, the exceptional morphologic preservation of the Proterozoic microfossils indicates that silicification occurred early in diagenesis. To understand the extent to which the microfossils were preserved, geochemical analyses were performed on the mats to determine whether the molecular chemistry of the organisms was also preserved by silicification. A secondary question addressed in the geochemical analyses is required sample size for reliable data. Valuable extraterrestrial samples are expected to be returned to Earth during a later mission to Mars. Approximately 15 g of sample will be allocated for scientific study; therefore, we need to have an understanding of the smallest sample size that we can use for destructive analyses, like GCMS analyses used to detect lipids. Two different sample sizes were used (5 g versus 50 g samples) to extract bitumen from the silicified mats. The first set of samples were collected in

1994 and stored in the collections for ~20 years prior to any organic geochemical analyses were performed. Samples size was limited for the 1994 samples, which allowed for testing the smaller sample size (5 g). The second set of samples were collected during a field season in 2017. These samples were not limited in sample size. Fifty grams of sample were used for the bitumen extractions.

Evidence for lipids (*n*-alkanes, hopanes, and steranes) was observed in the chromatograms of bitumen extracted from the 1994 samples. However, similar patterns of peaks in all 23 chromatograms suggest that the observed lipids are contamination. Although the source of the contamination is unknown. Chromatograms for the 2017 samples, which consisted of chert-only samples, chert-associated carbonate, and a carbonate sample, did not show much evidence for *n*-alkanes, hopanes, and steranes. In fact, the predominant peaks observed in many of the chromatograms (n=14), are identified as phthalates, phenols, and DEET. These compounds are interpreted to be contaminants. The data presented in this chapter indicate that although early diagenetic chert deposits contain exceptionally preserved microbial morphologies the chert does not preserve molecular biomarkers associated with the preserved microbes. Amorphous silica and chert deposits observed in lacustrine environments on Mars have been proposed as potential lithologies where we might find evidence of ancient life (McMahon et al., 2018), but these deposits may not be as fruitful as anticipated.

References

- Awramik, S. M., and Barghoorn, E. S., 1977, The Gunflint microbiota: *Precambrian Research*, v. 5, no. 2, p. 121-142.
- Bartley, J., Knoll, A., P Grotzinger, J., and Sergeev, V., 2000, Lithification and fabric genesis in precipitated stromatolites and associated peritidal carbonates, Mesoproterozoic Billyakh Group, Siberia.
- Bartley, J. K., 1996, Actualistic Taphonomy of Cyanobacteria: Implications for the Precambrian Fossil Record: *PALAIOS*, v. 11, no. 6, p. 571-586.
- Decho, A. W., 1990, Microbial Exopolymer Secretions in Ocean Environments: Their Role (s) in Food Webs and Marine Processes: *Oceanogr. Mar. Biol. Annu. Rev.*, v. 28, p. 73-153.
- Decho, A. W., *Exopolymers in microbial mats: Assessing their adaptive roles*, Berlin, Heidelberg, 1994, Springer Berlin Heidelberg, p. 215-219.
- Golubic, S., and Lee, Seong-Joo, 1999, Early cyanobacterial fossil record: preservation, palaeoenvironments and identification: *European Journal of Phycology*, v. 34, no. 04, p. 339-348.
- Hesse, R., 1989, Silica diagenesis: origin of inorganic and replacement cherts: *Earth-Science Reviews*, v. 26, no. 1-3, p. 253-284.
- Hofmann, H. J., 1976, Precambrian Microflora, Belcher Islands, Canada: Significance and Systematics: *Journal of Paleontology*, v. 50, no. 6, p. 1040-1073.
- Kah, L. C., Lyons, T. W., and Chesley, J. T., 2001, Geochemistry of a 1.2 Ga carbonate-evaporite succession, northern Baffin and Bylot Islands: implications for Mesoproterozoic marine evolution: *Precambrian Research*, v. 111, no. 1-4, p. 203-234.
- Knoll, A. H., 1985, Exceptional Preservation of Photosynthetic Organisms in Silicified Carbonates and Silicified Peats: *Philosophical Transactions of the Royal Society B: Biological Sciences*, v. 311, no. 1148, p. 111-122.
- Knoll, A. H., 2012, *The Fossil Record of Microbial Life, Fundamentals of Geobiology*, John Wiley & Sons, Ltd, p. 297-314.
- Knoll, A. H., Strother, P. K., and Rossi, S., 1988, Distribution and diagenesis of microfossils from the lower proterozoic duck creek dolomite, Western Australia: *Precambrian Research*, v. 38, no. 3, p. 257-279.
- Knoll, A. H., Wörndle, S., and Kah, L. C., 2013, Covariance of microfossil assemblages and microbialite textures across an upper Mesoproterozoic carbonate platform: *Palaios*, v. 28, no. 7, p. 453-470.
- Krylov, I., Orleanskii, V., and Tikhomirova, N., 1989, Chertification: Secular Preparations: *Priroda*, no. 4, p. 73-78.
- Maliva, R. G., Knoll, A. H., and Siever, R., 1989, Secular Change in Chert Distribution: A Reflection of Evolving Biological Participation in the Silica Cycle: *PALAIOS*, v. 4, no. 6, p. 519-532.
- Maliva, R. G., Knoll, A. H., and Simonson, B. M., 2005, Secular change in the Precambrian silica cycle: Insights from chert petrology: *Geological Society of America Bulletin*, v. 117, no. 7-8, p. 835-845.
- Maliva, R. G., and Siever, R., 1988, Mechanism and Controls of Silicification of Fossils in Limestones: *The Journal of Geology*, v. 96, no. 4, p. 387-398.

- McMahon, S., Bosak, T., Grotzinger, J. P., Milliken, R. E., Summons, R. E., Daye, M., Newman, S. A., Fraeman, A., Williford, K. H., and Briggs, D. E. G., 2018, A Field Guide to Finding Fossils on Mars: *Journal of Geophysical Research: Planets*, v. 0, no. 0.
- Milliken, R. E., G.A, S., Arvidson, R. E., Bishop, J. L., Clark, R. N., Ehlmann, B. L., Green, R. O., Grotzinger, J. P., Morris, R. V., Murchie, S. L., Mustard, J. F., and Weitz, C., 2008, Opaline silica in young deposits on Mars: *Geology*, v. 36, no. 11, p. 847-850.
- Oehler, J. H., and Schopf, J. W., 1971, Artificial Microfossils: Experimental Studies of Permineralization of Blue-Green Algae in Silica: *Science*, v. 174, no. 4015, p. 1229-1231.
- Ortega-Calvo, J. J., Hernandez-Marine, M., and Saiz-Jimenez, C., 1991, Biodeterioration of building materials by cyanobacteria and algae: *International Biodeterioration*, v. 28, no. 1, p. 165-185.
- Schopf, J. W., 1968, Microflora of the Bitter Springs Formation, Late Precambrian, Central Australia: *Journal of Paleontology*, v. 42, no. 3, p. 651-688.
- Schopf, J. W., 1975, Precambrian paleobiology: problems and perspectives: *Annual Review of Earth and Planetary Sciences*, v. 3, no. 1, p. 213-249.
- Sergeev, V. N., Gerasimenko, L. M., and Zavarzin, G. A., 2002, The Proterozoic History and Present State of Cyanobacteria: *Microbiology*, v. 71, no. 6, p. 623-637.
- Spear, N., Holland, H., Garcia-Veigas, J., Lowenstein, T., Giegengack, R., and Peters, H., 2014, Analyses of fluid inclusions in Neoproterozoic marine halite provide oldest measurement of seawater chemistry: *Geology*, v. 42, no. 2, p. 103-106.

VITA

Ashley Manning-Berg was born and raised in Georgia. She finished high school at Collins Hill High School in Suwanee, GA. After high school, she attended the University of West Georgia, where she registered for an academic first-year program focused on space science. Ashley was encouraged by one of the professors leading the program to take a geology course. She became a geology major at the end of that semester. Her interests in diagenesis, carbonate sedimentology, and understanding how microfossils enter the fossil record stem from the research opportunities she had as an undergraduate working with Dr. Julie Bartley and acting as a student operator in a scanning electron microscopy lab. After earning her bachelor's Degree, she worked for the Army Corps of Engineers at their Engineer Research and Development Center. During this time, she married, Dr. Christopher Berg. She left the Army Corps to obtain a master's degree at the University of Tennessee under the supervision of Dr. Linda Kah, where she investigated whether bright white limestone beds in the Atar Group, Mauritania represented calcitized evaporite deposits. She completed her master's degree in 2014 and stayed at the University of Tennessee in the Fall of 2014 to work towards her doctorate degree, under the guidance of Dr. Linda Kah. As a PhD student, she organized and led a field season to Baffin Island, Arctic Canada, mentored undergraduate student research, and worked as a visiting researcher and graduate student intern at NASA's Jet Propulsion Laboratory.